

Heat transport and related thermal Properties in Nanofluids and Nanostructured Materials

A Thesis
Submitted for the Degree of

Doctor of Philosophy

in the Faculty of Science
Jadavpur University

by

Rajesh Kumar Neogy



**Department of Condensed Matter Physics & Material Sciences
S. N. Bose National Centre for Basic Sciences
Block - JD, Sector - III, Salt Lake, Kolkata - 98
India**

July 2012

CERTIFICATE FROM THE SUPERVISOR

This is to certify that the thesis entitled *Heat transport and related thermal Properties in Nanofluids and Nanostructured Materials* submitted by **Sri/Smt. Rajesh Kumar Neogy** got his/her name registered on *5th* August, 2009 for the award of **Ph.D. (Science) degree of Jadavpur University**, is absolutely based upon his own work under the supervision of Prof. A. K. Raychaudhuri and that neither this thesis not any part of its has been submitted for any degree/diploma or any other academic award anywhere before.

.....
Signature of the Supervisor date with official seal

To my family...

Acknowledgment

This thesis is the outcome of my long cherished dream of becoming a scientist one day. This thesis will be the first stepping stone towards this. This is the result of the work that I have done in the last few years at the Department of Condensed Matter Physics & Material Sciences; SNBNCBS. This would not have been possible without the help and guidance of many people. In this list I will start with the name of my supervisor Prof. A. K. Raychaudhuri for introducing me to the wonderful world of experiments and that too in the field of Nanotechnology which is a buzz word now. I acknowledge the constant encouragement and live response that I received from him. Over these years, his advice has always influenced my perception towards research and the thirst to become an independent researcher one day. His criticism has always enhanced my ability to distinguish between the good, and the bad. One thing that I enjoyed under him is that he has given us immense freedom both professionally and socially. He enabled me to learn many things during my work. It has been a great experience working with him. He always helped me financially (from his project) whenever an aid needed for my work.

Secondly I would thank Mr. Subrato Sarkar, although he was my senior but he never let me felt that through his friendly and supportive attitude towards me. He gave me hand on experience in the 3 Omega technique and programming. On joining here I had to attend course work taken by Dr. S.S Manna, Dr. Sugata Mukherjee and I enjoyed their class very much and learned many new things.

I am highly indebted to IACS for providing me access to the facilities of TEM. They helped me in every way for getting good TEM images so that it is published.

I enjoyed the useful discussions and active support from my lab mates and project students. Ritwik Bhattacharyaa, Chinmay Gupta, Rajib Nath, Manotosh Chakroborty, Shahnawaz Mondal, Putul Malla Choudhuri, Rabeya Basori and the new comers like Sabyasachi Ghosh, Rishi Ram Ghimire. My seniors colleagues like M. Venkata Kamalakar, Tapati Sarkar, Soma Das, Sudeshna Samanta, Manoranjan Ghosh etc are very nice and gave me suggestions when needed in all types of problems. There were few seniors like Achyutda, P. Sai from IISc, Bangalore who had visited our lab and shared views and ideas with me. I thank Dr. Barnali Ghosh, Dr. Anindya Das, Dr. Kuntal Chakraborty, Dr. Kaustuv Das and Dr. Sarathi Kundu for their immediate help and support whenever I asked.

Talking individually for some of the above list, I would starts with the thanks to Kuntal da for giving suggestion to make the metal stencil masks from CTTC, Kolkata, without this life would not be so easy for me. Similarly Kaustuv da helped me whenever I asked and his useful suggestion out of his experience aided me much in my work both academically and socially.

Talking/debating with Shahnawaz on various issues like political, geo political, religious, current affairs etc. amused me very much. I learned lot of extracurricular things from him. Surely I am going to miss the company of Rajib, especially for cups of tea/snacks that we take from our so called “Dulal da” & “Kaka” etc. Manotosh was my good travelling company in both domestic and international tours.

Sudeshna di my senior helped me and gave suggestions various issues ranging from academic to domestic. Rabeya, Putul are like my sisters so I do not miss a chance to crack a joke or enjoy funny moments with them. New comers in our lab like Sabyasachi, Rishi, & Subarna are also nice persons to interact with them and guiding/suggestions are always forwarded to them whenever sought.

I would like to thank all my friends all walks of life, who were always a source of happiness and fun in my life irrespective of my failure or success. I cannot name all of them in this limited space but few of my batch mates like Nirupam Datta, Sudeep Gorai, Debabrata, Bipul da etc. have always given me enough boosts in my personal life as well as in research. Here I also like to thank one of my best friends Debabrata Bhattacharyya for his suggestions and help in academic and social life.

Last but not the least, Tandrima, my wife who has a very special place in my life, not only as my better half but also as a very good friend, with whom I shared all types of problems/happiness. She helped me to correct all my writing works grammatically and gave it a good cosmetic change. I could not have spent six years in research without the support and encouragement from my parents. I cannot express my gratitude towards them in simple words. All of them were in my heart every moment which provided me the courage for carrying out my research. I also want to thank my in-laws, especially to support me and make my life easy going. I can't forget to thank my "mama" and "kakas" who inspired me as well as extended helping hand in need.

I also like to express my thanks to our technical assistants of our centre who helped me in doing different types of measurement and characterisations etc. I apologize to all of them whose names I could not mention in this limited space but were always supportive in my research work.

At last I would thanks Department of Sciences (DST) and Technology, Govt. Of India for providing me the scholarship and funding for conferences attended by me etc.

Contents

Chapter 1: Introduction

1.1 Motivation.....	3
1.2 Reviews.....	4
1.2.1 Review on Nanofluids.....	4-9
1.2.2 Review of synthesis process of Nanofluids.....	9-12
1.2.3 Factors that influence the thermal conductivity enhancement.....	13-25
1.2.4 Review on 3 Omega technique.....	25-27
1.3 Importance.....	28
1.4 Motivation of the thesis and major issues addressed to.....	28-29
1.5 Structure of the thesis.....	30

References

Chapter 2: Experimental Techniques

2.1 Introduction	40
2.2 3ω Technique	40
2.2.1 Theory.....	40-43
2.2.2 Electronics.....	43-44
2.2.3 Experimental Setup Details.....	44-45
2.2.3.1 Heater/Thermometer.....	46
2.2.3.1.1 Heater Material.....	47-48
2.2.3.1.2 Heater Fabrication.....	49-52
2.2.3.1.3 Electrical Characterisation.....	53-55
2.2.3.1.4 Thickness Characterisation.....	55-60
2.2.3.2 Sample and heater holder.....	60-62
2.2.3.3 Wheatstone Bridge.....	63-65
2.2.3.4 Lock In Amplifier (LIA).....	65-68
2.2.3.5 Temperature Controller.....	68
2.2.3.6 Decade Resistance Box.....	69
2.2.3.7 CPU Interfacing (GPIB,C++)	69-71
2.2.4 Sources of possible error and its correction.....	71
2.2.4.1 Size Distribution of nanoparticles.....	72
2.2.4.2 Convective current in the liquids.....	73
2.2.4.3 Agglomeration of nanoparticles.....	74
2.2.4.4 Grounding of the setup.....	74
2.2.4.5 Instrumental error.....	75
2.2.5 Conclusion.....	76
Reference	

Chapter 3: Sample Preparation & Characterisation techniques...

3.1 Introduction	82-83
3.2 Synthesis of ZnO nanostructures	84-85
3.2.1 Characterisation.....	85-90
3.3 Synthesis of ZnO nanostructures with capping layer.....	90-91
3.3.1 Characterisation.....	91
3.4 Synthesis of Silver Nanofluids.....	92
3.4.1 Characterisation.....	93-94
3.5 Synthesis of Gold Nanofluids.....	95
3.5.1 Characterisation.....	95-96
3.6 Synthesis of Gold Nanonetwork.....	97-99
3.6.1 Characterisation.....	99-101
3.7 Characterization techniques	102
3.7.1 Scanning Electron Microscope (SEM)	102-104
3.7.2 Transmission Electron Microscopy (TEM).....	104-106
3.7.2.1 High Resolution TEM (HRTEM)	107
3.7.2.2 Selected Area Diffraction (SAD).....	107-108
3.7.2.3 Energy-dispersive X-ray (EDX) spectroscopy.....	108
3.7.3 UV-visible absorption measurement	108-110

References

Chapter 4: Heat Transport Measurement in ZnO Nanofluid.....

4.1 Introduction	117-118
4.2 Measurement process.....	118-121
4.3 Finite Size Effect.....	122-123
4.4 Calibration.	124-126
4.5 ZnO Nanofluid measurement.	127-130
4.5.1 Temperature Dependence.....	131
4.5.2 Volume fraction (ϕ) Dependence.....	131-133
4.6 Analysis of the frequency dependence.....	134-135
4.7 Physical interpretation.....	136-137
4.8 Conclusions.....	137

References

Chapter 5: Measurements in ZnO and ZnO with PVP Nanofluids.....

5.1 Introduction	144-145
5.2 Results.....	145-146
5.3 Separation of C_p and κ measurements.....	147
5.3.1 Measurement process of Thermal Conductivity (κ).....	147
5.3.1.1 Measurement Theory.....	147-148
5.3.1.2 Experimental Results.....	148
5.3.1.2.1 ZnO and ZnO + PVP Nanofluid.....	148-149
5.4 Calculation of temperature distribution of the heater.....	150
5.4.1 Substrate.....	150-151
5.4.2 Liquid.....	151-152
5.5 Discussion.....	153-156
5.6 Conclusion.....	156
References	

Chapter 6: Measurements in Metal Nanofluids.....

6.1 Introduction	163-164
6.2 Results... ..	165
6.2.1 Silver Nanofluids.....	165-167
6.2.2 Au Nanofluids.....	168-169
6.2.3 Au Network.....	170-171
6.3 Discussion.....	172-173
References	

Conclusion & Future works...

Summary and conclusions of the thesis	177-178
Experimental contributions made in the thesis	177
Physics contributions made in the thesis	178
Scope for further work	179
List of Publication.....	181

Chapter 1

Introduction

1.1 Motivation

Now a day the quest for more and more miniaturisation along with faster and faster processing speed of the devices has resulted in intense heat dissipation from such systems. This results in the hindrance of the efficiency. Such heat dissipation problem is not only associated with microelectronics but with all those things like machines, Industries, thermal plants, nuclear reactors etc. So in order to increase the efficiency as well as the longevity of these devices we must get rid of such heat radiations. For dissipating heat a cooling system is required for heat transfer.

In most of these applications, heat transfer is realized through some heat transfer devices. In such devices a working fluid is circulated by a pump, and they extract out the heat from the system. Improvements in heat transfer efficiency can minimize the associated power consumption. Conventional heat transfer fluids such as water, ethylene glycol, and engine oil have relatively low thermal conductivities inherently. So such conventional methods of heat removal have been found rather inadequate to deal with such high intensities of heat fluxes.

There are various ways to improve the heat transfer efficiency like utilization of extended surfaces, application of vibration to the heat transfer surfaces, usage of micro channel, and by increasing the thermal conductivity of the working fluid. Others factors though increases the thermal conductivity of the working fluid but not so impressive. Last factor is the most important one i.e. manipulating the working fluid. One of these attempts is the addition of nanoparticles to it and this mixed phase is now known as Nanofluid. This shows an anomalous increase in the heat transfer capability in contrast to heat transfer fluid.

We have tried to take one step further in this field by observing the effect of the application of external perturbation like electric field in nanofluid and its performance in enhancing the thermal conductivity. So we tried to capture the dynamic thermal parameters for the nanofluids using 3 ω method which is a dynamic heat transfer measurement technique.

1.2 Reviews

Review of my work consists into two parts. First part gives the review of my samples which are nanofluids of different types and second part is the review of different techniques which are employed for the measurement of different thermal parameters like thermal conductivity, specific heat or there combinations. Finally I narrowed down to dynamic measurement method the 3ω method, which was developed by Cahill in the 1980s [1] and was developed for liquid by Birge & Nagel [2]. This is the most popular method now of course much developed than earlier models. We will show that investigation of applying 3ω method for dynamic thermal conductivity measurements in nanofluids leads to new results that have not been observed before.

1.2.1 Review on Nanofluids

Back ground:

Today more than ever, ultrahigh-performance cooling plays an important role in the development of energy-efficient heat transfer fluids which are required in many industries and commercial applications. Conventional fluids, such as water, engine oil and ethylene glycol are normally used as heat transfer fluids however these conventional coolants are inherently poor heat transfer fluids. Although various techniques are applied to enhance the heat transfer, the low heat transfer performance of these conventional fluids obstructs the performance enhancement and the compactness of heat exchangers.

The use of solid particles as an additive suspended into the base fluid is a technique for the heat transfer enhancement. Improving of the thermal conductivity is the key idea to improve the heat transfer characteristics of conventional fluids. Since a solid metal has a larger thermal conductivity than a base fluid, suspending metallic solid fine particles into the base fluid is expected to improve the thermal conductivity of that fluid. The enhancement of thermal conductivity of conventional fluids by the suspension of solid particles, such as millimeter- or micrometer-sized particles, has been well known for more than 130 years [3]. However, they have not been of interest for practical applications due to problems such as sedimentation, erosion, fouling and increased pressure drop of the flow channel. The recent advance in materials technology has made it possible to produce nanometer-sizes particles that can overcome these problems. Innovative heat transfer fluids-suspended by nanometer-

sized solid particles are called ‘nanofluids’. These suspended nanoparticles can change the transport and thermal properties of the base fluid significantly.

Now in modern days the quest for more and more miniaturisation along with faster and faster processing speed of the electronics devices has resulted in intense heat dissipation from such systems. Such heat dissipation problem is not only associated with microelectronics but with all those things like machines, Industries, thermal plants, nuclear reactors etc. in order to increase the efficiency as well as the longevity of these devices we must get rid of such heat radiations. For dissipating heat a cooling system is required for heat transfer. In most of these applications, heat transfer is realized through some heat transfer devices; such as, heat exchangers, evaporators, condensers, and heat sinks. In these systems working fluid is circulated by a pump, and improvements in heat transfer efficiency can minimize the associated power consumption. So cooling is a very important part of such device and microelectronics industries. Cooling determines the efficiency of the production/processing system. Commonly used heat transfer fluids such as water, ethylene glycol, and engine oil etc. Though these liquids are used for heat transfer but they inherently poor thermal conductivity. Use of these fluids could be more beneficial if the thermal resistance of the heat transfer is decreased. Lots of efforts were made to increase the thermal conductivity of the coolants. One of the most widely used methods is addition of solid metal or metal oxide particles to these coolants. Since solids have much higher thermal conductivity than liquids it will cause an increase in the effective thermal conductivity of the resultant fluid system. Such idea of solid inclusion was very old and was predicted by Maxwell’s Effective Medium Theory (EMT) 140 years ago [3].

$$\kappa_{eff}^* = \frac{\kappa_p^*(1 + 2\phi) + 2(1 - \phi)}{\kappa_p^*(1 - \phi) + (2 + \phi)} \quad \kappa_{eff}^* = \frac{\kappa_e}{\kappa_m}, \quad \kappa_p^* = \frac{\kappa_p}{\kappa_m}$$

Where ϕ = Volume fraction of the solid inclusion. k = Thermal conductivity

κ_e = thermal conductivity of mixed phase

κ_p = thermal conductivity of the particle

κ_m = thermal conductivity of the medium

However these, early studies were limited to millimetre-or-micrometre sized particles. Although they show an enhanced heat transfer property according to Maxwell's prediction but not to that extent that it can be used in high processing industries for cooling purposes. Since the sizes of these particles used were big, so they do not make a stable suspension and the suspended particles tend to settle down at the bottom by their own weight. They also causes clogging and erosion of the channels through which they are made to flow. So such systems have many problems and it was necessary to overcome these by some new and innovative ideas to meet the challenges of these modern day high performance industries.

In fact when the sizes of these particles were reduced to nanometre level, the result was found to be miraculous. Such systems in which solid particles of size < 100nm suspended in a liquid was called "NANOFLUID" is the term first coined by Choi in 1995 [4] at the Argonne National Laboratory to describe the new class of nanotechnology-based heat transfer fluids that exhibit thermal properties superior to those of their base fluids or conventional particle fluid suspensions. This was a milestone in the field of heat management and transfer. This new class of fluids has generated a large interest from both academia and industry for its anomalous behaviour in the enhancement in thermal conductivity consequently its excellent potential for heat transfer applications. Similar anomalous results for the nanofluids are also reported by Keblenski et.al.[5].

For the last decade nanofluids sparked excitement as well as controversy for its reported dramatic increases of thermal conductivity with small nanoparticles loading, while others showed moderate increases consistent with the effective medium theories on well-dispersed conductive spheres. Accordingly, the mechanism of thermal conductivity enhancement continues to be a hotly debated topic. To explain different results different models were developed to explain the observation. However, till date, there is no single unified model which can be generalised for all the experimental results and for different types and systems. The models developed appear to have specificity that makes them applicable to one or few classes of nanofluids.

Without understanding the underlying heat conduction mechanism on the basic level our ability to tailor and predict performance of nanofluids is limited to empirical observation and thus limiting application of nanofluids to engineering systems only. In order to generalise the use we have to harness this system to the full capacity we have to do more experiments for understanding the system.

That effort in this direction has increased considerably over the past several years, as is evident from the increase of the yearly publications shown in table 1.1. We have used the data base of “Web of Knowledge” of Thomson Reuter to find out the number of papers published (peer reviewed) under the category of three fields namely Nanofluid, Nanofluid and its Heat transfer property and Nanofluid and other allied properties.

It was found that there is an exponential increase from 1993 to 2011 (December).

People started working in this field of Nanofluid around 1993. Then after 10 years there is a sharp increase in the numbers of paper/year and around 2005-07 alone, more than 200 research papers were published in *Science Citation Index* (CSI) journals. Around 2007 itself total number of papers published in the nanofluid related paper reaches around 1000. At the end of this year it is estimated that the paper count will be around 2500. It was also noticed parallely that the heat transfer related papers are much more than related to the other properties of the nanofluids. This is because an increasing number of industries got interested in the area and consequently make it a hot topic of research worldwide. However, the transition to industrial practice requires that nanofluid technology become further developed, and that some key barriers be overcome. Some of this publication increase is due to the establishment of nanofluid research groups at prestigious institutions worldwide.

<i>Duration</i>	<i>Phrase Searched</i>		
	<i>Nanofluids</i>	<i>Nanofluids & Thermal Conductivity/Heat Transfer</i>	<i>Nanofluids & its general properties</i>
1993-1995	1	0	0
1995-1997	1	0	0
1997-1999	2	0	0
1999-2001	5	2	0
2001-2003	15	7	4
2003-2005	77	42	20
2005-2007	207	117	56
2007-2009	488	282	134
2009-2011	893	589	255
<i>All Years (Total)</i>	2980	1852	828

Table 1.1

Above table summarises the finding about the no. of publications around different time of evolution. These results are plotted as a bar graph as a visual aid and it is shown in the Fig.1.1. It shows the result that as the time increases, popularity increases exponentially.

The anomalous behaviour in the thermal conductivity of the Nanofluid is the main reason behind this surge in interest of Nanofluids.

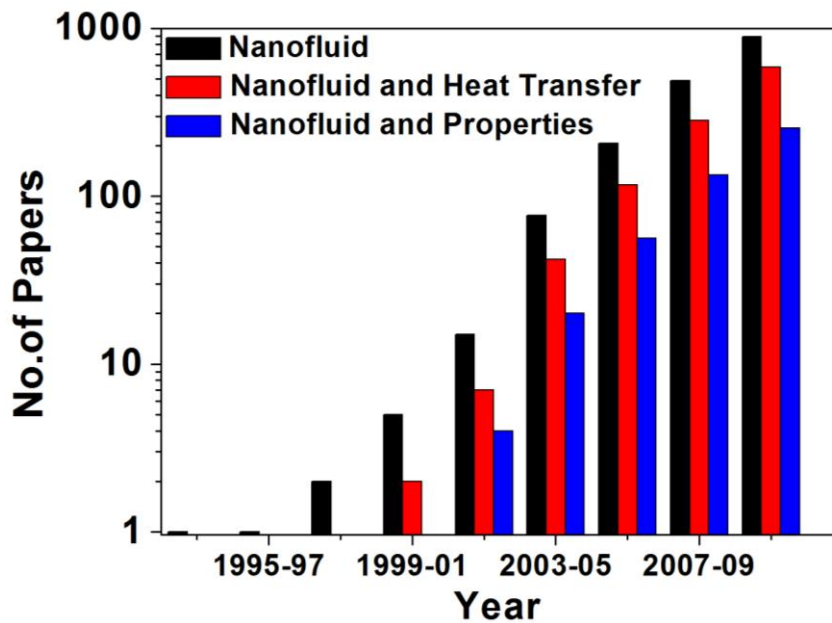


Fig.1.1 Bar graph showing the paper trend

Researchers have also tried to increase the thermal conductivity of base fluids by suspending micro- or larger-sized solid particles in fluids since the thermal conductivity of solid is typically higher than that of liquids [6]

1.2.2 Review of synthesis process of nanofluids

The samples used in this thesis work are the various types of nanofluids. Preparation of nanofluids is the first key step in experimental studies with nanofluids. Broadly nanofluids are generally prepared by two methods which are (a) One step method and (b) Two step method. These methods are described below. In nanofluids there is a liquids medium in which particles are dispersed these are usually called the heat transfer fluids.

» **One-step Method:** As the name suggests that this is a one pot synthesis process in which simultaneously makes and disperses nanoparticles directly into base fluid. This is best for synthesizing metallic nanofluids.

The single-step direct evaporation approach was developed by Akoh et al. [7] and is called the Vacuum Evaporation onto a Running Oil Substrate (VEROS) technique. The original idea of this method was to produce nanoparticles, but it is difficult to subsequently separate the particles from the fluids to produce dry nanoparticles. A modified VEROS process was proposed by Wagener et al.[8]. They employed high pressure magnetron sputtering for the

preparation of suspensions with metal nanoparticles such as Ag and Fe. Eastman et al. [9] developed a modified VEROS technique, in which Cu vapor is directly condensed into nanoparticles by contact with a flowing low-vapor-pressure Ethylene Glycol. Zhu et al. [10] presented a novel one-step chemical method for preparing copper nanofluids by reducing $\text{CuSO}_4 \cdot 5\text{H}_2\text{O}$ with $\text{NaH}_2\text{PO}_2 \cdot \text{H}_2\text{O}$ in ethylene glycol under micro wave irradiation. Results showed that the addition of $\text{NaH}_2\text{PO}_2 \cdot \text{H}_2\text{O}$ and the adoption of microwave irradiation are two significant factors which affect the reaction rate and the properties of Cu nanofluids.

A vacuum-SANSS (submerged arc nanoparticle synthesis system) method has been employed by Lo et al. [11] to prepare Cu-based nanofluids with different dielectric liquids such as de-ionized water, with 30%, 50%, 70% volume solutions of ethylene glycol and pure ethylene glycol. They found that the different morphologies, which are obtained, are mainly influenced and determined by the thermal conductivity of the dielectric liquids. CuO , Cu_2O , and Cu based nanofluids also can be prepared by this technique efficiently.

An advantage of the one-step technique is that nanoparticle agglomeration is minimized, while the disadvantage is that only low vapor pressure fluids are compatible with such a process. Recently, a Ni nanomagnetic fluid was also produced by Lo et al. [12] using the SANSS method.

In the recent days, Laser ablation is another much sought, single-step technique that simultaneously makes and disperses nanoparticles directly in the base fluids. A variety of nanofluids have been prepared by laser ablation method [13-16] by ablating solid metals, semiconductors, etc which are submerged in the base fluid (water, lubrication oils, etc). By creating a nanofluid in this way, stable nanofluids resulted without using any property-changing dispersants. This method is also useful for further splitting of nanoparticles present in the nanofluids to study effect of particle size on thermal conductivity.

Laser ablation in liquid medium occurs when a high-power laser is focused at the submerged surface for an appropriate time. Fig.1.2 shows the typical arrangement for laser method.

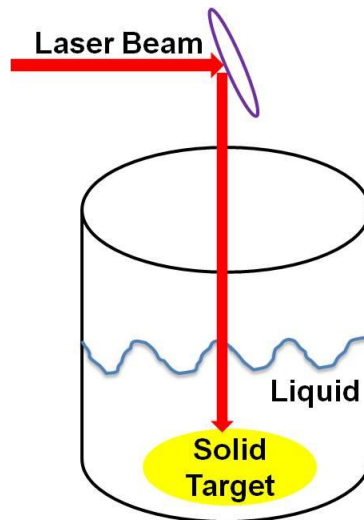


Fig.1.2 Laser based method

Some of the nanofluids made by these laser techniques are like Silver nanofluids [17]

A common difficulty encountered in nanofluid manufacture is nanoparticles tendency to agglomerate into larger particles, which limits the benefits of the high surface area nanoparticles. To counter this tendency, particle dispersion additives are often added to the base fluid with the nanoparticles. Unfortunately, this practice can change the surface properties of the particles, and nanofluids prepared in this way may contain unacceptable levels of impurities.

» **Two-step Method:** In this process as the name suggest there are two different steps are involved. In the first step nanoparticles are synthesized and in the second step are dissolved and dispersed in some liquid medium. This method is usually applied for oxide nanofluids (“Kool-Aid” method), nanoparticles are produced by evaporation and inert-gas condensation processing, and then dispersed (mixed, including mechanical agitation and sonification) in base fluid.

All the nanofluids made by using the commercially available nanopowders come under this method. In this method, nanoparticles were first produced and then dispersed the base fluids. Generally, ultrasonic equipment is used to intensively disperse the particles and reduce the agglomeration of particles. For example, Eastman et al. [9], Lee et al. [13], and Wang et al. [14] used this method to produce Al_2O_3 nanofluids. Also, Murshed et al. [15] prepared TiO_2 suspension in water using the two-step method. Other nanoparticles reported in the literature

are gold (Au), silver (Ag), silica and carbon nano tubes. As compared to the single-step method, the two-step technique works well for oxide nanoparticles, while it is less successful with metallic particles.

Except for the use of ultrasonic equipment, some other techniques such as control of pH or addition of surface active agents, are also used to attain stability of the suspension of the nanofluids against sedimentation. These methods change the surface properties of the suspended particles and thus suppress the tendency to form particle clusters. It should be noted that the selection of surfactants should depend mainly on the properties of the solutions and particles. Xuan and Li [16] chose salt and oleic acid as the dispersant to enhance the stability of transformer oil–Cu and water–Cu nanofluids, respectively. Oleic acid and cetyltrimethylammoniumbromide (CTAB) surfactants were used by Murshed et al. [15] to ensure better stability and proper dispersion of TiO₂–water nanofluids. Sodium dodecyl sulfate (SDS) was used by Hwang et al. [18] during the preparation of water-based MWCNT nanofluids since the fibers are entangled in the aqueous suspension.

List of various types of nanoparticles and the corresponding base fluids are given in table 1.3

<i>Nanoparticle materials include</i>	<i>Base fluids include</i>
Oxide ceramics – Al ₂ O ₃ , CuO	Water
Metal carbides – SiC	Ethylene/tri-ethylene-glycols and other coolants
Nitrides – AlN, SiN	Oil and other lubricants
Metals – Al, Cu	Bio-fluids
Nonmetals – Graphite, carbon nanotubes	Polymer solutions
Layered – Al + Al ₂ O ₃ , Cu + C	Other common fluid
PCM – S/S	
Functionalized nanoparticles	

Table 1.3 [19]

1.2.3. Factors that influence the thermal conductivity enhancement

There are large numbers of factors that affects the thermal conductivity of the nanofluids which are determined and summarised from the different experimental results. These factors are as follows

- (1) Nanoparticle Volume fraction(ϕ)*
- (2) Nanoparticle material*
- (3) Nanoparticle Size*
- (4) Nanoparticle Shape*
- (5) Base fluid Material*
- (6) Operating Temperature*
- (7) Surfactant/Stabilizer*
- (8) External perturbation/excitation*

Each factor are explained below one by one

(1) Nanoparticle Volume fraction (ϕ)

The basic concept of Nanofluid originated from the very simple idea that the thermal conductivity of solid is much higher than the liquids (for example κ for Water=0.6 W/mK, Cu=400W/mK & diamond 3300W/mK) so if these are mixed then the resulting thermal conductivity will increase as predicted by Maxwell's Effective Medium Theory (EMT) [3]. Volume fraction (ϕ) is defined as the volumetric concentration of the particle present in the whole volume of the nanofluid. Particle volume fraction is the most common factor which is measured in all experiment with nanofluid and the results are almost in agreement qualitatively. The general trend is that there is an increase in the enhancement of thermal conductivity κ/κ_0 with the volume fraction or loading of the Nanoparticles, where κ and κ_0 are the thermal conductivity of the mixed phase and the base fluid.

Fig.1.3 shows the graph from reference [20] which shows the variation of the ratio of the thermal conductivities w.r.t volume fraction for all types of nanofluids like oxide, metal, carbon nanotubes also showing the value obtained theoretically from the Hamilton- Crosser model.

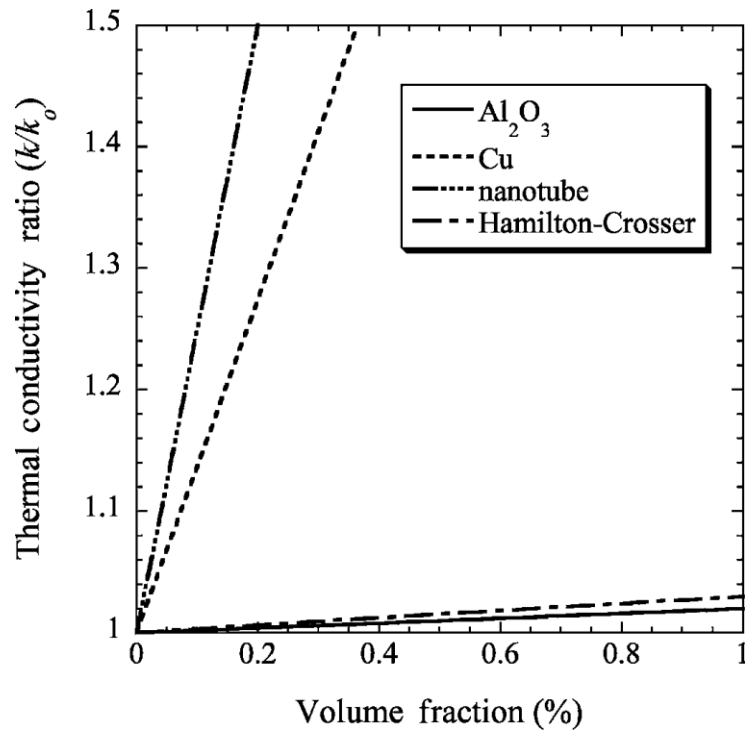


Fig.1.3 Thermal conductivity enhancement ratios of the nanofluids as a function of nanoparticle loading. [20]

Same results were obtained with other material particles with similar sizes. This parameter seems to be the same for all the other observations and results. The same is not true for the other parameters as we will show. The same result i.e linear dependence is obtained by us in our experiment with ZnO Nanofluid with Ethanol as a base fluid in our lab.

(2) Nanoparticle Size

The size of the nanoparticle is an important factor determining the thermal conductivity of the nanofluid. The general trend in the experimental data is that the thermal conductivity of nanofluids increases with decreasing particle size [21]

This trend is theoretically supported by two mechanisms of thermal conductivity enhancement; Brownian motion of nanoparticles & liquid layering around nanoparticles.

Fig 1.4 shows the graph from reference [21] which shows the variation of the ratio of thermal conductivity w.r.t particle size.

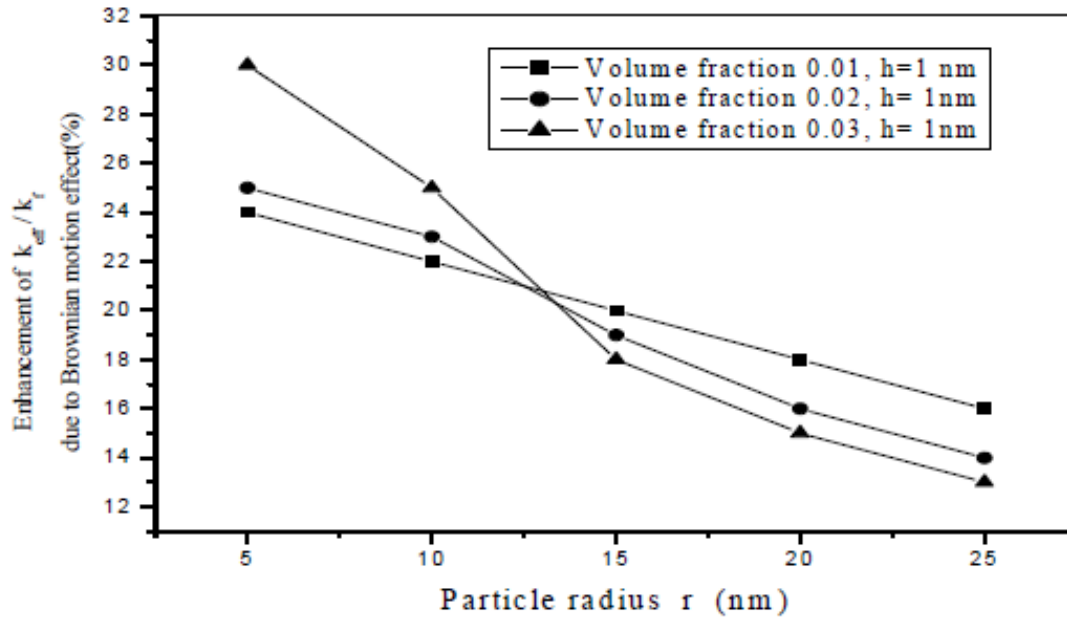


Fig.1.4 Thermal conductivity enhancement of the nanofluids as a function of size of NP

As the particle size is decreased the Brownian/ random motion becomes larger and it results in the increase of the convection effect. The larger the convection larger is the thermal conductivity [22]. Although Brownian motion cannot solely/directly result in an enhancement of the thermal transport properties, it could have an important indirect role in producing particle clustering, which as described below, could significantly enhance thermal conductivity.

This size dependent behaviour makes Nanofluid more promising for practical application than ever.

(3) Nanoparticle Material

The thermal conductivity ratio is observed to increase faster for metal than oxide nanoparticles. Fig 1.5 shows the graph from reference [23] shows the variation of the ratio of thermal conductivity w.r.t particle material.

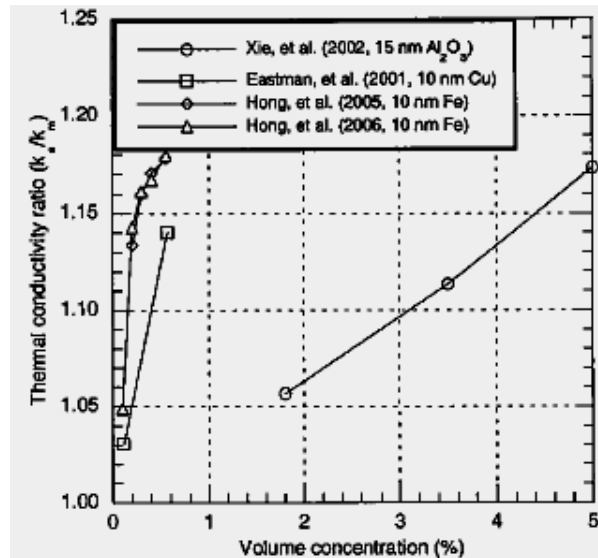


Fig.1.5. Thermal conductivity enhancement of the nanofluids as a function of NP material

Later on it was found that the effect of particle material is much more pronounced when CNTs are used in nanofluids. Choi et al.[23] shows that 1 vol. % of MWCNT (dia=25nm,length=50 μ m) immersed in poly oil shows an enhancement in thermal conductivity by 160% which is very large.

They said that this anomalous enhancement can be explained by the formation of the liquid nanolayer around the nanotube, which acts like a solid layer and helps in conduction of heat to the neighbouring tubes. Also the shape effect has a major role to play in this enhancement as the length is much larger so transfer can takes place to a larger length which is absent in spherical nanoparticles if there is no clustering.

(4) Nanoparticle Shape

Enhancement in thermal conductivity is compared with the geometrical shape of the nanoparticles. It was found that the nanoparticles with elongated and extended shapes have more thermal conductivity than spherical nanoparticles. The comparison shown in the fig.1.6 which shows the graph from reference [20] clearly indicates that, nanofluid with SiC nanoparticles (dia.=26nm) have less thermal conductivity than the nanofluid with SiC cylinders (dia.=600nm). This is due to the mesh like structure formed by the elongated nanoparticles and that assist in faster transfer of heat through them. The length of the nanotubes is on the order of micrometers, and this enables rapid heat conduction across relatively large distances, which is not possible for spherical nanoparticles as long as there is no clustering. But the synthesis of spherical particles is much easier than the cylindrical structures and they are widely available commercially also. But there is another factor which should be noted that in case of cylindrical particles viscosity of the nanofluid is usually very high in comparison to the spherical particles [24] consequently there should be an increase in the pumping power and this aspect reduces the feasibility of using nanofluids with cylindrical particles in heat transfer application.

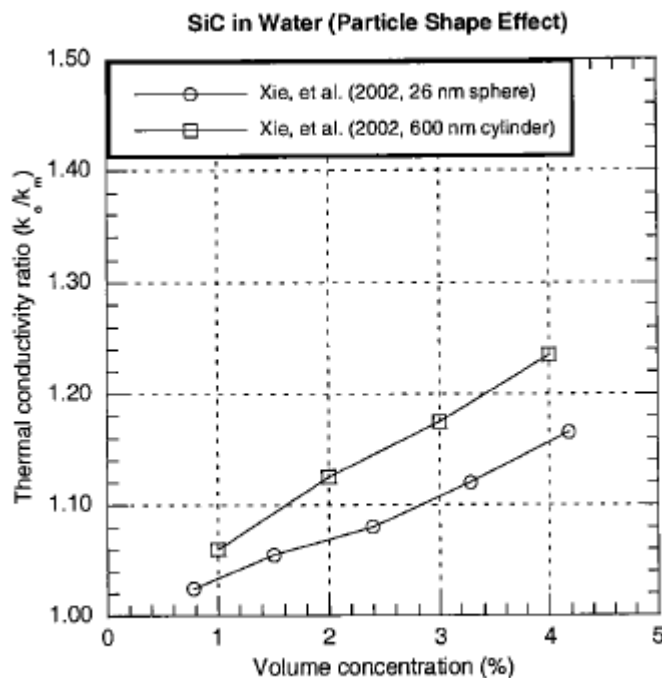


Fig.1.6 Thermal conductivity enhancement ratios of nanofluids as a function of shape of NP

(5) Base fluid Material

From the Maxwell's EMT theory we get that with the increase of the thermal conductivity of the base fluid there is a decrease in the thermal conductivity of the mixture. Experimentally it is also established that the relation between the enhanced thermal conductivity ratios of the nanofluids and the thermal conductivities of the base fluids [25] as shown in fig.1.7 which shows the graph from reference [25]. It is clearly seen that no matter what kind of nanoparticle was used, the thermal conductivity enhancement decreases with an increase in the thermal conductivity of the base fluid. If the viscosity of the base fluid is high then there will be a decrease in the mobility of the nanoparticles resulting in the decrease of the thermal conductivity

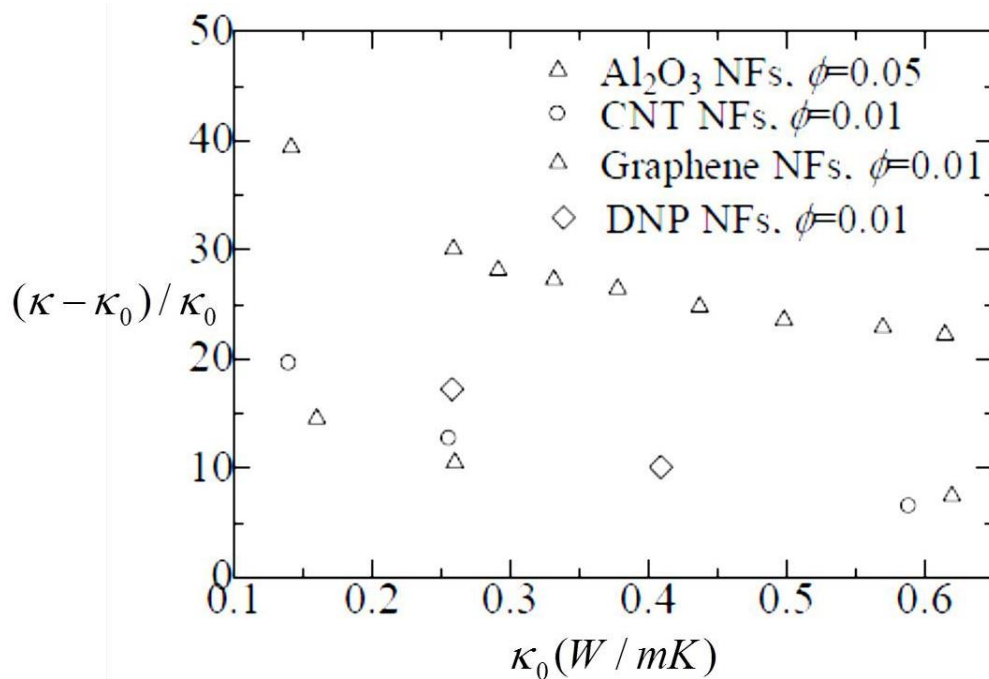


Fig.1.7 Thermal conductivity enhancement ratios of nanofluids as a function of the thermal conductivity of the basefluids.

There is also a study by Lee [26] on the effect of Electric Double Layer (EDL) (forming on the nanoparticles) and found that thermal conductivity and thickness of the EDL depends on the fluid material.

In the previous study Wang et. Al [14] used Al_2O_3 and CuO nanoparticles were used to form nanofluids with different base fluids ranging from Water, Ethylene Glycol (EG), Vacuum pump oil and engine oil. The highest thermal conductivity ratio was observed when EG was used as the base fluid. Engine oil showed somewhat lower thermal conductivity ratios than EG. Water and pump fluid showed even smaller ratios, respectively.

In the case of Carbon NanoTubes (CNT) the dependency on the base fluid is observed to be least. No matter what kind of base fluid is used, the thermal conductivity enhancement of CNT nanofluids is much higher than that for Al_2O_3 nanoparticle suspensions [27] at the same volume fraction. The reason behind this large difference in thermal conductivity is the substantial difference in thermal conductivity and morphology between alumina nanoparticle and carbon nanotube.

(6) Operating Temperature

In conventional microfluids the dependence of the thermal conductivity on operative temperature is only due to the dependence of the constituting part's thermal conductivity on the temperature. With the case of nanofluids various other factors emerges like clustering and Brownian motion of the nanoparticles which results in the dramatic change in the thermal conductivity with temperature.

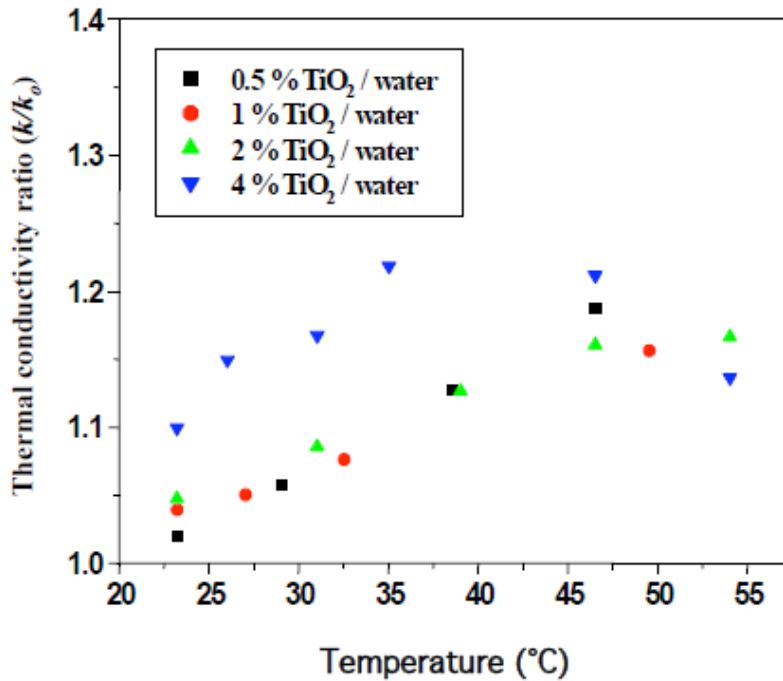


Fig.1.8. Thermal conductivity ratio of nanofluids as a function of the operating temperature.

In general it is found that at low temperature there is a linear relationship between temperature rise and increase in thermal conductivity [19] and after certain temperature there is a decrease in the thermal conductivity as shown in the Fig.1.8 which shows the graph from reference [19]. May be at higher temperature there is an increase in the tendency of the agglomeration of the nanoparticle and consequently settling down of these agglomerate and hence causing a decrease in the thermal conductivity of the nanofluids.

(7) Surfactant/Stabiliser

Stability of the nanofluid is a very important factor in deciding the thermal conductivity. If the nanofluid is not stable then the nanoparticles will show a tendency to get agglomerated and form a cluster and after certain limit it gets saturated. Tae-Keun et.al [28] investigated on the dispersion dependence of the thermal conductivity of nanofluids.

Another observation on the effect of the stability of the nanofluid was done by Eastman as shown in fig.1.9 which shows the graph from reference [29]. Freshly prepared Cu nanofluid shows more enhancement than the older one. This is because in the freshly prepared nanofluids, nanoparticles are well dispersed.

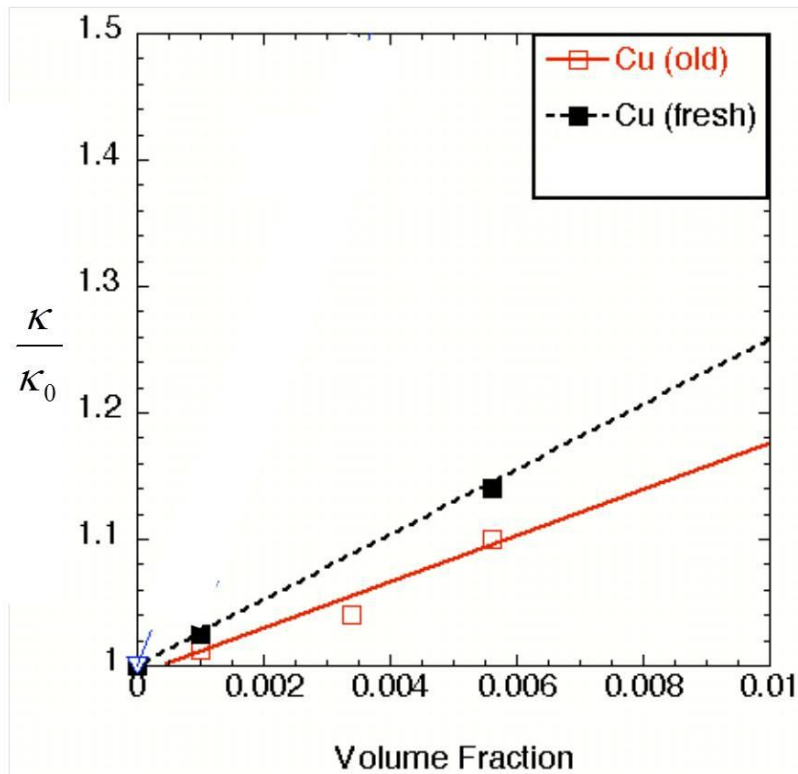


Fig.1.9. Thermal conductivity enhancement ratios of the nanofluids as a function of vol. fraction wrt stability of the Cu nanofluid.

(8) External Perturbation/Excitation effect

So far we have discussed about the dependence of the thermal conductivity of nanofluid on the structural factor, volume fraction, temperature, time etc. All these measurements were done in static condition but there is very few report of work that shows the dependence of thermal parameters of the nanofluid submitted to the action of an external excitation i.e. in dynamic condition.

A dynamic measurement in this aspect is very important in the sense that it gives more insight in to the system. It can give an idea of the time scale (so length scale also) of agglomeration of the nanoparticles. This is a very important aspect which will throw light on understanding thermal transport behaviour of nanofluids fundamentally, which is needed for developing a new generation of highly efficient heat transfer fluids. So we also tried to explore this aspect of nanofluids and shed some light for understanding its thermal behaviour.

It is now well-known that nanoparticles dispersed in a solvent can easily be manipulated by external forces which bring them into non equilibrium situations in a controllable manner

[30]. They question on the possibility of enhancing the heat transport coefficient of a nanofluid from external actuations.

One of the simplest ways to generate such a force field can be achieved by focusing a laser beam with an appropriate wavelength on the colloidal suspension which provides a momentum to the nanoparticles. Another simple way of excitation is applying an oscillating force field like Electric field, Magnetic field etc. There is some report of simulation work in this direction, one of such work is done by Cle´ment Le Goff et.al.[31]. In this work they study to what extent the motion of nanoparticles, respond to the action of an external oscillating force field, and affect the thermal conductivity of nanofluids. A temperature gradient is established through the solvent and an oscillating force field is applied in the same direction and then in the opposite direction. Using the non equilibrium molecular dynamics (NEMD) simulation technique they calculated the thermal conductivity of fluid in the direction of force field and in the transversal direction also. For periodic excitations in the radio frequency and microwave ranges, they showed that the thermal conductivity of nanofluid can be enhanced. From this they identify the best frequency conditions to enhance heat transport in nanofluids and examine whether the thermal conductivity of nanofluids can be carried out without clustering in presence of external forces.

This enhancement has been closely related to the hydrodynamic behaviour of fluid. After applying the external excitation the fluid is collectively driven by the motion of nanoparticles they showed that the thermal conductivity of nanofluid can be strongly enhanced both in the direction of force field and in the transversal direction.

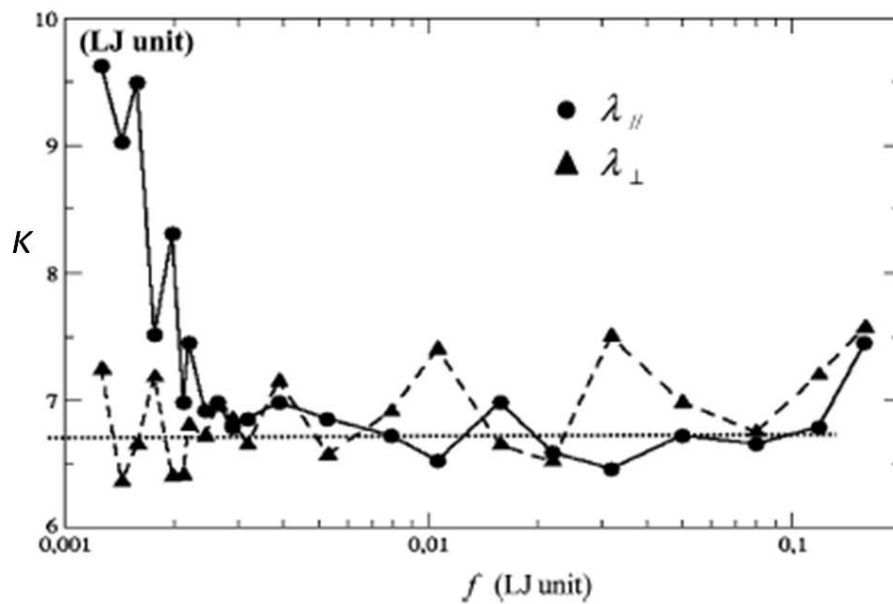


Fig.1.10. Thermal conductivity of nanofluid in a LJ fluid in the direction parallel and perpendicular to the excitation. The dashed horizontal line stands for the thermal conductivity of nanofluid without excitation.

From fig.1.10 shows the graph from reference [31] it is clear that there is a large enhancement in the thermal conductivity at the frequency end and as the frequency is increased there is a reduction in it.

They also showed interesting results in all simulations they have performed with an oscillating force in the radio frequency and microwave ranges is the absence of cluster formation. This result is radically different to what they have already observed [32, 33] in presence of steady force fields and allow to avoid the negative effects of clogging in nanofluidic devices. With an oscillating force field, they found that during a half period of the force many nanoparticles tend to stick together. However, they have noticed that these particles separate as soon as the sign of the force changes.

Recently there is a report of 4 to 5 times enhancement in thermal conductivity of the magnetic Nanofluid than that of the base fluid [34] in an applied magnetic field. The nanofluid used was a stable colloidal suspension of magnetite (Fe_3O_4) nanoparticles of average diameter 6.7 nm, coated with oleic acid and dispersed in kerosene. Here they used external magnetic field as an excitation. Their experimental result is shown in fig.1.11 shows the graph from reference [34].

For a particle loading of 0.65–1.71 vol%, the enhancement of thermal conductivity was drastic when the magnetic field strength was above 12.6 mT. As the external magnetic field strength increased to 44.1 mT, the thermal conductivity ratio increased from 1.33 to 2.25. The highest enhancement of thermal conductivity observed for 1.71 vol% of particles was 125%. In the case of 4.9 and 6.3 vol%, the thermal conductivity started to increase drastically at very low magnetic fields. The highest value of enhancement in thermal conductivity for 6.3 vol% of Fe_3O_4 was 300 ($k/k_f = 4$). A drop in the thermal conductivity was observed above 8.2 and 16.0 mT respectively for 6.3 and 4.9 vol% of nanoparticles.

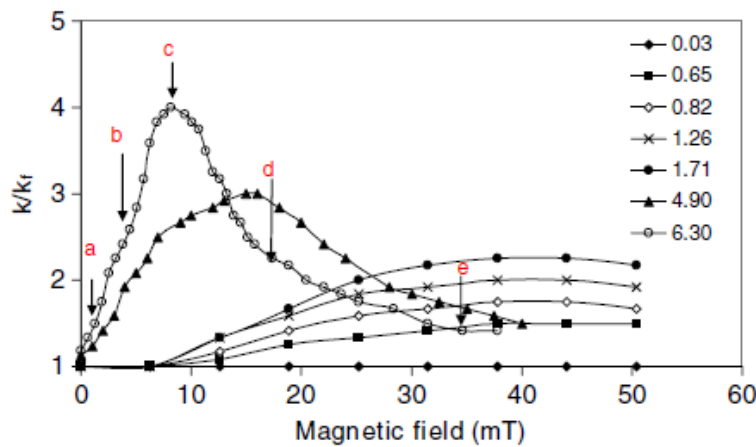


Fig.1.11. The thermal conductivity ratio (k/k_f) in the presence of an external magnetic field, parallel to the temperature gradient, at different volume fractions (ϕ) of Fe_3O_4 .

This results shows that there is a switchable transfer of alignment in the arrangement in the nanoparticle as shown in fig.1.12 taken from reference [34].

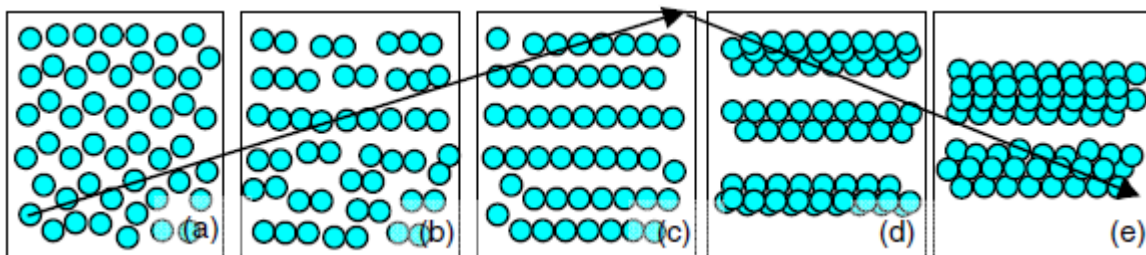


Fig.1.12. A schematic of the chain-like structures formed in the fluid at different magnetic fields. The arrow shows the increasing and decreasing trend of thermal conductivity.

This is an important observation as it provides experimental proof of the dynamic aspect of the thermal conductivity in which it varies with the frequency of the applied excitation force. So we have discussed the different properties and parametric dependence of Nanofluid. There are many issues which are to be addressed before commercial application like problems of

nanoparticles agglomeration, settling, and erosion potential. Nanofluids used in experimental research need to be well characterized with respect to particle size, size distribution, and shape in order to make the results most useful.

The results were presented and discussed in this study using results from multiple research groups as verification. Some parametric trends still require substantiation, and the use of additives has barely been addressed.

The results to date are not sufficient to identify all the trends and magnitudes in nanofluid heat transfer enhancement. More experiments have to be done in order to understand underlying mechanism of such superior as well as anomalous behaviour of the nanofluids.

1.2.4 Review on 3ω technique

The 3ω method is a dynamic method of measuring the specific heat C_p and thermal conductivity (κ) of a material. It is an accurate method of measuring these properties. The 3ω method uses a simple heater geometry, whose behaviour can be solved from the heat diffusion equation [35]. The heater is excited at a frequency of ω , this excitation produces temperature fluctuations in the material at a frequency of 2ω . The thermal excitation at 2ω mixes with the applied voltage at ω through dR/dT term and produces frequencies at 3ω and difference frequency response at ω . The response at 3ω is used for the determination of the thermal properties of the samples. In this method the heater is used simultaneously as a heater and a thermometer, so no additional probes are required to carry out the measurement.

The history of the development of this method was very old. The idea of this transient measurement was first conceived by Corbino in 1911. It was he who first proposed that the 3rd harmonic of output voltage from the sample can be relate to its thermal properties. From this idea the study of the time-dependent or frequency dependence of linear response of materials was started. It forms a very important part of condensed matter physics. It provides a very powerful tool to explore the slow/fast dynamics of different systems in condensed matter physics.

There are various type of susceptibilities like dielectric the magnetic susceptibility, the dynamic structure factor (accessible by neutron scattering). In contrast to these dynamic susceptibilities, thermal variables such as the specific heat C_p were considered to be static and well-defined only for systems in equilibrium. However, it has been shown that, dynamic frequency dependence of C_p in some special type of materials like Glassy or super cooled material. In such material specific heat shows dispersive behaviour i.e $C_p(\omega)$ [36]. Any system, that may have a slow relaxing component and has a substantial energy associated with it can have ω dependent C_p .

The concept of a time or frequency dependent specific heat arises in systems where a subset of the degrees of freedom (DOF) (for example localized modes) couple weakly to the predominant modes which are mainly responsible for heat conduction. Dilute Molecular gas is an example where the vibrational or rotational DOF of the molecules couple weakly to sound waves [37]. A more subtle situation is the case where the coupling is not necessarily weak, but where some of the degrees of freedom have a long relaxation time compared to the dominant modes. An example of this type of system is a supercooled liquid near the glass transition [38]. Here the heat-carrying modes are the small-amplitude molecular vibrations that will become the phonons in the glassy state. The slow degrees of freedom are molecular rearrangements, which relax on ever longer timescales as the glass transition is approached on cooling. This separation of molecular motions into these two classes is not obvious on a microscopic scale; nevertheless, a supercooled liquid exhibits the separation clearly in a measurement of its time-dependent specific heat. The first observation of slow time dependence in the enthalpy absorbed or released by a supercooled liquid was made 60 years ago [39].

A treatment of the frequency-dependent specific heat as a linear-response susceptibility – on the same footing as other dynamic susceptibilities - awaited the work of Birge and Nagel [40-

42] and of Christensen [43] in 1985. Christensen used the adiabatic technique of specific heat measurement; hence his measurements were limited to a narrow frequency range.

The technique used by Birge and Nagel, called ‘specific heat spectroscopy’ (SHS), relies on one dimensional heat diffusion from a planar heater as well as the sample thermometer. Birge and Nagel exploited the fact that the heat diffusion equation maintains its simple form in the frequency domain, even if the specific heat is frequency-dependent. With this method, they achieved a frequency range of 5 decades.

A drawback of the original technique is that it measured only the product of the specific heat and thermal conductivity [44]. Since then, the technique has been enhanced and the frequency range extended by Dixon and Nagel [45] and by Menon [46]. Similar data as that obtained from frequency dependent measurement have been obtained from time dependent measurement by Rajeshwari & Raychaudhuri [47].

For measurements of thermal conductivity, if a steady state conduction method is used, errors can be introduced by the parasitic heat flow through the substrate and by radiation losses from the test sample. If the thermal conductivity of the substrate is relatively high, then the total heat flow through the substrate will be large compared to the heat flow through the superlattice and subtraction of the substrate’s contribution to heat conduction will significantly magnify measurement errors. If the thermal conductivity of the substrate is low, then radiation losses from the surface will dominate the heat flow through the test sample and the uncertainties of the radiative behavior will complicate the measurement of the thermal conductivity of the superlattice when measurements are made at room temperature or above.

It was also determined by Cahill that the effect of black-body radiation produced less than 10% error in the measurement at 1000K and that this error was proportional to T^3 , quickly becoming insignificant at lower temperatures [48]. The 3ω method has been used to produce a number of significant measurement results, which have been published in the literature [35], [48-49].

Although the 3ω method is extensively used for thermal conductivity measurement, the formulas generally used are based on the zero heater-thickness approximation. It is therefore necessary to provide a complete analysis of the problem to determine the limits of its applicability. Experimental details and the limits of 3ω methods are discussed in details in chapter 2.

1.3 Importance

The measurement of thermal parameters like thermal conductivity, specific heat etc. is important because it is necessary to study the properties of newly developed materials and determine what contribution they may be able to provide to the advancement of technology. Once new materials are discovered and characterized, they can be developed and adapted into systems which can provide an improvement in the performance over existing technology. For example, with the development of carbon nanotubes and the discovery that they possess very high values of thermal conductivity, the concept was put forward of using carbon nanotubes as an enhanced thermal interface material. The improved thermal interface performance provided by carbon nanotubes is significantly better than commercially available thermal greases and other thermal interface methods. This improved thermal interface can be used to aid with power dissipation in high performance computer processors, as the newly developed processors are steadily making greater and greater demands on cooling technology [47].

We also synthesised the samples that are used for measurement. A novel Au nanonetwork structure was synthesised in which the individual nanoparticles are attached with each other forming a network structure.

1.4 Motivation and major issues addressed in the thesis

We all know that nanofluids are a class of materials which show enhancement in the thermal conductivity values that are much higher than that obtained theoretically from the Effective Medium Theory (EMT). These observations are made in static condition. There are scanty reports on what will happen to the thermal conductivity values when we apply an external perturbation or excitation (like a.c electric field) to it i.e in dynamic thermal condition. In this regard some simulation work was reported in 2008 [31], in which they apply an electric field to the nanofluid and found an enhancement in the thermal conductivity at low frequency.

Our major issue in this thesis work is to address a very basic question: *whether such anomalous enhanced heat transport in nanofluid systems has any time/frequency dependence associated with them or not.*

Reasons for such curiosity is that one of the likely models for such type of anomalous enhancement in thermal conductivity of nanofluid suggests that local aggregation [50] of nanoparticles can enhance local thermal transport. We argue that local aggregation will have

a length scale associated with it and heat diffusion thus will get a time scale that will reflect the thermalization time of the aggregated region [51]. In this thesis we also make materials which have longer scale of aggregation than that allowed by thermal effects, these are networked nanofluids. Enhancement of thermal properties in such networked nanofluids has been observed.

1.5 Structure of the thesis:

The thesis has been presented in such a way that it starts with the following chapters:

The **1st Chapter** covers the literature review of the Nanofluids with their allied properties and also review of the 3ω technique which is used to carry out the thermal measurements.

The **2nd Chapter** gives a detail description of the method used to carry out the dynamic thermal measurement. During thesis it was set up from the scratch and developments of its different parts like fabrication of heater/thermometer are described. We also describe its calibration with standard materials.

The **3rd Chapter** gives a description of different samples (which are nanofluids) and interesting Au nanonetwork structure, from its synthesis to characterisations. Discussions of the different techniques which are employed for the characterisation in this work.

The **4th Chapter** covers Heat Transport Measurement in ZnO nanofluid and discuss the basic interesting results which we get from the experiment. In this chapter we show that the thermal transport parameters can have frequency dependence.

The **5th Chapter** covers Heat Transport Measurement in capped ZnO (with PVP) nanofluid and discuss the results and conclusions. The main result here is that we show that by capping the nanoparticles in the fluid, the frequency dependence of thermal parameters can be controlled.

The **6th Chapter** covers the measurement on metal nanofluids like Ag, Au etc. In particular we work with a novel Au nanonetwork structure.

The Last **Chapter** gives summary and conclusions of this thesis.

It also involves a discussion of the achievements of the thesis and the future challenges.

References

- [1] D.G Cahill and R.O.Pohl, Phys.Rev.B 35, 4067 (1987)
- [2] N.O. Birge, S.R. Nagel, Rev. Sci. Instrum. 58, 1464 (1987)
- [3] J.C. Maxwell, A Treatise on Electricity and Magnetism, second ed., Clarendon Press, Oxford, UK, 1881.
- [4] S.U.S. Choi, Enhancing thermal conductivity of fluids with nanoparticles, Developments & Applications of Non-Newtonian Flows, FED-vol.231/MD-vol. 66, pp. 99, 1995
- [5] P. Keblinski, J.A. Eastman, D.G. Cahill, Nanofluids for thermal transport, Materials Today 8 (6), 36, 2005
- [6] U.S. Choi and J.A. Eastman, "Enhanced Heat Transfer Using Nanofluids," U.S. Patent #6,221,275
- [7] H. Akoh, Y. Tsukasaki, S. Yatsuya, A. Tasaki, Journal of Crystal Growth 45, 495, (1978)
- [8] M. Wagener, B.S. Murty, B. Gunther, S. Komarnenl, J.C. Parker, H.J. Wollenberger (Eds.), Nanocrystalline and Nanocomposite Materials II, vol. 457, Materials Research Society, Pittsburgh, PA, pp. 149, 1997
- [9] J.A. Eastman, U.S. Choi, S. Li, L.J. Thompson, S. Lee, vol. 457, Materials Research Society, Pittsburgh, PA, USA, Boston, MA, USA, pp. 3, 1997
- [10] H. Zhu, Y. Lin, Y. Yin, Journal of Colloid and Interface Science 227, 100, 2004
- [11] C.-H. Lo, T.-T. Tsung, L.-C. Chen, Journal of Crystal Growth 277,1-4, 636, 2005
- [12] C.-H. Lo, T.-T. Tsung, L.-C. Chen, Fluids and Thermal Engineering 48, 4, 750, 2006

- [13] S. Lee, S.U.S. Choi, S. Li, J.A. Eastman, *Journal of Heat Transfer* 121, 280, 1999
- [14] X. Wang, X. Xu, S. Choi, *Journal of Thermophysics and Heat Transfer* 13, 4, 480, 1999
- [15] S.M.S. Murshed, K.C. Leong, C. Yang, *Journal of Thermal Sciences* 44, 4, 367, 2005
- [16] Y. Xuan, Q. Li, *International Journal of Heat and Fluid Transfer* 21, 58, 2000
- [17] *Optics and Lasers in Engineering* 45, 1099, 2007
- [18] Y.J. Hwang, Y.C. Ahn, H.S. Shin, C.G. Lee, G.T. Kim, H.S. Park, J.K. Lee, *Current Applied Physics*, vol.6, 242, 2006
- [19] *Mechanisms of Enhanced Heat Transfer in Nanofluids* by J.A. Eastman, *Fluctuations & Noise in Out of Equilibrium Systems*, Sept 14-16, 2005
- [20] J.A. Eastman, S.R. Phillpot, S. Choi, P. Keblinski, *Annu. Rev. Mater. Res.* 34, 219, 2004
- [21] P.C. Mukesh Kumar et. al., *International Journal of Engineering Science and Technology* Vol. 2(7), 2846, 2010
- [22] Seok Pil Jang and Stephen U. S. Choi, *APL* vol. 84, 21, 2004
- [23] Choi, S.U.S., Zhang, Z.G., Yu, W., Lockwood, F.E., and Grulke, E.A., *Appl. Phys. Lett.* 79(14). Pp. 2252, 2001
- [24] Timofeeva, E.V., Routbort, J.L., and Singh, D., *J.A.P.*, 106(1), 2009
- [25] Xie et al. *Nanoscale Research Letters*, 6:124, 2011
- [26] Lee, D., *Langmuir*, 23(11), pp. 6011, 2007
- [27] Xie H, Lee H, Youn W, Choi M, *J Appl Phys*, 94:4971, 2003
- [28] Tae-Keun Hong and Ho-Soon Yang *Journal of the Korean Physical Society*, Vol. 47, , S321, September 2005
- [29] J.A. Eastman et al., *Appl. Phys. Lett.*, 78, 718, 2001

- [30] Ashkin A, Dziedzic JM, Bjorkholm JE, Chu S (1986) *Opt Lett* 11:288–290. See also Ben-Abdallah P, Ould El Moctar A, Ni B, Aubry N, Singh PJ (2006) & *J Appl Phys* 99:094303 and refs. Therein
- [31] Cle´ment Le Goff, Philippe Ben-Abdallah, Gilberto Domingues, Ahmed Ould El Moctar *J Nanopart Res*, 10, 1115, 2008
- [32] Ben-Abdallah P (2006a) *Appl Phys Lett* 89:113117
- [33] Ben-Abdallah P (2006b) *Phys Rev E* 74:041407
- [34] John Philip¹, P D Shima and Baldev Raj, *Nanotechnology* **19**, 305706, 2008
- [35] R. Venkatasubramanian, The American Physical Society, 2000
- [36] T. Christensen, *Journal De Physique*, C8-635, 1985
- [37] K.F. Herzfeld and T.A. Litivitz, Academic Press, New York and London, 1959
- [38] For a review of the phenomenology of glasses, see J. Wohlg and C.A. Angell, *Glass: Structure by Spectroscopy* (Dekker, New York, 1976). A more recent review is given by M.D.Ediger, C.A. Angell and S.R. Nagel, *J. Phys. Chem.* 100, 13200, 1996
- [39] P.G. Oblad and R.F. Newton, *J. Am. Chem. Sec.*, 59, 2495, 1937
- [40] N.O. Birge and S.R. Nagel, *Phys. Rev. Lett.*, 54, 2674, 1985
- [41] N.O. Birge, *Phys. Rev. B*, 34, 1631, 1986
- [42] N.O. Birge and S.R. Nagel, *Rev. Sci. Instrum.*, 58, 1464, 1987
- [43] T. Christensen, *J. Phys. (Paris)*, 46, C8-635, 1985
- [44] Efforts by Birge (ref. 6) to separate the thermal conductivity from the specific heat by combining the data from a planar heater with those from a second experiment using a wire geometry were not successful in the temperature range where the specific heat was frequency-dependent.
- [45] P.K. Dixon and S.R. Nagel, *Phys. Rev. Lett.*, 61, 341, 1988
- [46] N. Menon, *J. Chem. Phys.*, 105, 5246, 1996

[47] M. Rajeswari and A. K. Raychaudhuri, *Europhys. Lett.* 10 153, 1989

[48] D.G. Cahill, American Institute of Physics, 1990

[49] N.O. Birge, S.R. Nagel, American Institute of Physics, 1987

[50] R.Prasher et.al. *Nano Letters*, Vol. 6, No. 7, 1529, 2006

[51] R.K.Neogy, A.K.Raychaudhuri, *Nanotechnology* 20, 305706, 2009

Chapter 2

Chapter 2: Experimental Techniques

2.1 Introduction	40
2.2 3ω Technique	40
2.2.1 Theory.....	40-43
2.2.2 Electronics.....	43-44
2.2.3 Experimental Setup Details.....	44-45
2.2.3.1 Heater/Thermometer.....	46
2.2.3.1.1 Heater Material.....	47-48
2.2.3.1.2 Heater Fabrication.....	49-52
2.2.3.1.3 Electrical Characterisation.....	53-55
2.2.3.1.4 Thickness Characterisation.....	55-60
2.2.3.2 Sample and heater holder.....	60-62
2.2.3.3 Wheatstone Bridge.....	63-65
2.2.3.4 Lock In Amplifier (LIA).....	65-68
2.2.3.5 Temperature Controller.....	68
2.2.3.6 Decade Resistance Box.....	69
2.2.3.7 CPU Interfacing (GPIB,C++)	69-71
2.2.4 Sources of possible error and its correction.....	71
2.2.4.1 Size Distribution of nanoparticles.....	72
2.2.4.2 Convective current in the liquids.....	73
2.2.4.3 Agglomeration of nanoparticles.....	74
2.2.4.4 Grounding of the setup.....	74
2.2.4.5 Instrumental error.....	75
2.2.5 Conclusion.....	76
Reference	

2.1 Introduction

Establishment of the dynamic thermal measurement using 3ω detection technique is an important component of the thesis. Though it is a known technique, it has not been used so much in the context of nanofluids. We have employed this technique for the dynamic measurement of the thermal conductivity of the nanofluid which is first of its kind and not reported earlier. Below we describe the basis of the technique by its working principal and then its realisation as has been done in this thesis.

2.2 3ω Technique

3ω technique is the main/central technique in the thesis work. This is very old technique which was first conceived by Corbino in 1911. We employed this to find the thermal conductivity. So we will discuss this in details like theory, its different parts required for measurement. Then we characterise/ standardise this method with some known samples.

2.2.1 Theory

The 3ω method [1] is based on heat diffusion from a thin heater which is producing a heat flux that is sinusoidal in time and is immersed in a bath of the liquid sample to be studied. If the heater has a simple geometry, such as a plane or a wire, then the temperature oscillations at the heater itself will be simply related to the thermal properties of the surrounding liquid. With this technique frequency limit is determined by the width and thickness of the heater thermometer itself. When the heater is a film on a substrate the thermal parameters of the substrate also contributes to the response of the oscillating heater. One needs to properly subtract out the substrate contribution to extract the numbers for the liquid. This is described later on.

To start, we use the situation of a free standing heater of resistance R (shown in fig.2.1) and we pass a sinusoidal current through it

$$I = I_0 \cos \omega t \quad \text{where } \omega (=2\pi f) \text{ angular frequency}$$



Fig.2.1 Thin film through which sinusoidal current is passing

This flowing current cause a resistive heating in the film due to the power dissipation in it and it is given by the following equation eqn.2.1

$$P = I_0^2 R * \cos^2 \omega t = \frac{1}{2} I_0^2 R * (1 + \cos 2\omega t) \quad [2.1]$$

All the following stages of the process are depicted in the fig.2.2

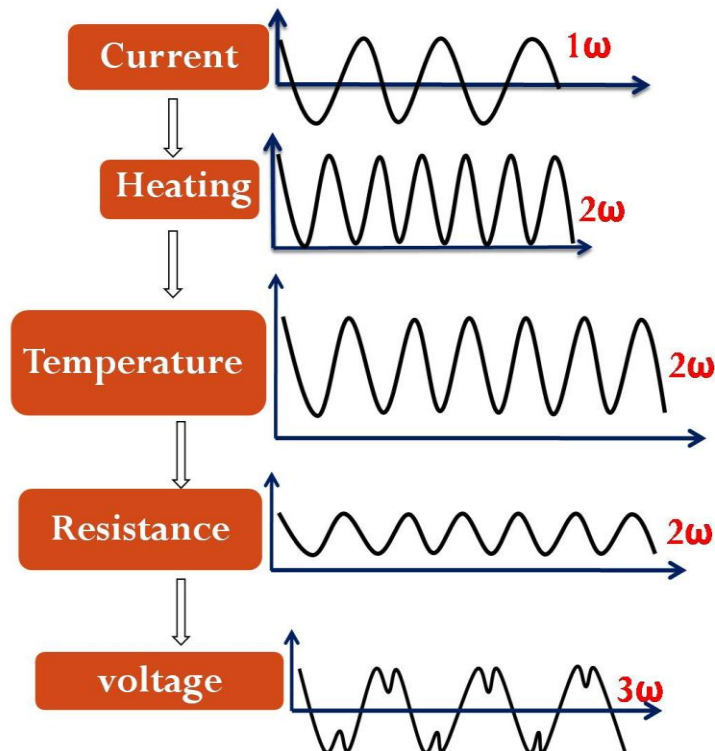


Fig.2.2 Pictorial description of the 3ω method. [2]

» From eqn.2.1 **power** oscillates at twice the frequency of the applied voltage i, e 2ω

» This oscillating power also causes a modulation in the temperature of the film and oscillates at an angular frequency 2ω .

The temperature can be written as $\delta T = T_\omega \cos(2\omega t - \phi)$

where ϕ = phase lag between temperature and resistance

Now this fluctuating temperature can be related to the resistance of the film via the eqn given below

$$R(t) = R_0 + R_\omega \quad \text{where} \quad R_\omega = \alpha R_0 T_\omega$$

Where α is the temperature coeff. of resistance and given by $\alpha = \frac{1}{R} \frac{dR}{dT}$

Therefore resulting voltage (V) across the film is given by the product of the current $I(\omega)$ and resistance $R(2\omega)$.

$$V = I(\omega)R(2\omega) = I_0 R_0 \cos \omega t [1 + \alpha T_\omega \cos(2\omega t - \phi)]$$

After simplification using cosine formulae we get the expression in eqn.2.2

$$V = I_0 R_0 \cos \omega t + \frac{1}{2} I_0 R_0 [\alpha T_\omega \cos(\omega t - \phi)] + \frac{1}{2} I_0 R_0 [\alpha T_\omega \cos(3\omega t - \phi)] \quad [2.2]$$

If we separate the terms as function of angular frequency ω we get the final expression as eqn.(2.3)

$$V = V_\omega \cos(\omega t - \phi') + V_{3\omega} \cos(3\omega t - \phi) \quad [2.3]$$

Thus V_ω is the sum of the $I_0 R_0$ plus a small contribution from the Mixing of I_0 and R_ω . This voltage at first harmonics causes d.c power dissipation at the heater and sets up a static temperature gradient in the cell. We have calculated the average temperature change introduced by dc power in the cell is about 0.5 K over the set temperature of the cell.

$V_{3\omega}$ on the other hand, is exactly equal to $\frac{1}{2} I_0 R_\omega$ which is proportional to T_ω , the temperature oscillation of the heater. Thus third harmonic of the output voltage across the film purely contains information about the thermal properties of the sample under investigation.

After determining the phase and magnitude of the $V_{3\omega}$ we define the normalized value of it as

$$Z = \frac{|V_{3\omega}|}{|V_{\omega}|} \quad [2.4]$$

We can connect this quantity directly to the thermal properties of the substrate (Z_S) on which the film is deposited and further to the liquid (Z_L) in which it is submerged via the eqn.2.5 [3] details are discussed in 4th chapter.

$$Z e^{i\phi} = \frac{2area}{\alpha^*power} \sqrt{2\pi f} V_{heater} (3\omega) = \frac{e^{-i\pi/4}}{(\sqrt{(C_p\kappa)_S} + \sqrt{(C_p\kappa)_L})} \quad [2.5]$$

Simple calculation gives the final $C_p\kappa$ of the sample as given by the eqn.2.6.

$$(C_p\kappa)_L = \left[\frac{Z_S - Z_L}{Z_L} \right]^2 (C_p\kappa)_S \quad [2.6]$$

where C_p stand for specific heat and κ for thermal conductivity.

In short we can say that a sinusoidal current at frequency ω leads to Joule heating with a 2ω component. The magnitude and phase of the resulting temperature rise at 2ω depend on Z . Due to the temperature coefficient of resistivity α ; the electrical resistance of the heater also contains a modulation at 2ω . Finally, the current at ω mixes with the resistance at 2ω leading to a voltage signal at 3ω . This third harmonics contains the thermal information of the surrounding liquids by using the eqn. (2.5). Thus in this straight forward way 3ω technique is used for finding thermal parameters.

2.2.2 Electronics

A schematic diagram of the electronics involved in the experiment is shown in fig.2.3.

The 3ω signal from the Platinum heater is very small ($\sim\mu V$) as compared to the voltage applied at ω ($\sim V$). In this method the primary voltage acts as an out of phase signal for the system so in order to extract out $V_{3\omega}$ signal from this large out of phase signal, the heater is placed in one of the four arm of the bridge so that signals at ω can be eliminated from the system.

Bridge balancing helps to reduce V_{ω} as much as possible so that the ratio $V_{\omega}/V_{3\omega}$ is well within the dynamic reserve of the Lock-in amplifier that was used to measure $V_{3\omega}$ at the third harmonic. If this does not happen then Lock in will not be able to measure and it will show “overload”. So Wheatstone bridge is an important part of this measurement. OPAMP are also being used for this purpose also.

The schematic diagram of the experimental set up is given in the fig.2.3.

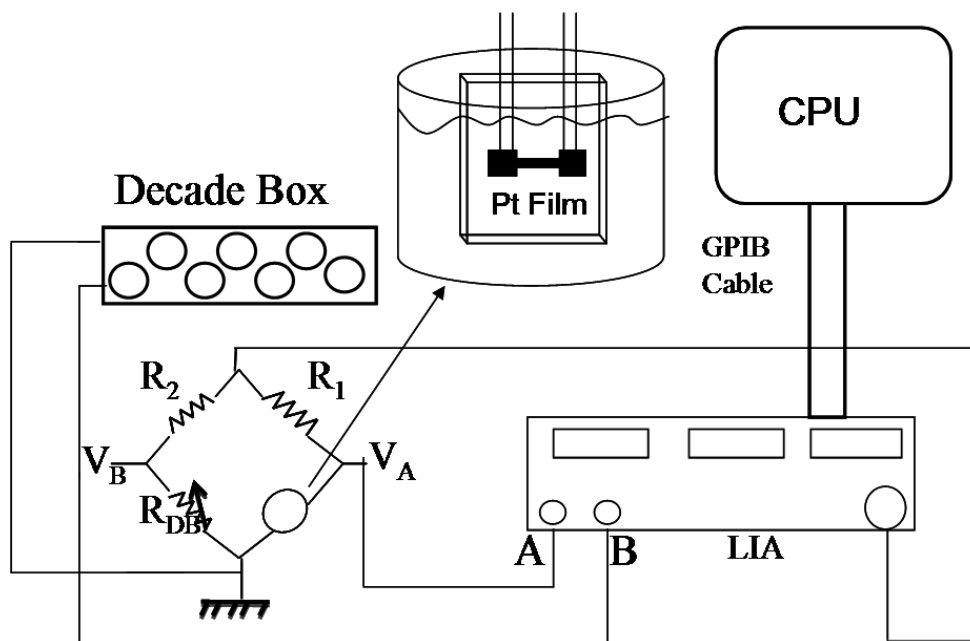


Fig.2.3. Sketch of the whole 3ω measuring set up

2.2.3 Experimental Setup details.

In the experimental setup there are different parts these are as follows.

- (1) Heater/Thermometer
- (2) Sample and heater holder
- (3) Wheatstone Bridge
- (4) Lock In Amplifier (LIA)
- (5) Temperature Controller
- (6) Decade Resistance Box
- (7) CPU Interfacing (GPIB,C++)

Now the picture of the complete experimental set up is shown in fig.2.4. Each part is marked side by side.

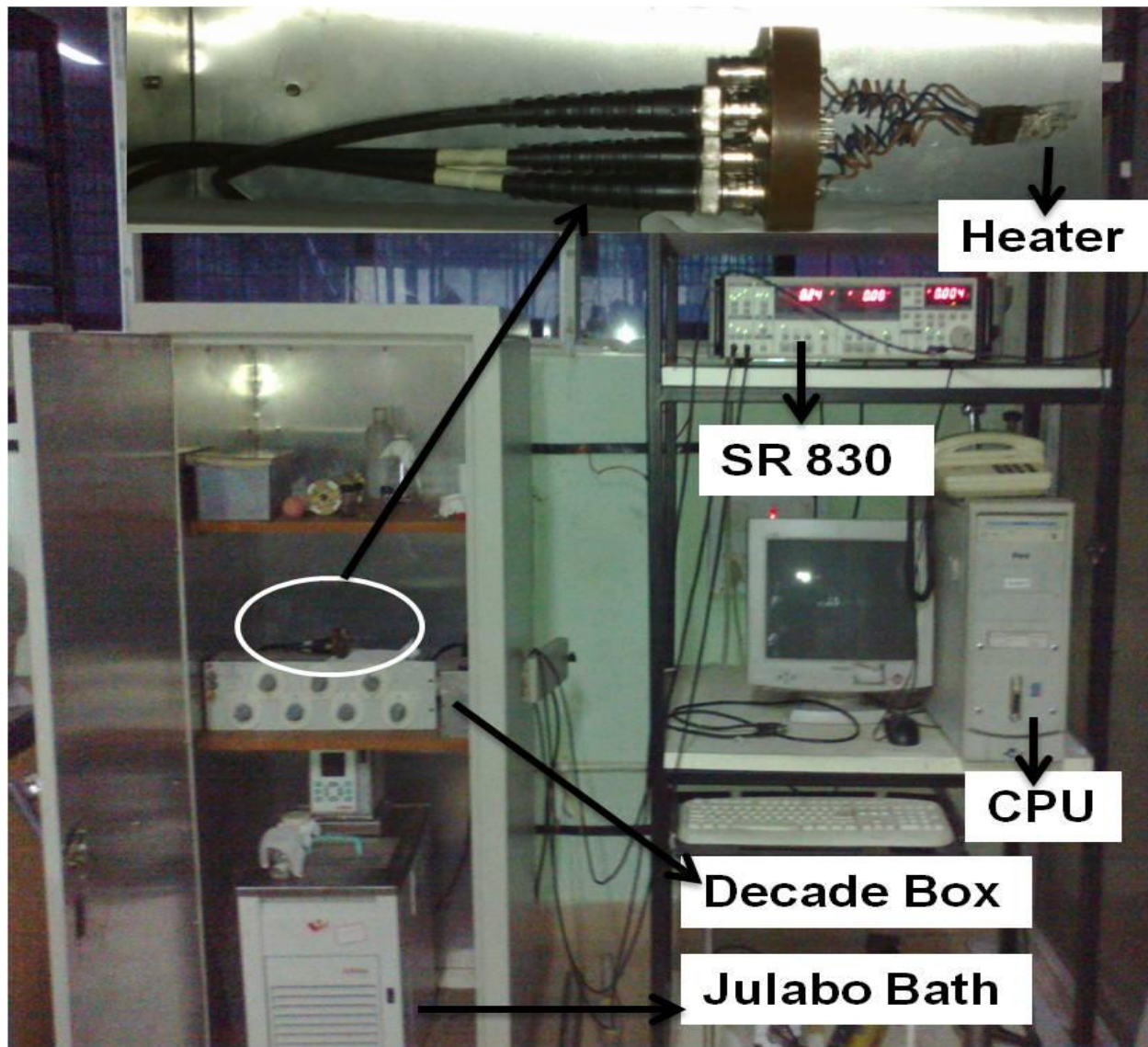


Fig.2.4. Picture of the experimental set up

All these parts are discussed separately below.

2.2.3.1 Heater/Thermometer

The heater is an important part of the whole experimental set up. 3ω method uses radial flow of heat from a single element that is used both as heater as well as thermometer. The main thing in this method is the use of the frequency dependence of the temperature oscillation instead of time domain response.

The heater/ thermometer in the experiment is a Platinum (Pt.) film evaporated on to an optically flat glass square substrate (18mm x 18mm) optical window. The heater configuration is shown in the fig. 2.5

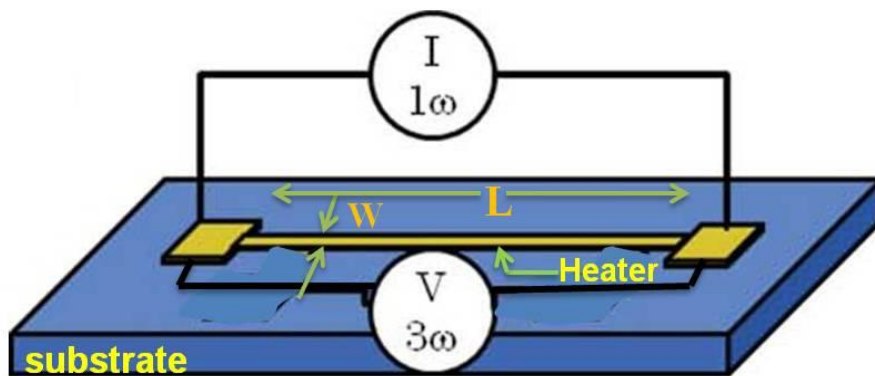


Fig.2.5. Top view of the heater configuration on a substrate

Here it is assumed that heat flows from an infinitely narrow line source of heat on the surface of a substrate. For this reason our film has $L \gg W$. For the film used typical $L \sim 5\text{mm}$, $W \sim 0.3\text{mm}$.

The film has dual pads for making electrical connections to the external world. Since it is to be placed in one of the arm of the Wheatstone bridge, in order to cancel out the more pronounced 1ω signal, it cannot be used in ordinary four probe method. For this the Pseudo four probe configuration was used for carrying electrical measurements. Such Pseudo Four probe configuration is shown in fig.2.6. Initially the lead wires connected to the pads using conducting Silver paste however when it was dipped in Ethanol (the base fluid) it got dissolved in it consequently opening the closed circuit connections. As a result we cannot use such conducting metal pastes as it gets dissolved in the base fluid. We use a high quality soldering material which is alloyed with Indium at high temperature in vacuum condition. This alloy helps us to solve our electrical contact problem.

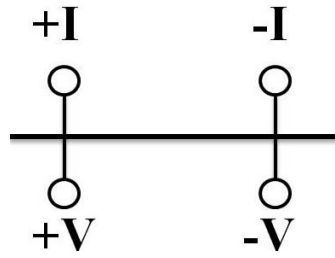


Fig.2.6. Pseudo Four Probe configuration

2.2.3.1.1 Heater Material

Choosing the material of the heater is the most important step towards successfully completing the measurement in this method. There are many factors which determine the nature of the materials which is to be selected. The requirements are mentioned below.

- 1) Reasonable temperature coefficient of resistance ($\alpha = \frac{1}{R} \frac{dR}{dT}$) which is very important to allow it is to be used for thermometer. Higher the value of it higher is the response/resolution from the system.
- 2) Since $V_{3\omega} \propto R_0$ (resistance of the film), it should have a relatively high resistivity (ρ) at room temperature. However, too much high ρ can reduce α as well. Thus a trade-off is needed.
- 3) It should be very inert i.e. it does not interact easily in ambient condition and as well as in different medium which we will use for nanofluids.

First we started with the Silver (Ag), Copper (Cu) film by thermal evaporation, but problem with this is that it slowly gets oxidized and passivated. Then we worked with the Platinum (Pt) film made by RF magnetron sputtering method of deposition.

We carry out the experiment by using the thin films made from both these metals. The response from these films are shown in fig.2.7 is result of the measurement. It clearly shows that the response with the Pt is much more pronounced than the Ag film with same dimension and under the same experimental conditions. At the low frequency end the $V_{3\omega}$ voltage for Pt. film is almost 3 times than that for the Ag film. Thus the response with Pt is much more than the Ag film. Since the resistivity of the film determines the amount of power/heat generated

in it, thus higher the resistivity better is the heater. Pt has much more resistivity than the Ag. Hence we found that Pt is the best candidate for this system. So much higher resolution consequently more accurate result is obtained with the Pt heater. More over Pt is a noble metal and least corrosive.

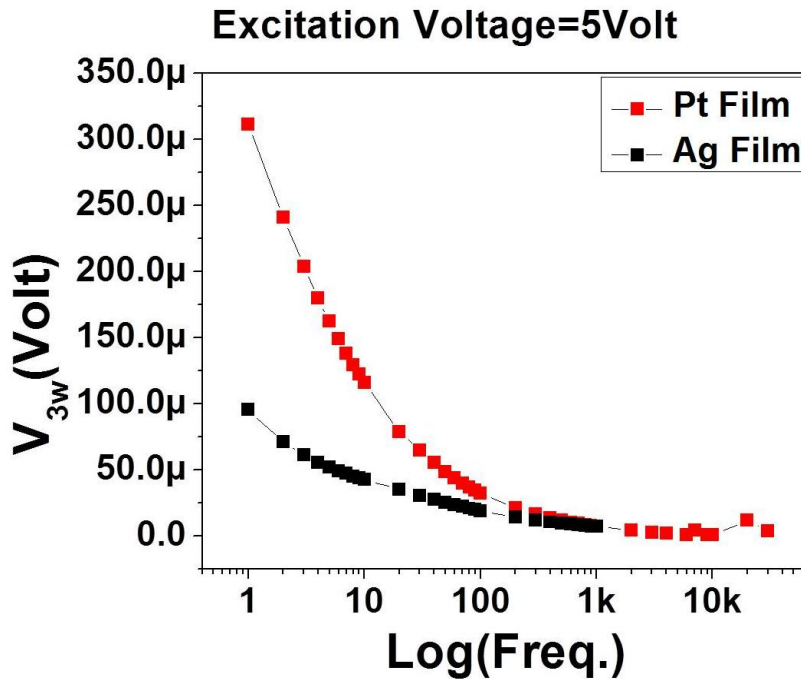


Fig.2.7. 3ω response for the two thin films under similar conditions.

Another important thing in this system is the good adhesion of the film/heater with the substrate on which it is deposited. It is very important for the good performance of the film as a heater.

We started with depositing Pt film on the quartz substrate we find that the pattern was highly resistive and sticking was also not good. Pt sticks very well with the glass substrate kept at high temperature in vaccum.

Another problem that we face while doing the measurement is that with the bare substrate one can get good results. But when the film is dipped inside the nanofluid suddenly there is a large jump in the output voltage. Then we found that since the nanofluids are electrically conducting when the film is inside the fluid the whole fluid acted as a conducting medium and contributing in the output result which is not correct. Thus we have to isolate the conducting film from the neighboring conducting medium. We deposit a very thin insulating layer of SiO over the length of the Pt film. This layer acts as a protective coat and isolates the film.

2.2.3.1.2 Heater Fabrication

We employed RF Magnetron sputtering method for depositing Pt film for our heater.

Sputtering is a widely used process for deposition of thin films. It is a process whereby coating material is dislodged and ejected from the solid surface due to the momentum exchange associated with surface bombardment by energetic particles. It is used in those substances whose melting point is very high and it is very difficult to achieve it by simple evaporation methods. Sputtering is done by means of plasmas which generate free charged particles which can be accelerated towards a targeted surface/substrate electrically.

In RF magnetron sputtering a magnetic field is applied perpendicular to the electric field and this result in the increase in the time of interaction of the ions with the target atoms. This is an enhanced sputtering method which results in a higher deposition rate at low operating pressure and also increases the quality of the film. Such $E \times B$ arrangements are shown in fig.2.8 [4]

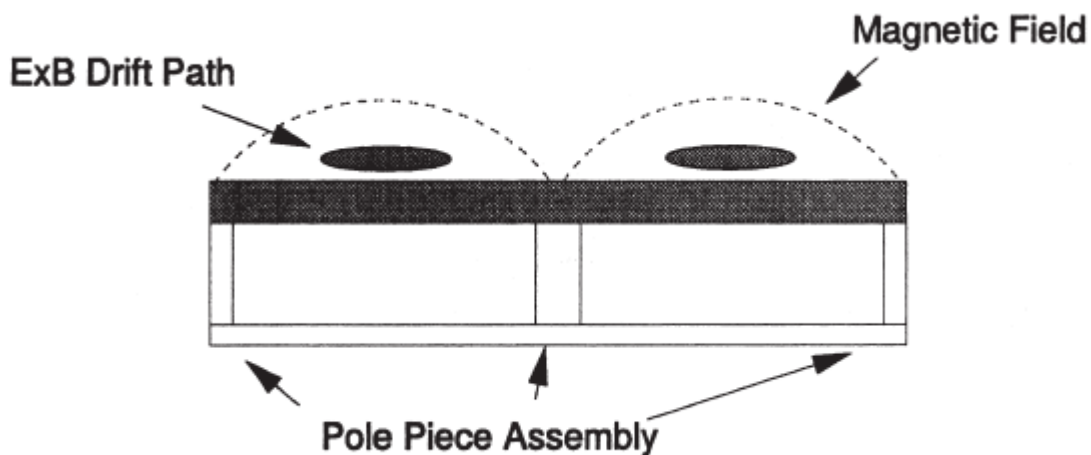


Fig.2.8. The magnetic field configuration for a circular planar magnetron cathode

Magnetron sputtering is presently the most widely commercially practiced sputtering method. These are typically an order of magnitude higher than rates attained by conventional sputtering techniques. The RF diode system requires impedance matching to operate most efficiently. This matching network, adjacent to the vacuum system, helps to optimize the transfer of power. A typical sputtering system is shown in fig.2.9 of Hind Hi vac made.

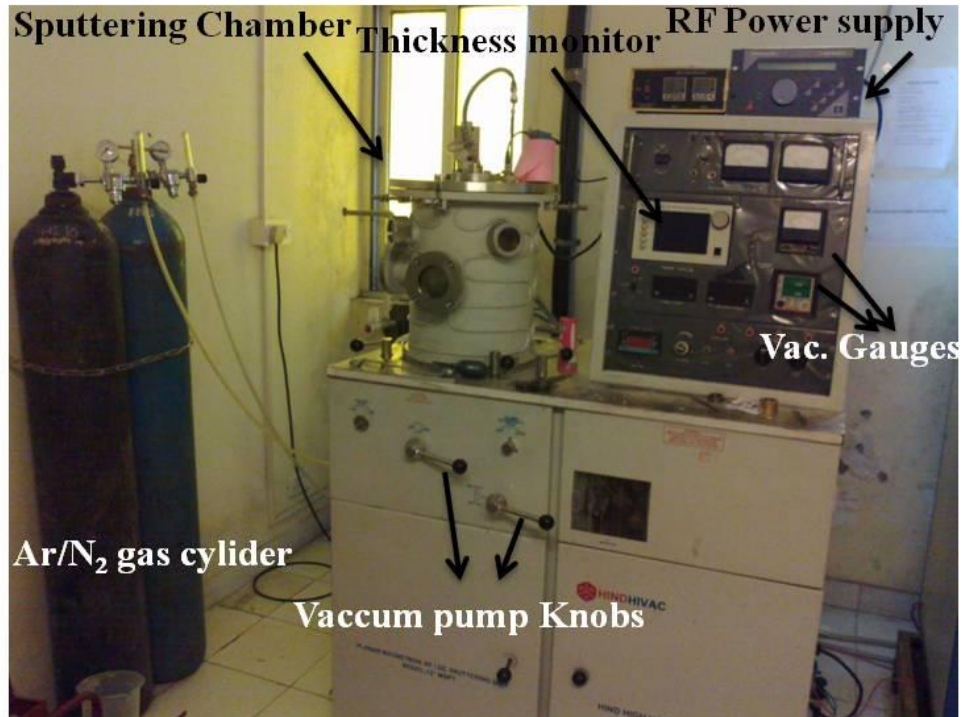


Fig.2.9. Evaporation cum sputtering system of S.N.Bose Centre

Vacuum Chamber measures 12 inch. dia. x 10 inch. height steel chamber with both ends open and achieve vacuum sealing with top plate and bottom plate. A target holder, for the material to be sputtered, made of copper with provision for cooling by water circulation is provided. Substrate holder (anode) is a copper plate of 5" dia. is provided at the bottom plate. A dedicated DC power supply of 2 KW is provided for DC Sputtering. Huttinger (GmbH) PFG 300 RF model is used for RF excitation of the gases in the chamber for Plasma formation. A high speed vacuum pumping system fully integrated with necessary piping and valves, all operated manually is rated for high gas through put handling and to produce clean and high vacuum in the chamber. All the electrical controls and instruments are housed in the main unit at convenient place for smooth operation of the system. After the excitation voltage is applied to high pressure chamber containing Ar there is a formation of the Plasmonic state of the Ar gas and glows brilliantly purple coloration as shown in fig.2.10. Pt target and substrate are kept already inside it and the heavy ions of Ar bombarded on to Pt surface knocking out the Pt atoms from the surface layer. These atoms slowly settle down on to the hot substrate and giving a fine Pt thin film on it.

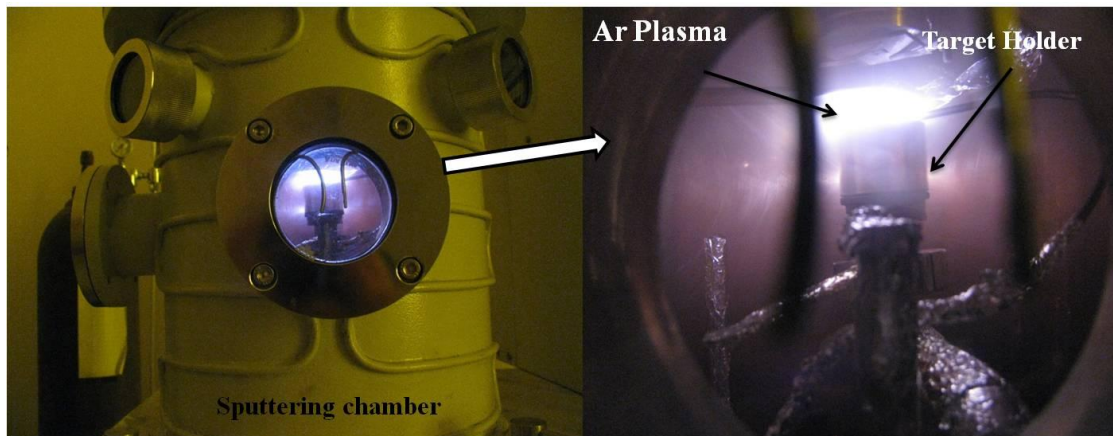


Fig.2.10 Argon Plasma formation inside the Sputtering chamber for Pt. film synthesis

The film was patterned by sputtering through a hard steel stencil mask. These hard stainless steel masks (1mm) were designed by AutoCAD and given to Central Tool Room & Training Centre (CTTC, Govt. of India), Bon Hooghly are shown in the fig.2.11. Using these masks heater of different widths like 300 μ m, 400 μ m and 500 μ m were deposited on Glass microslides was used as a substrate after cleaning it by RCA process (It is a three step chemical process of substrate cleaning). Mask was put on the sized substrate and fixed inside the vaccum chamber. Vaccum was maintained at 10⁻⁶ mbar. In the mean time the substrate was maintained at a high temperature 400 °C. After lots of research and repeations we optomise the systems different parameters and we were able to grow a good, smooth and high quality thin Pt. films

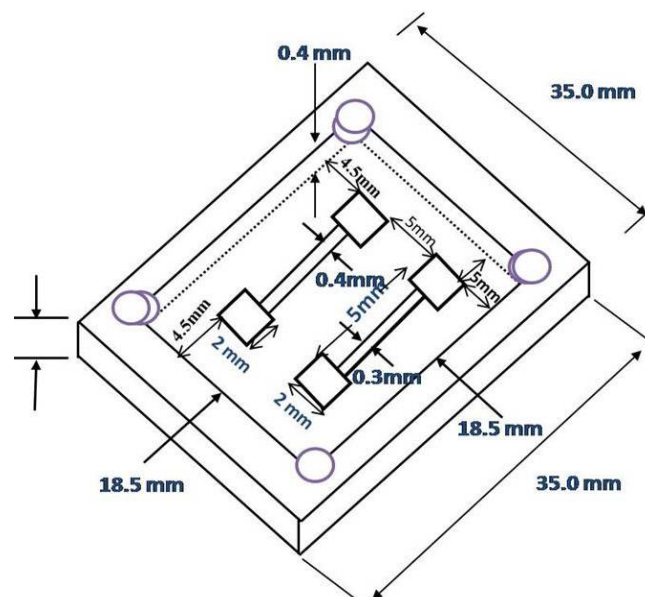


Fig.2.11. AutoCAD design of the mask stencil

In the system there are various parameters which determine the thickness, quality etc of the Pt film. We have fix the conditions for the desired growth of our Pt film by are given below.

- (1) *Initial rate*=10
- (2) *Final Thickness*= 1.0kA°
- (3) *DC Bias*=180V
- (4) *Base Pressure*=0.03mbar
- (5) *Working Pressure of Argon gas*=0.02mbar
- (6) *Power*=20W
- (7) *Forward Power (FWDP)*=20W
- (8) *Reverse Power (RWDP)*=0W
- (9) *Z Factor*=0.529
- (10) *P Term*=70
- (11) *I Term*=5
- (12) *D Term*=0

After applying the above conditions a Pt thin film was formed with predefined pattern and desired dimension of whose optical image is shown in fig.2.12 . To characterise the film we used SEM, EDAX etc.

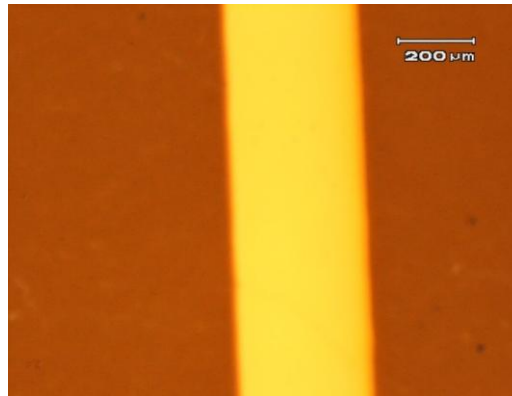


Fig.2.12. Top View of Pt film under Optical Microscope

From above figure it is clear that there edges of the Pt films are very sharp and clear with desired accurate dimension. We have also compared this with dimension of the slit and find it is of the same dimension

2.2.3.1.3 Electrical Characterisation/Calibration

Electrical characterisation of the film is done by using low temperature measurement setup [5] for determining the a.c resistance variation with the operating temperature. Photograph of the set up is shown in fig.2.13. It consists of three main parts comprising of hardware and software namely the cryocooler for producing low temperature, external instrumentation for measurement, computer program for automation.

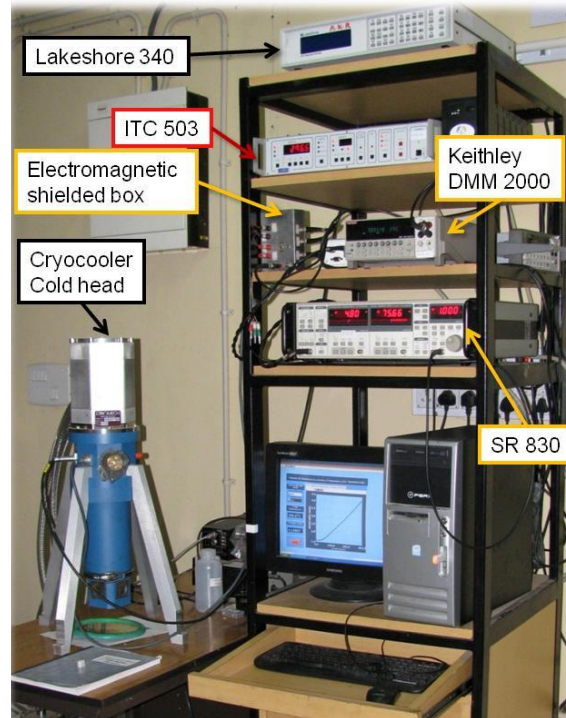


Fig.2.13. Setup for measuring the A.C resistance

The thin film so formed by the sputtering is not defect free (e.g strained etc.) which causes reduction in the quality consequently the functionality of the film. For improving its quality it is annealed at high temperature (500 °C) in vacuum before performing electrical measurement on it.

Two important electrical parameters can be used to determine the quality of the metal films. These are as follows with their calculated values.

(1) **Residual Resistance Ratio (RRR)**,

It is the ratio of resistances of the film at room temperature (300K) to Helium boiling temperature (4.2K). When the metal films are annealed it gets defects free and improves the quality of it. Higher the value of this quantity better is the quality. In my case for Pt (annealed) it comes out to be around 3.

$$RRR = \frac{R_{300K}}{R_{4.2K}} \approx 3$$

(2) *Temperature coefficient of resistance (α)* i.e change in resistance per unit change of temperature. If the film has to be used also as a thermometer then this parameter plays a very important role. Higher the value of this for a material higher is its sensitivity as a thermometer.

$$\alpha = \frac{1}{R} \frac{dR}{dT} \approx 0.0039\text{K}^{-1}$$

Both the above quantities can be determined from the slope of the Resistance vs Temperature (RT) curve of the film. So we have done the very low temperature A.C Resistivity measurement to calculate the value of RRR for our Pt. thin film.

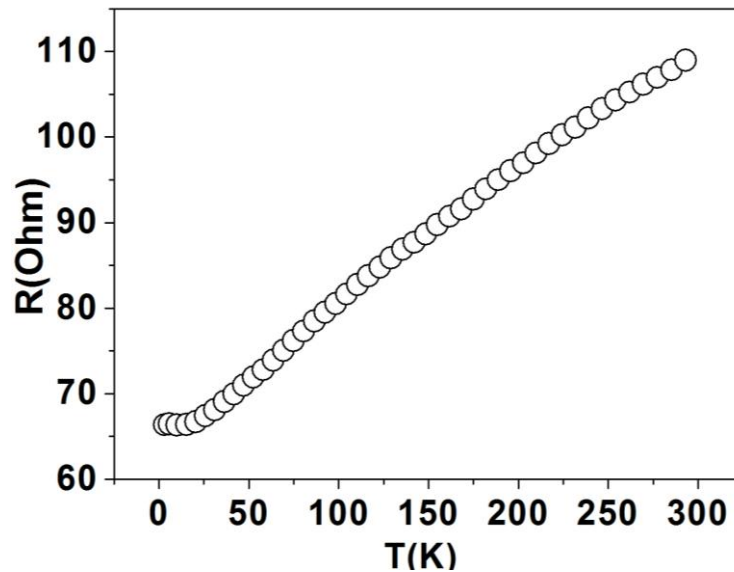


Fig.2.14. R vs T data of the Pt. film

A typical resistance data are shown in fig.2.14 above. The values of the parameters for the film compared with the bulk values are listed in table 2.1

<i>Parameters</i>	<i>High purity bulk Pt [6]</i>	<i>Film used</i>
α	0.003	0.029
ρ	$0.10 \times 10^{-6} \Omega\text{m}$	$0.35 \times 10^{-6} \Omega\text{m}$

Table 2.1

The resistivity of thin Pt. thin film comes out to be three times that of the corresponding bulk value. This value allows us to get a film with higher resistance. Since we are using voltage

biasing, this is desirable. However, α is reduced from the bulk giving us lesser sensitivity. However, the film was to have good enough sensitivity for our work.

SEM image of the surface of the Pt film is shown in fig.2.15. From image it appears that the film surface is very smooth and continuous.

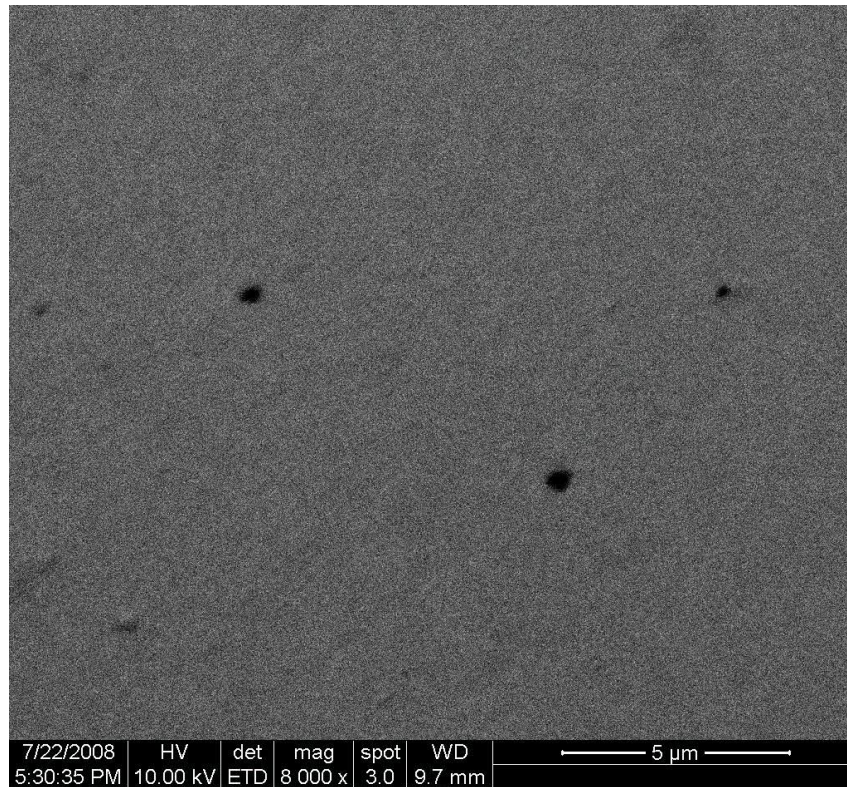


Fig.2.15.SEM image of the Pt thin film

2.2.3.1.4 Thickness Characterisation

For measurement of thickness of the thin films we used Ellipsometry technique. It is a non-destructive, Non contact method of optical characterisation and then determination of the thickness of thin film. Schematic diagram of the ellipsometre is shown in fig.2.16.

A light source produces unpolarized light which is then sent through a polarizer. The polarizer allows light of a preferred electric field orientation to pass. The polarizer axis is oriented between the p- and s- planes, such that both arrive at the sample surface. The linearly polarized light reflects from the sample surface, becomes elliptically polarized, and travels through a continuously rotating polarizer (referred to as the analyzer). The amount of light allowed to pass will depend on the polarizer orientation relative to the electric field “ellipse” coming from the sample. The detector converts light to electronic signal to determine the

reflected polarization. This information is compared to the known input polarization to determine the polarization change caused by the sample reflection.

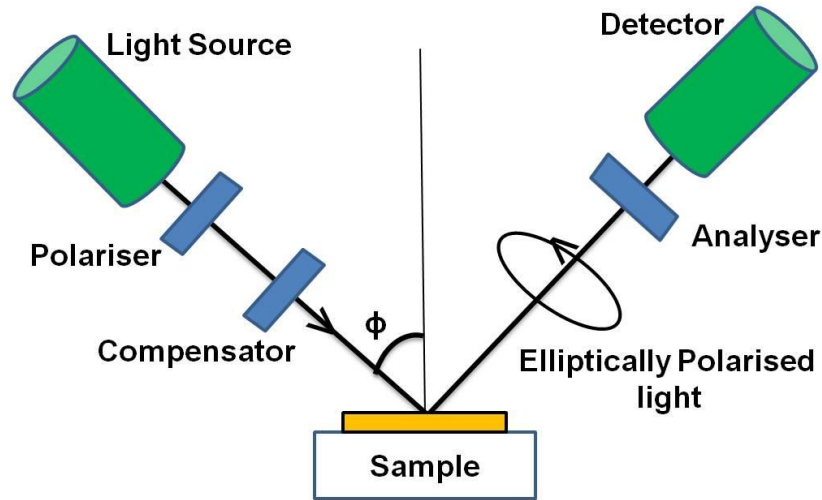


Fig.2.16. Schematic diagram of an Ellipsometre showing optical arrangement of the device

Ellipsometry measures a change in polarization as light reflects or transmits from a material structure. The polarization change is represented as an amplitude ratio, Ψ , and the phase difference, Δ . The measured response depends on optical properties and thickness of individual materials. Thus, ellipsometry is primarily used to determine film thickness and optical constants. However, it is also applied to characterize composition, crystallinity, roughness, doping concentration, and other material properties associated with a change in optical response. Fig.2.17 shows the elliptically polarised light from the sample and going towards the detectors.

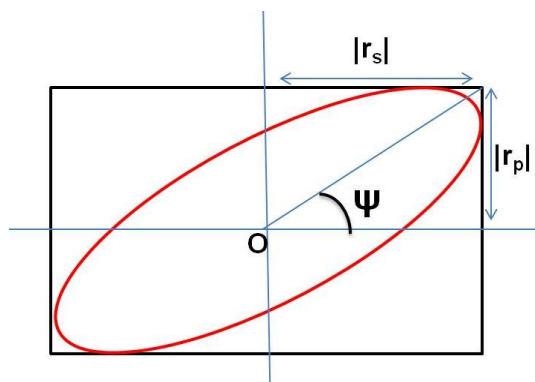


Fig.2.17. Elliptically polarised light with different parameters [7]

$$\frac{r_p}{r_s} = \tan \Psi \exp(j\Delta)$$

We take the measured values of Δ and ψ , typically as a function of wavelength and angle of incidence (Variable Angle Spectroscopic Ellipsometry (VASE)).

We have to first clean the sample and then placed it on the stage of the device which is held firm by a vacuum pump through a hole. Then taken data by varying the angle of the incident polarised light as it was VASE. These data are obtained by measuring the change in polarization state of light that occurs when light is reflected off the surface of (or transmitted through) a sample. The VASE system accomplishes this by supplying a light of known wavelength and polarization state and determining the polarization state of the light after being reflected off the sample.

Then we fit the models which are preloaded in the system for Pt. and SiO thin films. In this model there is a tabulated values of n and k for the given material for different wavelengths of light used. Then by using the Regression algorithms of Levenberg-Marquadt are used to vary the unknown parameters and try to minimise the difference between experimental data and the data which is generated as a result of the model. It is bit lengthy process as we have to arbitrarily vary the unknown parameter and minimise the value of the Mean Squared Error (MSE). The parameter which minimises this difference is taken and the thickness corresponding to this value is taken as the most appropriate value for the given material.

Fig.2.18 shows the photograph of the Ellipsometre which we used for determining the thickness of the Pt film. It is product of J.A Wollam (VASE) model.



Fig.2.18 VASE Ellipsometer in our lab

We start with the Pt film. The typical output result fitting the experimental data with the fitted data generated by the model fit for this system is shown in fig.2.19. It is clear that error in the fit is very small. The MSE ($2.594e-005$) calculated for the fit has come out to be very small consequently there is almost an overlap between the experimental data and the fitted data. Thickness of the film comes out to be around 75.583 ± 29.2 nm.

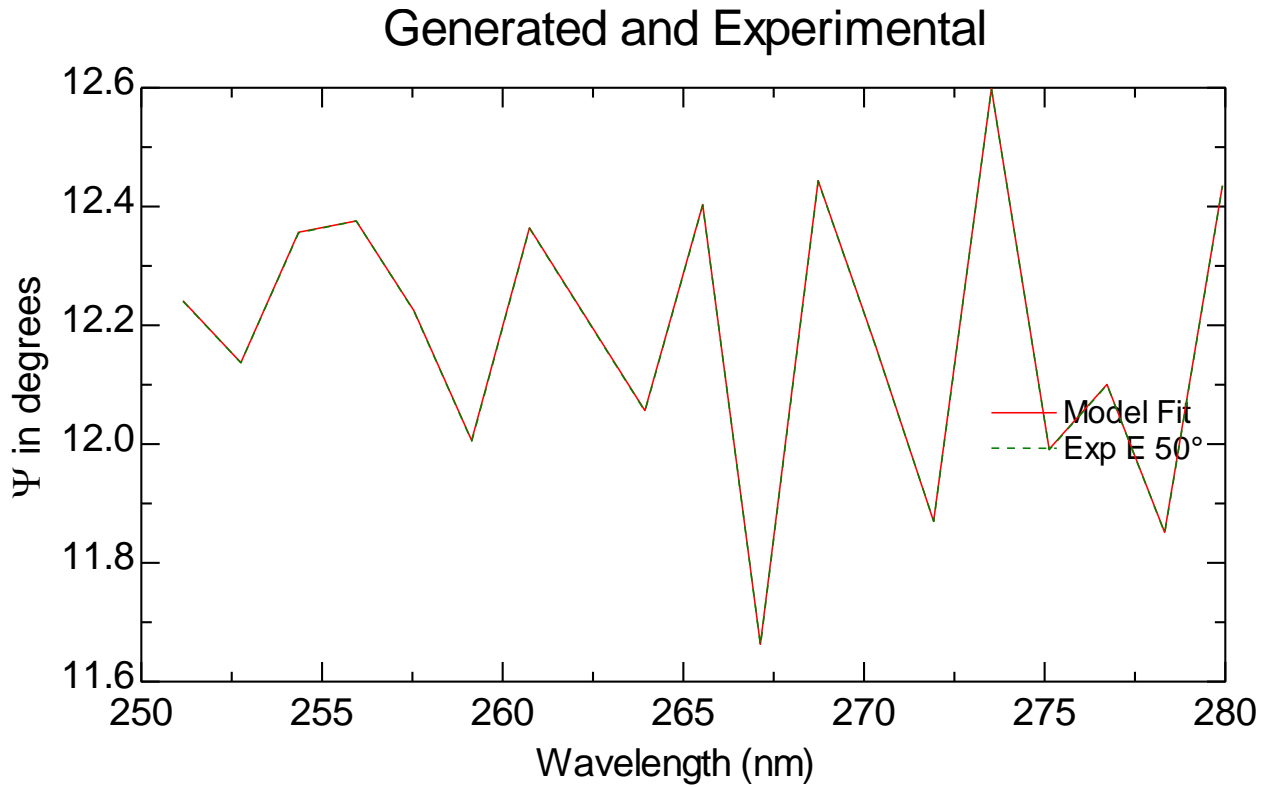


Fig.2.19. Experimental and fitted data for Pt thin film

Similarly for finding the thickness of the insulating SiO layer, we repeat the above experiment and the results are shown in fig.2.20. Data are taken for a series of varying incidence angle. From the fitting we found that it is not as good as with the Pt film because the thickness of this passivating layer is very small and secondly it is over a parent layer.

The MSE (2.47) calculated for the fit has come out to be not so small. Thickness of the film SiO layer comes out to be around 53.014 ± 1.02 nm.

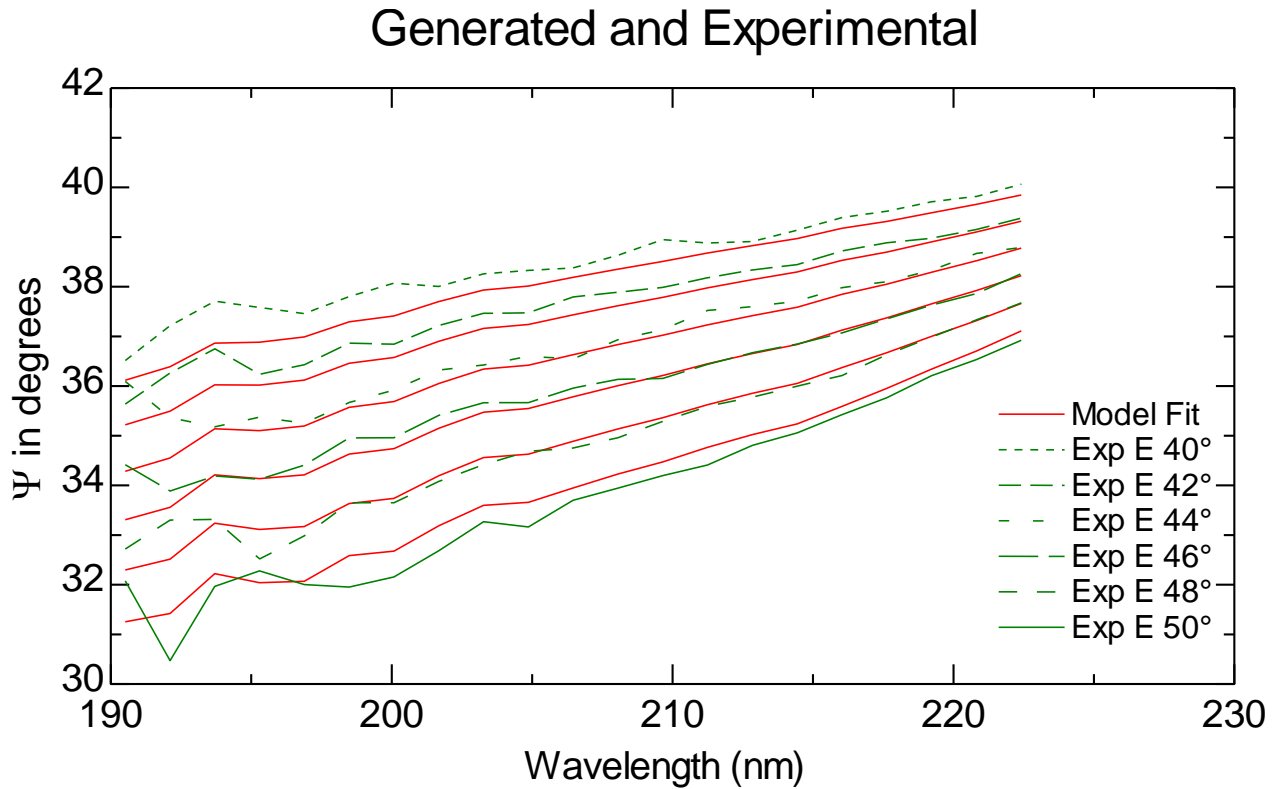


Fig.2.20. Experimental and fitted data for thin film of SiO coating

The results are also verified by the AFM also in which we cut a trench in the film and then measure the thickness of it.

2.2.3.2 Sample and heater holder

Pt film grown by above described method acts as both heater and thermometer. The film on substrate and the nanofluid to be investigated are which is kept inside a Cu vessel placed inside the temperature controller bath so its body should be of conducting material like Copper. Details of it is shown in the fig.2.21.

In the head four BNC connectors are there for making electrical connections to the external instruments. The current and voltages across the film is send and measured by the four probe arrangement. This is connected to the lock in and Wheatstone Bridge by BNC cables.

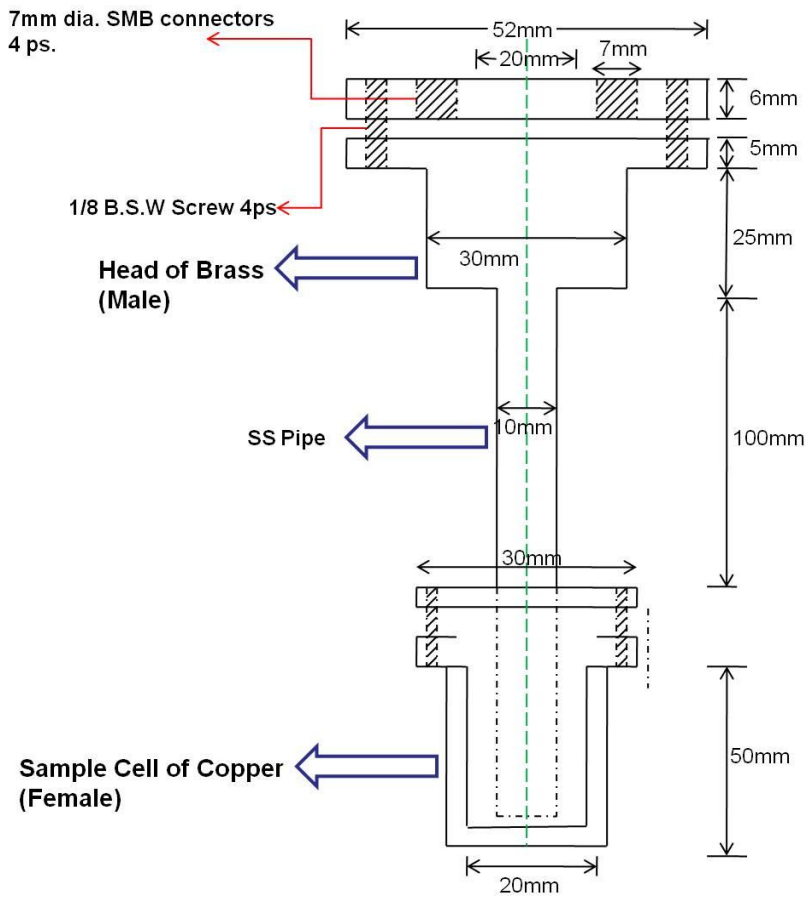


Fig.2.21 AutoCAD design of the sample holder (side view)

The current and voltages across the film is send and measured by the Four probe arrangement. This is connected to the lock in and Wheatstone Bridge by BNC cables.

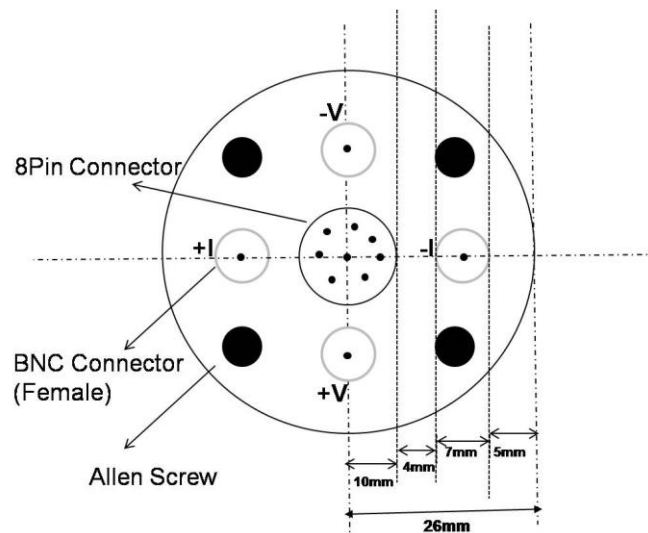


Fig.2.22. Top view of the sample holder showing four probe arrangements

The actual picture of the above schematic of fig.2.22 is shown in fig.2.23. Heater is connected at the end of the BNC connectors. Heater is dipped inside the liquid solution as as shown below.

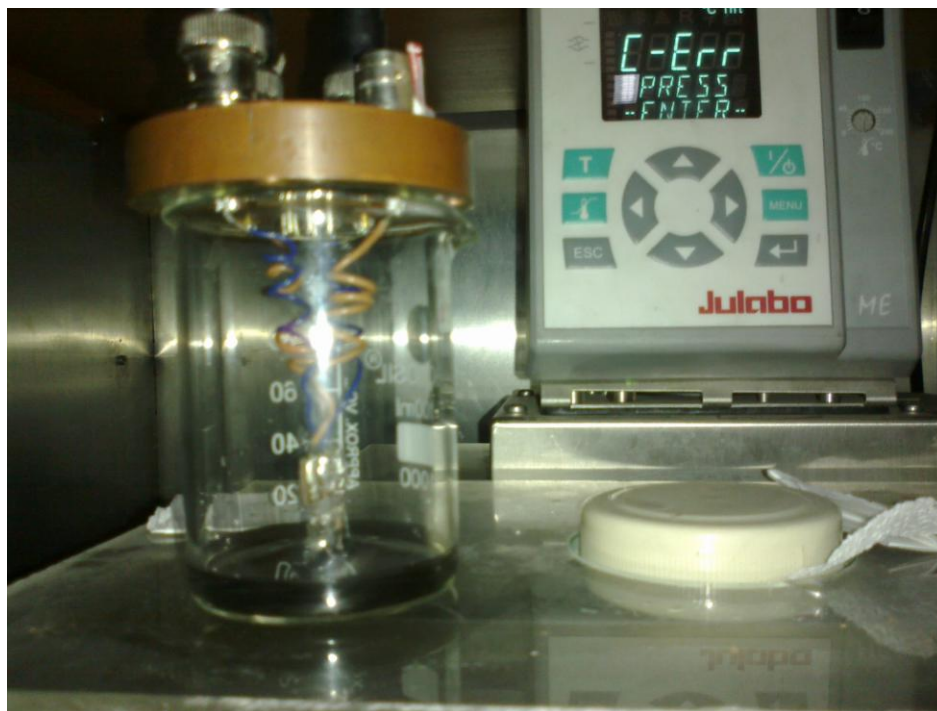


Fig.2.23. Heater arrangement with the BNC connector

2.2.3.3 Wheatstone Bridge

This is also an important part of the setup. Here we place the heater with other resistances.

Now the question arises why we should use this bridge circuit in this measurement.

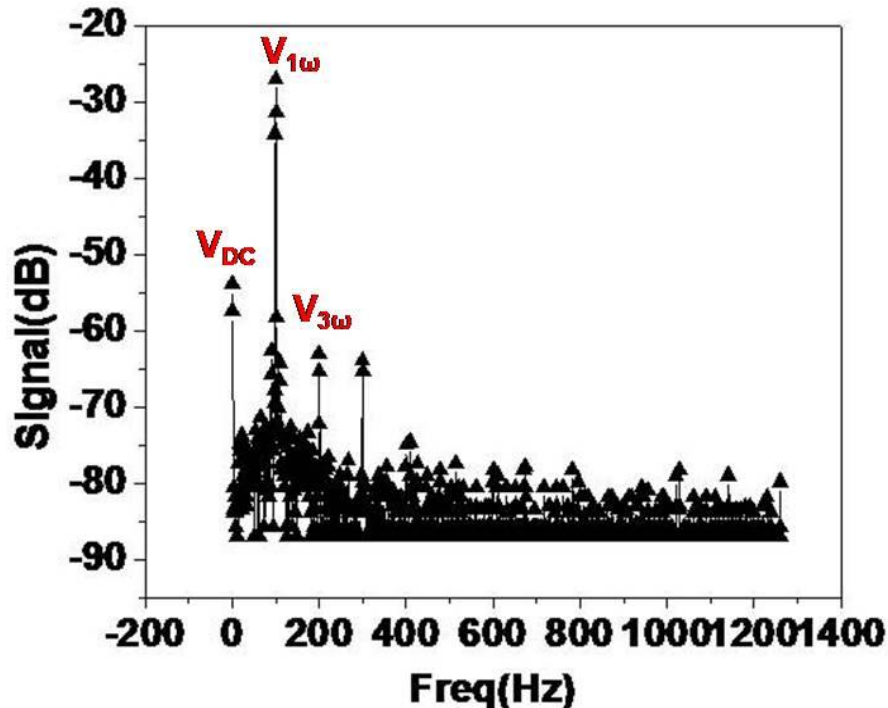


Fig.2.24. FFT of the output signal in Oscilloscope

We fed the output signal coming directly from the heater into an Oscilloscope to visualise it, and to get the FFT of the signal. The FFT looks as it is shown in the fig.2.24. It is clear that the magnitude of the 1st harmonic of the output voltage (1ω) is very high compared to the 3rd harmonics. If we convert dB to ratio of the two signals then ~ 100 . To measure this small signal which is immersed into the large magnitude signal we will have to suppress the ω signal. This can be done simply by using Wheatstone bridge. When the bridge is in the balanced condition it effectively nullifies the 1ω signal and the differential output (A-B) of LIA contains only the 3rd harmonic component.

For understanding the action of the Wheatstone bridge we will see the circuit diagram of it and allied things with this. Consider the circuit shown in fig.2.25 where

R_1, R_2 = Standard resistances,

R_{DB} = Resistance in the decade box after balancing the bridge with it,

R_{pt} = Resistance of the Platinum heater.

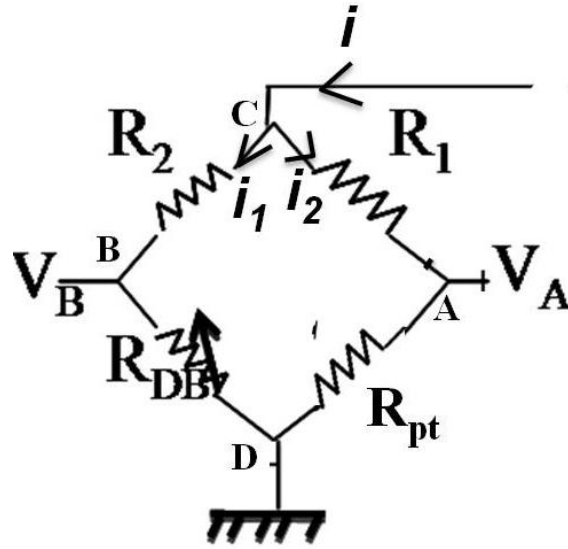


Fig.2.25. Wheatstone Bridge arrangement

Differential Output Voltage is measured across A and B is, $V_{out} = V_A - V_B$

$$\text{Using the voltage divider relation } V_{out} = V_{in} \left[\frac{R_{pt}}{R_{pt} + R_1} - \frac{R_{DB}}{R_{DB} + R_2} \right] \quad [2.6]$$

Applying Kirchhoff's current law at point C,

$$i = i_1 + i_2 = V_{in} \left[\frac{1}{R_{pt} + R_1} + \frac{1}{R_{DB} + R_2} \right] = V_{in} \left[\frac{R_1 + R_2 + R_{DB} + R_{pt}}{(R_1 + R_{pt})(R_2 + R_{DB})} \right] \quad [2.7]$$

Combining eq.(2.6) and eq.(2.7) we get

$$V_{out} = i \left[\frac{R_{pt}R_2 - R_{DB}R_1}{R_1 + R_{pt} + R_2 + R_{DB}} \right] \quad [2.8]$$

If now change ΔR_{pt} shown up as $R_{pt} \rightarrow R_{pt} + \Delta R_{pt}$

Then there will be a corresponding change in the output voltage as $V_{out} \rightarrow V_{out} + \Delta V_{out}$

When the Wheatstone bridge is in balanced condition we have $V_{out} = 0$ and let $R_1 = R_{pt} = R$ then eqn.(2.8) reduces to

$$V_{out} + \Delta V_{out} = i \left[\frac{(R_{pt} + \Delta R_{pt})R_2 - R_{DB}R_1}{R_1 + R_2 + R_{DB} + R_{pt} + \Delta R_{pt}} \right] \quad [2.9]$$

$$\Delta V_{out} = i \left[\frac{(R + \Delta R_{pt})R_2 - R_{DB}R}{2R + R_2 + R_{DB} + \Delta R_{pt}} \right] \quad [2.10]$$

Further simplification gives the final expression for the ΔV_{out} when there is a slight change in the resistance of the Pt. heater.

$$\Delta R_{pt} = \frac{(R_2 - R_{DB})R - (2R + R_{DB} + R_2) \frac{\Delta V_{out}}{i}}{\frac{\Delta V_{out}}{i} - R_2} \quad [2.11]$$

Thus eqn.(2.11) gives ΔR_{pt} in terms of ΔV_{out} (measured signal), input current and bridge resistance. This fluctuating resistance gives a fluctuating voltage across it and we extract out the 3rd harmonic signal from it by using the Lock in Amplifier. Once this 3ω signal is derived then we can find the thermal properties of the substrate and the nanofluids as mentioned earlier.

2.2.3.4 Lock In Amplifier

Lock in Amplifier, model SR 830 of Stanford Research is used in our set up. It is the most important part of the 3ω measurement set up. It plays a dual role in the experiment. It provides sinusoidal excitation voltage to sample as well as measured the output voltage coming from the sample after excitation. It is shown in fig.2.26.

A.C Sinusoidal voltage of amplitude 5V is passed through the internal source of the LIA through the “sine out” port. The frequency of the applied voltage is varied through the external CPU command.

Differential Output Voltage is measured across A and B i.e $V_{out}=V_A-V_B$ is fed into the signal inputs of the LIA and then bridge is balanced so that primary signal get suppressed and then we detect the 3rd harmonics of the signal by pressing the “Harm#” button of the LIA. In this mode LIA all other harmonics as noise so suppresses them and detects only the 3rd harmonics. All the voltages are measured in terms of RMS value.



Fig.2.26. LIA of Stanford Research; Model SR830 DSP

Working Principal of Lock in Amplifier

A lock-in amplifier is a device which is useful for measuring the amplitude and phase of a signal. The output will typically be a DC voltage which is proportional to the input amplitude. The device has two inputs as shown in fig. 2.27. One is the input signal that is to be measured, and the other is a reference. The reference should have the exact same frequency as the input. This signal is usually a synch-signal originating from the same source as the input signal. The input signal is first amplified in an amplifier. The gain of this amplifier is adjustable and is used to control the sensitivity of the lock-in. The reference signal is first led through a sine-former. This is a block consisting of many components which transforms the signal to ensure it has sinusoidal form and specific pre-determined amplitude.

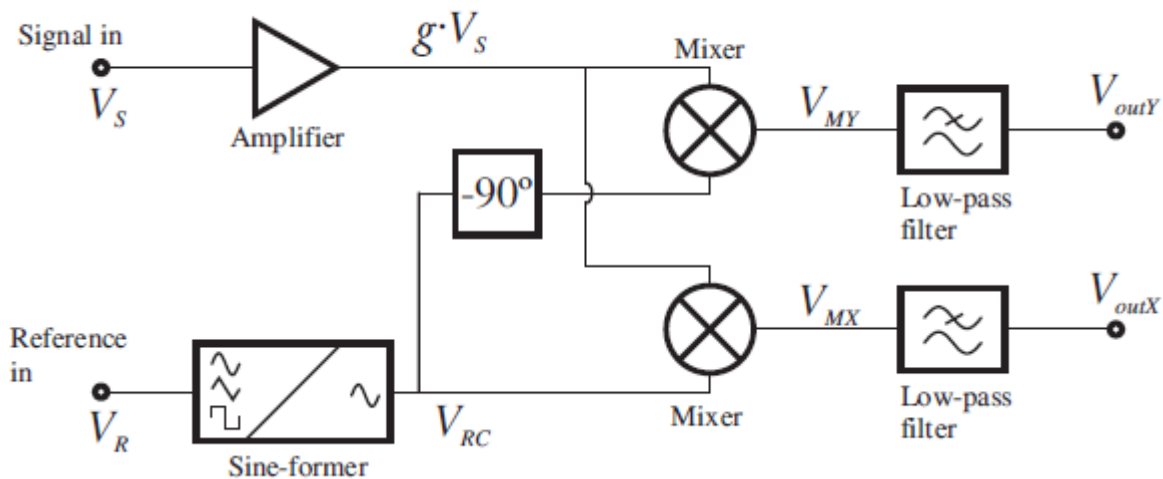


Fig.2.27. Simplified principle sketch of a dual lock-in amplifier [8]

A basic lock-in amplifier can be split into 4 stages: an input gain stage, the reference circuit, a demodulator and a low pass filter.

- **Input Gain Stage:** The variable gain input stage pre-processes the signal by amplifying it to a level suitable for the demodulator. Nothing complicated here, but high performance amplifiers are required.
- **Reference Circuit:** The reference circuit allows the reference signal to be phase shifted.
- **Demodulator/Mixer:** The demodulator is a multiplier. It takes the input signal and the reference and multiplies them together. When you multiply two waveforms together you get the sum and difference frequencies as the result. As the input signal to be measured and the reference signal are of the same frequency, the difference frequency is zero and you get a DC output which is proportional to the amplitude of the input signal and the cosine of the phase difference between the signals. By adjusting the phase of the reference signal using the reference circuit, the phase difference between the input signal and the reference can be brought to zero and hence the DC output level from the multiplier is proportional to the input signal.
- **Low Pass Filter:** As the various noise components on the input signal are at different frequencies to the reference signal, the sum and difference frequencies will be non zero and will not contribute to the DC level of the output signal. This DC level (which

is proportional to the input signal) can now be recovered by passing the output from the demodulator through a low pass filter.

The above gives an idea of how a basic lock-in amplifier works. Actual lock-in amplifiers are more complicated, as there are instrument offsets that need to be removed, but the basic principle of operation is the same.

2.2.3.5 Temperature Controller

Here the temperature controller is not that of usual where a concentrated area in vacuum condition is cooled down by cryocoolers which is controlled electrically by RTD controller. Since in our experiment the samples are in liquid state so no question of vacuum condition and the temperatures control by RTD etc. We used JULABO (model F32 ME) temperature controller bath. Glycol was used as the circulating liquid shown in the fig.2.28.



Fig.2.28. JULABO temperature controller

Here the sample holder is dipped inside the circulating liquid from the top. Its temperature stability is about 0.01°C.

2.2.3.6 Decade Resistance Box

Decade resistance box is a collection of high precision standard resistances in a box. We have used resistance box of General Radio, USA.

The **1433** Decade Resistors are a family of instruments providing a very broad choice of high-performance resistance sources. Any number of decades from one to eleven is available.

The **1433** is a precision resistance source with excellent characteristics of stability, temperature coefficient, power coefficient, and frequency response. The **1433** Series employs stable, very-low-resistance switches with silver-alloy contacts. A special design keeps zero-resistance to less than 1 m Ω per decade.

The dials marked “**0**” to “**10**”, offer smooth rotation from position to position with no stops. Each dial has an overlap “**10**” position for maximum convenience and flexibility in setting and adjusting resistance values. The resistance per step and maximum current of each dial are clearly shown on the front panel. Electrical shielding is provided by Aluminium cabinet and front panel. The resistance elements have no electrical connection to the cabinet and panel; a separate shield terminal is provided.

High-quality gold-plated tellurium-copper binding posts serve to minimize the thermal emf effects which can introduce errors into dc resistance measurements, with a minimum resistance as low as 1 m Ω and a maximum available resistance of over 111 M Ω .

2.2.3.7 CPU Interfacing (GPIB, C++)

After all these hardware arrangements there is a need of software and interfacing programs for automatic data acquisition through the CPU of the computers. We used GPIB for communication. These GPIB cards are from IEEE.

Command is sent to the instruments by a code written in C++ programming language. Typical code for my experiment is given below. This program records output voltage set at 3rd harmonic of the Lock in Amplifier (LIA) along with the frequency of the applied a.c voltage.

Typical source code is given below. The time gap between two frequencies is about 5 min and at a given frequency, it takes output voltage after averaging over 1000 data.

```

#include<iostream.h>
#include<fstream.h>
#include<stdio.h>
#include<stdlib.h>
#include<math.h>
#include "IEEE_32.h"
#define lin 8
double valueLin(char[]);
int main()
{int i,j,k,m,n,p,status,l,t,flag=0; double f,v1,vR,vP,v2; char r[100], r1[100],freq[30];

ofstream datafile ("Trial(5V).dat");
if (! datafile.is_open())
{ cout << "Error opening file"; exit (1); }
initialize (21,0);
send(lin,"SLVL 5.00",&status);
send(lin,"S2",&status);
send(lin,"ISRC 1",&status);
// send(lin,"SENS 20",&status);
send(lin,"OFLT 13",&status);
for(int o=0;o<=8;o++)
{for(n=1;n<=9;n++)
sprintf(freq,"FREQ %f",f);
send(lin,freq,&status);
t=50000;
if(f>=1)
{t=25000;
if (flag==0) flag=1;
}
if(f>=10) t=20000;
if (flag==1) { send(lin,"OFLT 12",&status); flag=2; cout << "OFLT 12" <<endl;
for(i=1;i<=t;i++)
{send(lin,"Q1",&status);
enter(r,25,&l,lin,&status);
cout << f << " " << i << endl;
}

{send(lin,"Q1",&status);
enter(r,25,&l,lin,&status);
v1=atof(r);
vR=vR+v1;
send(lin,"Q2",&status);
enter(r,25,&l,lin,&status);

v2=atof(r);
vP=vP+v2;
}
vR=vR/1000.0; vP=vP/1000.0;
cout << f << " " << vR << " " << vP << " " << t << endl;
datafile << f << " " << vR << " " << vP << endl;
}
}
return 0;
}

```

Typical outcome of the above code is shown in fig. 2.30. We can directly find the variation of the magnitude of 3ω voltage w.r.t to the frequency of the externally applied sinusoidal excitation.

f	$V_{3\omega}(r)$	θ
1	4.41254e-05	146.76
2	3.70943e-05	148.431
3	3.19615e-05	147.79
4	2.88932e-05	148.202
5	2.66376e-05	148.633
6	2.527e-05	148.902
7	2.4235e-05	149.26
8	2.313e-05	149.593
9	2.2591e-05	149.651
10	2.193e-05	149.365
20	1.7681e-05	150.173
30	1.53392e-05	147.268
40	1.35456e-05	145.113
50	2.26976e-05	32.833
60	7.84541e-06	123.7
70	1.07269e-05	144.533
80	1.049e-05	145.317
90	9.775e-06	144.553
100	9.28491e-06	142.757
200	7.21321e-06	145.085
300	5.97793e-06	145.513
400	5.484e-06	147.005
500	4.99553e-06	146.912

Fig.2.30 output of the C++ coding for the case of substrate (glass)

2.2.4 Sources of possible error and its correction

For any kind of experimental set up there is a probability of occurrence of error in the measuremental results due to many reasons. There is also a resolution limit of the measurement of certain quantities by the measuring equipments. We have to take care of all the sources from which the error may encroach in the result. In our set up there are various points which have to be taken care of during the measurement. These factors are mentioned below.

2.2.4.1 Size Distribution of nanoparticles

An important source of uncertainty in these experiments can be the effect arising out of size distributions, in particular when we are comparing solutions of different concentrations.

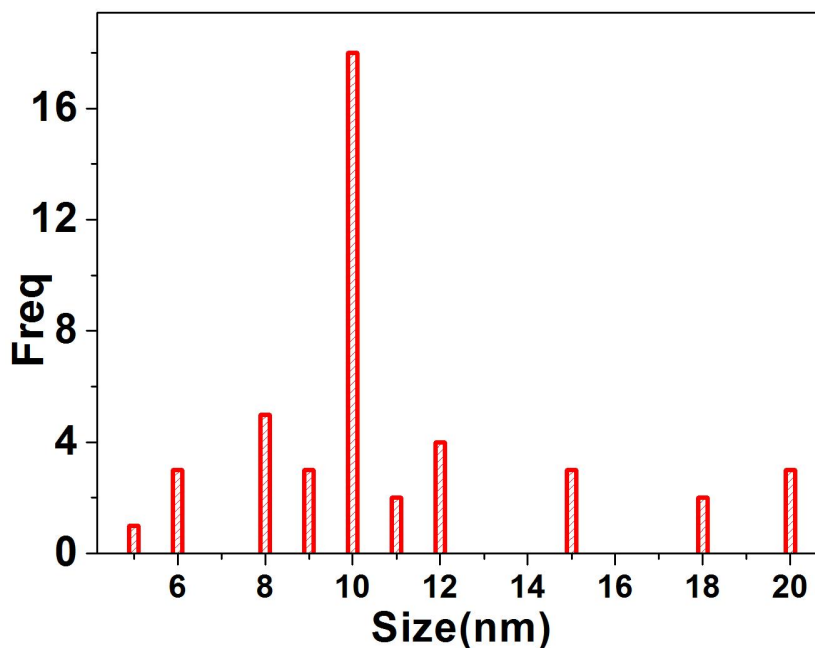


Fig.2.31. Size distribution chart of the ZnO nanoparticles

To have a control on this we checked through TEM analysis of the particles that 80% of them have a size lying in the range 10 ± 1.5 nm as shown in fig.2.31. The bigger size particles precipitate out. To prepare samples with different concentrations we have the same size stabilized batch and different concentrations were obtained by dilution of a mother batch. In this way any uncertainty arising from sample size variation has been avoided.

2.2.4.2 Convective current in the liquids

We have to carry out the experiment in such a way so that there is no setting up of convection current in liquid due to density gradient so that there is no convective heat transfer effect (present at the aqueous solution interface) that affects the measured thermal conductivity.

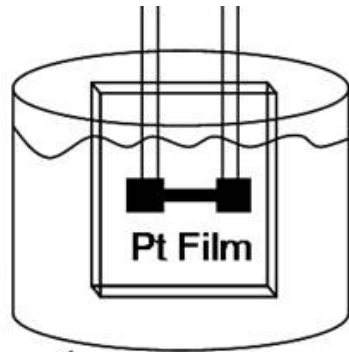


Fig.2.32. Schematic of the heater dipped inside the nanofluid solution

For minimising the transfer of heat due to convection process, the heater was dipped vertically in the fluid as shown in the above fig. 2.32. We know that in convection process the fluid which is near the heat source get heated up first and it moves up and denser fluid layer comes up. So there is an up down movement (convective current) due to density gradient of fluid. So if the heater is placed horizontally parallel to the bottom of the vessel then this up down movement will become effective. Also the fluid was in static condition and no macroscopic movement was observed within the fluid.

We have estimated the convective contribution and it is very small compared to the conduction part. This is because the maximum temperature swing in the measurement (i.e., the amplitude of the temperature oscillation) is very small. The $\delta T_{2\omega}$ is $\sim 25\text{mK}$. Due to the smallness of the value of $\delta T_{2\omega}$ the system has a very low Reynolds number R_a . For our experimental set-up $R_a < 200$. If $R_a < 10^3$, the natural convection decreases towards zero [15]. Thus, the heat transport in our experiment mainly arises from the conduction process and the convective contribution is negligible.

2.2.4.3 Agglomeration of nanoparticles

Since the nanoparticles has a tendency to get agglomerate and form a bigger cluster and finally settled down at the bottom. This hampers the enhanced thermal conductivity activity of the nanofluids. So it is very important to make sure that during the experiment the nanoparticles are well dispersed by taking some measures like ultrasonication etc.

Regarding agglomeration we monitor the stability of the ZnO nanofluid graph in fig.2.33 shows that the 3ω signal which is coming from the freshly prepared ZnO (in which particles are separated apart and does not coagulated) stays for a time period of 1.5hrs to 2hrs from the time of preparation of the nanofluid. We took our data within this time limit. Also to minimise the affect of coagulation, sample was ultrasonicated for a long time before every run of data.

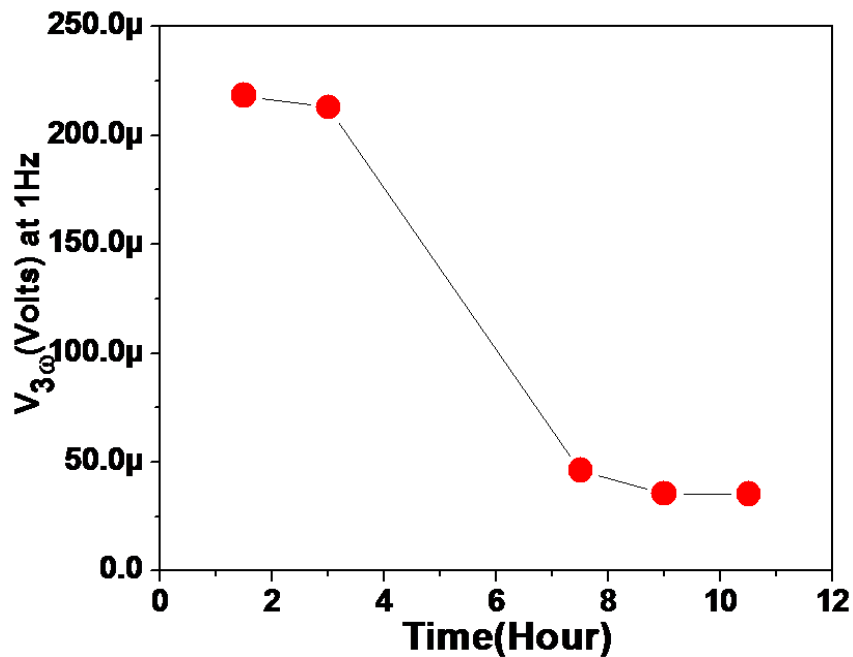


Fig. 2.33. 3ω signal of freshly prepared ZnO with the shelf life time (hrs)

2.2.4.4 Grounding of the setup

Such types of dynamic measurements are very precision measurements. Very small voltages of the order of few μ Vs are detected from the samples during the measurement process. In order to acquire a good noise free data we have to ensure a proper care of the grounding of

the setup and the chassis grounding of other allied electrical components so that stray noise and signals are directed to the ground for removal from the system. To ensure a efficient grounding we used very thick, good quality copper strips for making dedicated grounding other than the line grounding. 3 ω method involves frequency scan, we have to take care at those frequencies or multiples of them, which matches the AC supply main line frequency. In India AC supply takes at 50Hz so we have to skip the frequencies like 50,100,150 Hz etc so that there is no chance of interference with the measurement signals thereby eliminating the spurious signals. Bridge should be balanced and contact should give a noise signal as minimum as possible.

To ensure further protection from the environmental and neighbouring stray signals and other electrostatic fields we put the whole set up inside a specially built cage of μ metals which acts as a shield against such unwanted fields.

2.2.4.5 Instrumental error

Source of the error arises from eqn. (8) where one has to subtract two numbers Z_S and Z_{NF} which may in some cases are of comparable magnitude then it will induce error and more over it is squared again, cascading the error further.

We calculate all the things from the calculation of the Z as given by $Z \approx \frac{2A}{\alpha P} V_{3\omega}$

In terms of dimension we have $[Z] = \frac{[L^2 R]}{[V]}$

Now
$$\frac{\delta Z}{Z} = 2 \frac{\delta L}{L} + \frac{\delta R}{R} + \frac{\delta V}{V} \approx 2 \left(\frac{\delta L}{L} + \frac{\delta V}{V} \right) = 2(0.01 + 0.001) = 0.022$$

Since
$$\frac{\delta L}{L} \approx \frac{10^{-6}}{10^{-4}} \text{ \& \ } \frac{\delta V}{V} \approx \frac{10^{-9}}{10^{-6}} \text{ from resolution of microscope and LIA}$$

so
$$\frac{\delta Z}{Z} \approx 0.022, \text{ So the \% of error} = \frac{\delta Z}{Z} \times 100\% = 2.2\%$$

For frequencies, $f > 1$ KHz the detected voltage (μ V) becomes of the order of the instrumental resolution.

2.2.5 Summary

We describe the details of the setup for thermal measurement of the nanofluids. When everything is ready for action then the whole system is put inside especially made Faraday cage which insulate it from the outer electrostatic or electromagnetic disturbances.

Another important factor which is very important in such high precision low noise measurement is that the whole system should be well grounded with a dedicated thick special copper sheet.

Details of the experimental data, calibration, results are discussed in details in the Chapter 4 of this thesis.

References

- [1] O.M. Corbino, Phys. Z. 12, 292, 1911
- [2] Review of Scientific Instruments 76, 124902, 2005
- [3] Menon N, J. Chem. Phys. 105, 5246, 1996
- [4] Seshan, K. Handbook of Thin-Film Deposition Processes and Techniques - Principles, Methods, Equipment and Applications (2nd Ed.), William Andrew Publishing/Noyes, 2002
- [5] Doctoral Thesis of Dr. Venkat Kamalakar, arXiv: 1110. 5260v1, Oct 2011
- [6] Lide D R, Handbook of Chemistry and Phy. 81st ed. (Boca Raton, NY: CRC Press), 2000
- [7] J.A Woolam VASE Product Manual.
- [8] www.iet.ntnu.no

Chapter 3

Chapter 3: Sample Preparation & Characterisation techniques...

3.1 Introduction	82-83
3.2 Synthesis of ZnO nanostructures	84-85
3.2.1 Characterisation.....	85-90
3.3 Synthesis of ZnO nanostructures with capping layer.....	90-91
3.3.1 Characterisation.....	91
3.4 Synthesis of Silver Nanofluids.....	92
3.4.1 Characterisation.....	93-94
3.5 Synthesis of Gold Nanofluids.....	95
3.5.1 Characterisation.....	95-96
3.6 Synthesis of Gold Nanonetwork.....	97-99
3.6.1 Characterisation.....	99-101
3.7 Characterization techniques	102
3.7.1 Scanning Electron Microscope (SEM)	102-104
3.7.2 Transmission Electron Microscopy (TEM).....	104-106
3.7.2.1 High Resolution TEM (HRTEM)	107
3.7.2.2 Selected Area Diffraction (SAD).....	107-108
3.7.2.3 Energy-dispersive X-ray (EDX) spectroscopy.....	108
3.7.3 UV-visible absorption measurement	108-110

References

3.1 Introduction

This chapter will be dedicated towards the synthesis of nanofluids and then their characterisation by different methods. The system we have used is a very interesting one.

In this thesis we synthesise all the samples of nanofluids used in the present work. As a result syntheses of nanofluids, along with experimental measurement make an important component of the thesis.

Nanofluids are the two component system consisting of the base fluid, the liquid (continuous) medium and the solid nanoparticles which are dispersed in this medium as shown in fig.3.1.

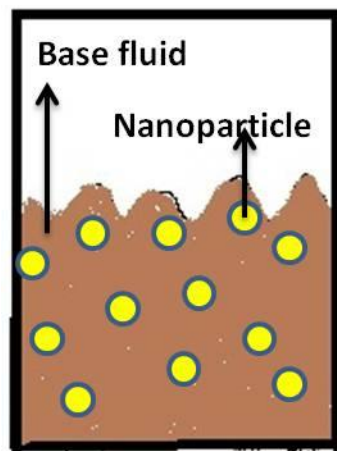


Fig.3.1 Schematic representation of the Nanofluid

There are various types of Nanofluids. Those have wide range of dispersion fluids and nanoparticles. In fig.3.2 it is showing the different kinds of material fluids which can act as the base fluid for such nanofluid systems. Similarly there is a wide range of nanoparticles material like metals, metal oxide, organic, inorganic, semiconductor etc.

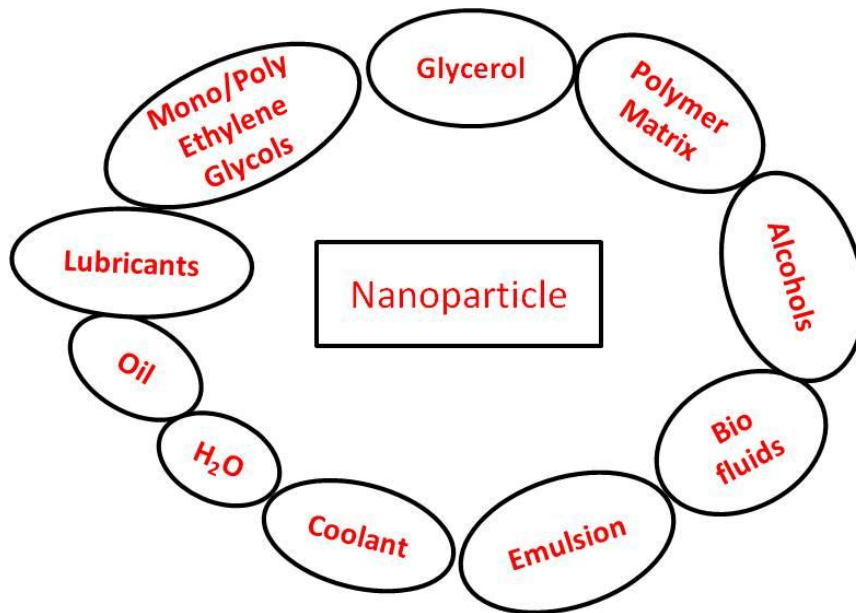


Fig.3.2. Diagram showing the nanoparticles with different types of base fluids

These nanofluids can be synthesised in two processes namely

- (a) **One Step process:** In this method the nanoparticles are made and simultaneously dispersed in the base fluid. This can be termed as the one pot synthesis process. This method is mainly used to synthesize metal nanofluids like Cu, Ag, Pt etc.
- (b) **Two Step process:** In this nanoparticles or other nanostructures are made separately by one of the physical or chemical processes (e.g., evaporation and inert-gas condensation processing) in the form of a dry powder and in the second step they are dispersed in the base fluid resulting a formation of nanofluids. Most of the nanofluids are made by this process. For example it is used for the materials like oxide and nanowires and nanotubes, graphite etc.

The two-step and one-step methods are discussed in more detail in Sections 2.1.1.1 and 2.1.1.2 respectively.

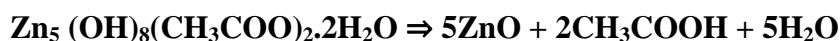
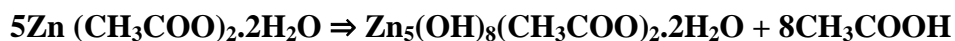
Now I will discuss in details about the synthesis of different nanofluids and nanostructures from our laboratory. We have made nanofluids using ZnO, Stable ZnO, Silver, Gold materials. An interesting Gold network structure is also synthesized by using PLD. These materials are widely used in our day to day to life and available abundantly.

3.2 Synthesis of ZnO nanostructures

One of the most famous and widely used research materials in nanotechnology field is Nanocrystalline ZnO particles. There are various reasons for it due to its easy availability, inexpensivity, biocompatibility. In technical terms Zinc oxide is a wide band gap (~3.3 eV) n type direct semiconductor having Wurtzite structure. Recently it has attracted enormous attention because of its unique optical properties [1,2].

ZnO Nanofluids is prepared by Acetate route (wet chemical method) which is a one step synthesis technique. These can be prepared from alcoholic solutions of zinc acetate dihydrate with or without using a base solution such as NaOH or KOH through a colloid process carried out at a temperature above 60°C [3].

First we prepare a 50mM Zinc acetate dihydrate and 100mM NaOH solution in ethanol separately. Then Zinc solution is heated for 1hr at temperature 60-65°C, and then slowly add NaOH solution to it the drop by drop with continuous magnetic stirring. Half an hour post heating, the solution is ready to produce 10nm size (average) ZnO nanocrystal. Reaction performed above 60°C avoids precipitation of Zn (OH)₂ and results in the formation of colloidal ZnO nanostructures of such a size range which appear sky blue because of Rayleigh scattering. It is revealed that layered hydroxide zinc acetate is formed as an intermediate and its transformation into ZnO is a key reaction step in any of the alcoholic solutions. The overall chemical reaction leading to the formation of ZnO from zinc acetate precursor follows the following chemical reactions [4].



After this heating process the resulting solution is centrifuge at high speed so that the solid white colored powder gets separate out and settle down at the bottom. Then it is separated out and again dissolved in the fresh alcohol solution. By this way any residual like Na etc are removed, then this solution is sonicated at high power for half an hour for proper dispersion of the nanoparticles in the base liquid. By this way the first sample of nanofluid containing ZnO nanoparticles was ready and it was for carrying out the measurement on it shown in fig. 3.3. This ZnO is without any capping agent or surfactant. Depending on the particle size, it has a finite shelf life. A freshly sonicated dispersion is stable for over an hour, which as we will see is long enough for experimental measurement.



Fig.3.3 Photo of the freshly prepared ZnO nanofluid

3.2.1 Characterisations

Solutions that are prepared are subjected to characterisation analysis using TEM, HR TEM, UV-Visible absorption spectra, EDAX on it. (All these techniques will also be discussed in details at the end of this chapter). We start with the TEM characterisation for finding the shape, size, size distribution, crystal structure of the nanoparticles. For this we have to prepare sample for TEM characterisation. TEM imaging requires a good sample preparation before investigation. Here Copper (Cu) grid with 1000 mesh is used as a matrix in which samples are imbedded. For this nanofluids are stirred vigorously for some time then by using micropipette 1 to 2 μl of the sample is dropped on the carbon coated side of the grid and then it is allowed to dry so that there is no liquid trace is there. Then it is put inside the TEM machine for analysis of the nanoparticles.

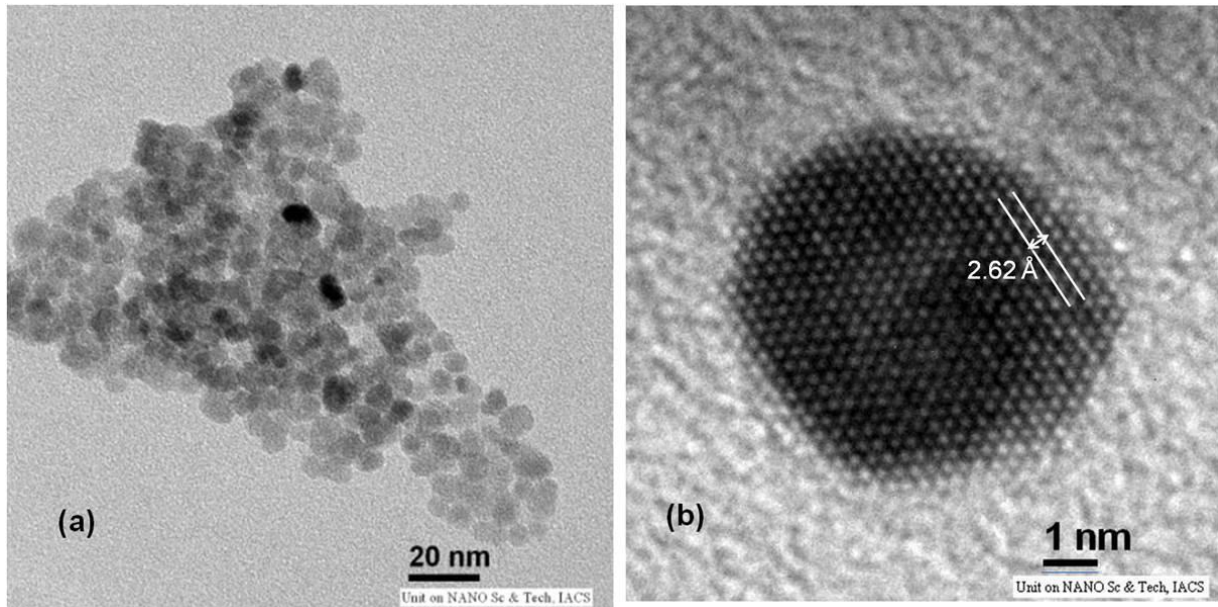


Fig.3.4. (a) TEM images of ZnO Nanoparticles (b) HRTEM image

TEM images are shown in fig.3.4. (a) These were taken from JEOL Ltd. (Japan) made TEM at an accelerating voltage of 200kV. We also took the High Resolution (HR) TEM image of a site on the nanoparticles as shown in fig.3.4. (b). In this a high concentration of e beam is focussed over a very small cross section on the crystal so that a very high resolution images can be taken with finer details which is evident from the criss cross of the lattice fringes of ZnO crystal as in fig.3.4. (b). It clearly shows that the particles are single crystal and show facetating with hexagonal shape. The distance between the parallel lattice fringes of the ZnO particle is 2.62 Å. This shows that it is a ZnO crystal.

We determine the size distribution of the nanoparticles from these TEM images. A typical size distribution of ZnO nanoparticles is shown in fig.3.5.

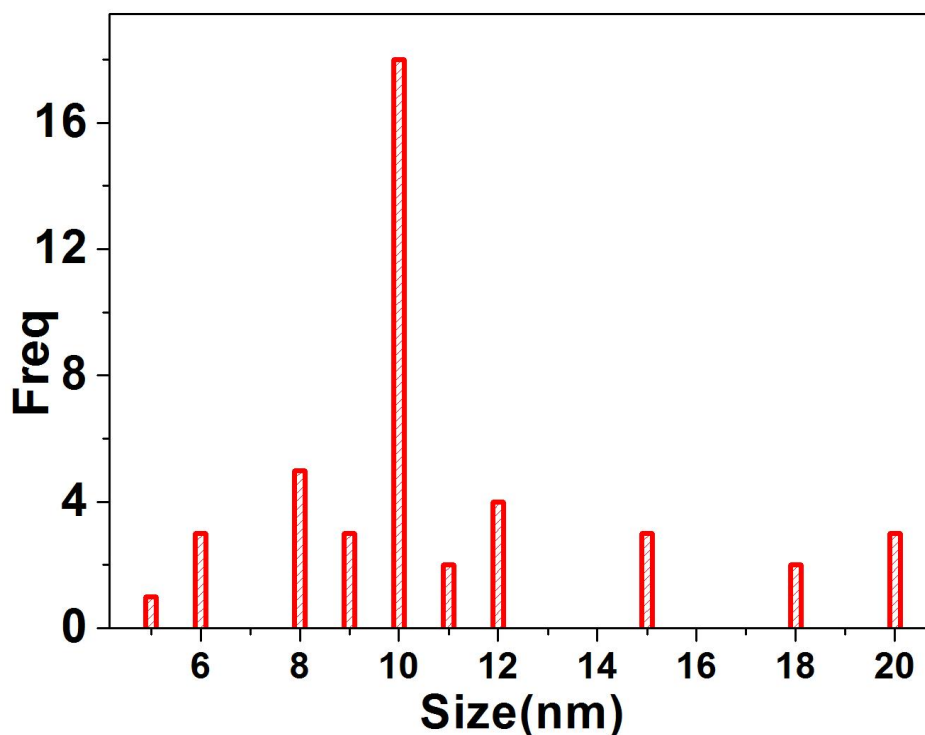


Fig.3.5. Size distribution chart of the ZnO nanoparticles

From above distribution we find that 80% of the particles have size lying in the range 10 ± 2 nm. The bigger size particles precipitate out. During the experiment we have used the solutions with different concentrations. To prepare samples with different concentrations we have the same size stabilized batch and the different concentrations were obtained by dilution of a mother batch.

Then to determine the actual elements presents in the solution we have done an EDX analysis by TEM itself. Data taken at an accelerating voltage of 200KV.

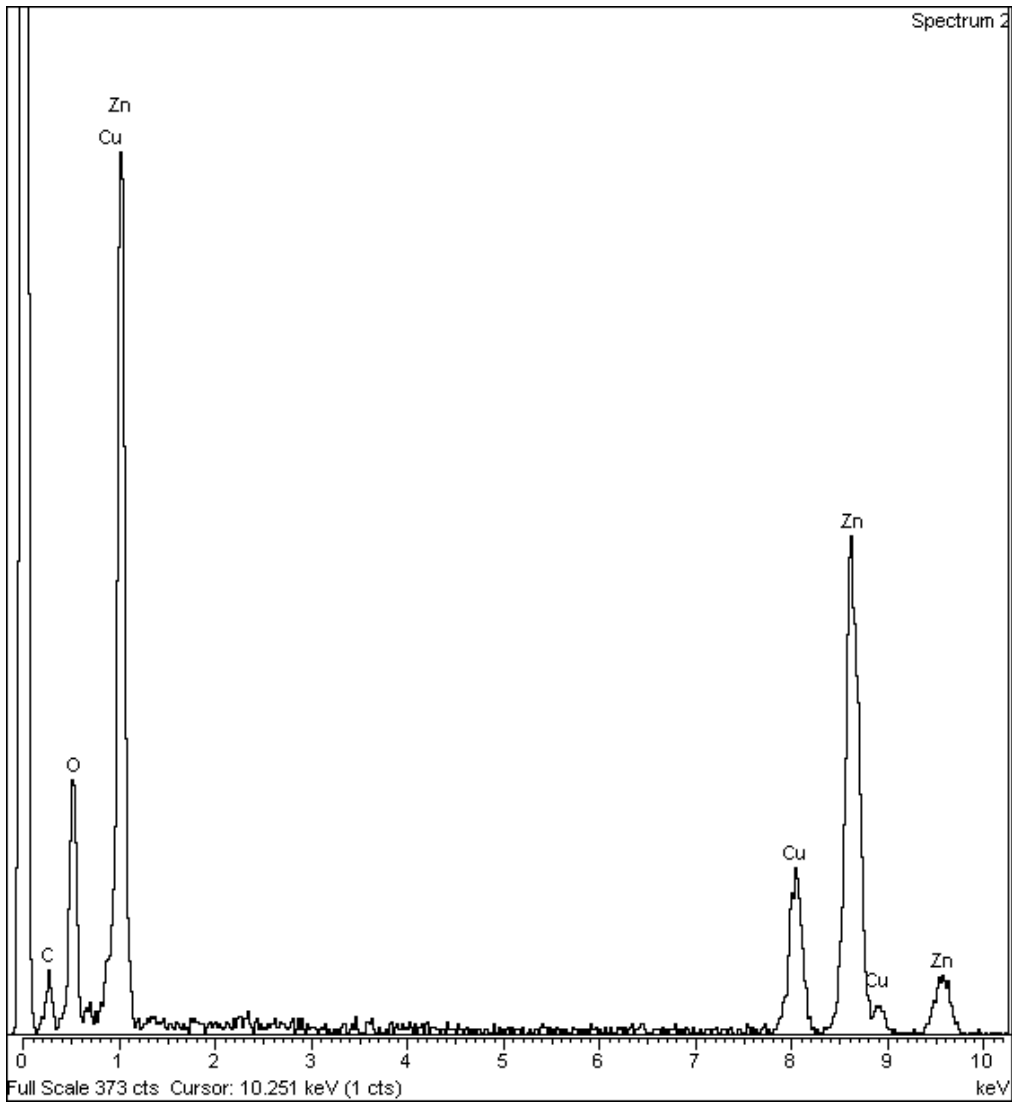


Fig.3.6. EDX spectrum of the ZnO nanoparticles on Cu grid/matrix

Table 3.1 shows the elements present with their corresponding weight %. Table clearly shows the abundant presence of Zn, O in the system.

Element	Peak	Area	k	Abs	Weight%	Weight%	Atomic%
	Area	Sigma	factor	Corrn.		Sigma	
C K	135	27	1.504	1.000	1.21	0.24	5.42
O K	658	51	1.309	1.000	5.14	0.40	17.22
Cu K	1070	59	3.363	1.000	21.45	1.05	18.11
Zn K	3160	96	3.832	1.000	72.20	1.10	59.25
Totals					100.00		

Table 3.1 Element analysis table for ZnO nanofluids

Fig.3.6 shows the SAED pattern of ZnO crystal. SAED patterns are a projection of the reciprocal lattice, with lattice reflections showing as sharp diffraction spots. SAED patterns can be used to identify crystal structures and measure lattice parameters [5]. The Pattern clearly shows the hexagonal facets of ZnO crystal.

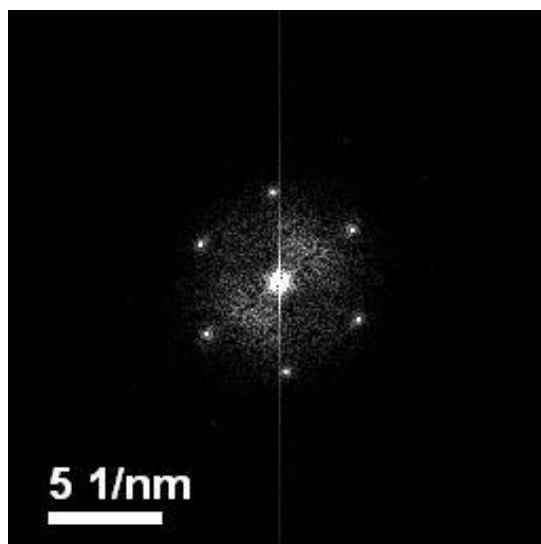


Fig.3.7. SAED pattern of ZnO crystal

After the structural characterisation, optical characterisation was done using UV-Visible absorption spectra for determining the band gap of the semiconducting ZnO. Absorption of light by solution is one of the oldest and still one of the most useful instrumental methods. The wavelength of light that a compound will absorb is characteristic of its chemical structure. Specific regions of the electromagnetic spectrum are absorbed by exciting specific types of molecular and atomic motion to higher energy levels.

Graph in fig.3.8 shows the absorption spectra of bare ZnO nanofluid at different time scale, starting with the freshly made sample. It is clear that there is decrease in the absorption as well right shift in the absorption spectra of the ZnO nanofluids as it is ages with time. The absorption peak is around the wavelength of 360nm and in terms of band gap energy it comes out to be 3.3 eV [6]

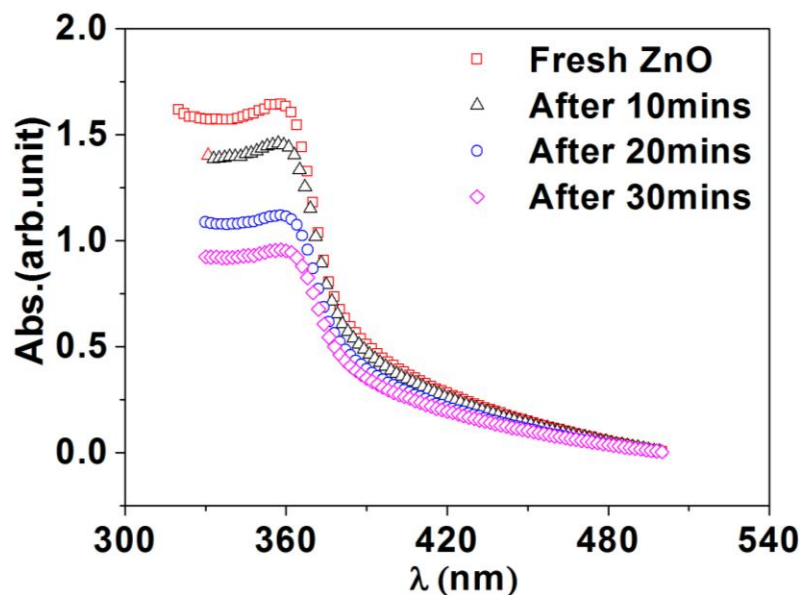


Fig.3.8. UV-Vis absorption spectra of ZnO nanofluid

This also provides an additional proof of the presence of the ZnO nanoparticles in the solution. When all these characterisation process are completed on this sample is finally ready to put inside the sample cell for measurements.

3.3 Synthesis of ZnO nanostructures with capping layer

Two things that make nanoparticles in to stable suspension are

- (1) Surface charge
- (2) Brownian motion (it is for this reason small particles are stable)

ZnO nanofluid which was synthesised by the above mentioned method are not so stable since they show a tendency to agglomerate and after some time they settle down at the bottom of the container. Hence they have very short shelf life.

To counter this tendency, particle dispersion additives are often added to the base fluid with the nanoparticles. This capping layer prevents the agglomerating nature of the nanoparticles by covering them with a thin layer. We have used PVP (PolyVinyl Pyrrolidone) to make stable ZnO nanofluids.

Synthesis of this nanofluid is same as that for bare ZnO nanofluid only additional step is mixing PVP powder to boiling solution before carrying out the final chemical reaction.

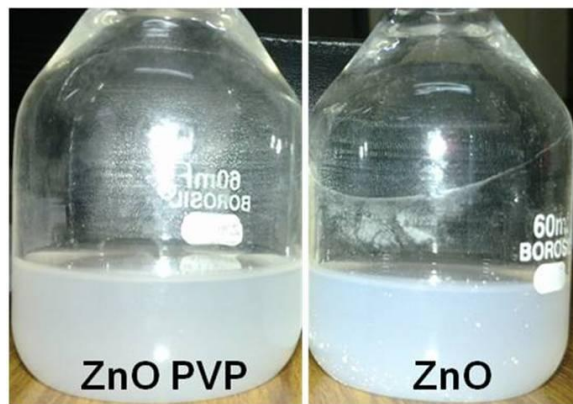


Fig.3.9. Photograph of the samples

3.3.1 Characterisation

This solution is stable and its stability is checked over a month. We monitor its stability by using UV absorption spectra time to time. This is shown in fig.3.10.

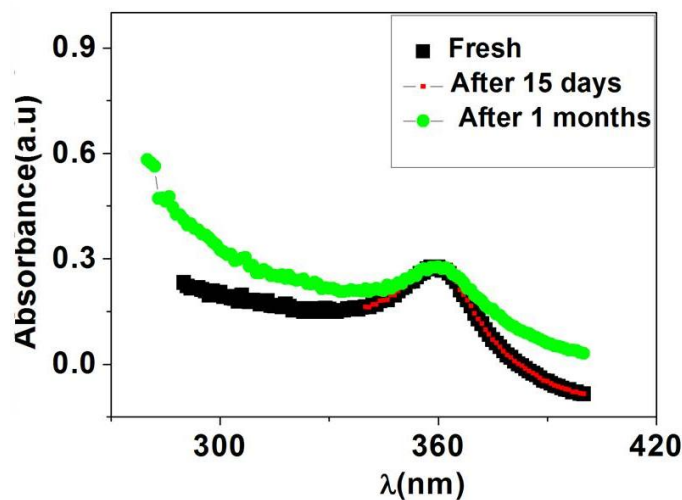


Fig.3.10 Absorption spectra of stable ZnO with time

3.4 Synthesis of Silver Nanofluids (AgNF)

We made Silver nanofluid by using wet chemical method in which the chemical reaction is carried out inside a microwave. It is a single step process in which Silver nanoparticles are synthesised and dispersed in the base fluid simultaneously. Recently, microwave irradiation has been widely applied to material science. Due to intense friction and the collision of molecules created by microwave irradiation, microwave irradiation not only provides the energy for heating but also greatly accelerates the nucleation. With microwave irradiation on the reactant solution, temperature and concentration gradients can be avoided leading to uniform nucleation and the obtained nanofluids have good stabilization. Microwave-based synthesis method is one of the easiest, energy-saving, and quick methods for largescale production of nanofluids [7].

Microwave synthesis has been applied to prepare stable silver nanofluids in ethanol by reduction of AgNO_3 with polyvinylpyrrolidone (PVP), used as stabilizing agent, having Ag concentrations of 1% by volume. The nanofluid with AgNO_3 to PVP weight ratio of 1:10 (vol. conc.=0.0114). Microwave synthesis of AgNF resulted in a formation of solution as shown in fig 3.11.



Fig.3.11. Photograph of the AgNF with UV absorption spectra alongside

3.4.1 Characterisation

We started characterisation of the nanofluid with the UV-Vis absorption spectra. Since it is a metal nanoparticle it has lots of free electrons on its surface and when they are fired with EM waves of proper wavelength they undergo a resonance at a particular wavelength and at this wavelength an absorption peak is observed there. For AgNF corresponding UV absorption which peaks at 420 nm is shown in fig.3.12.

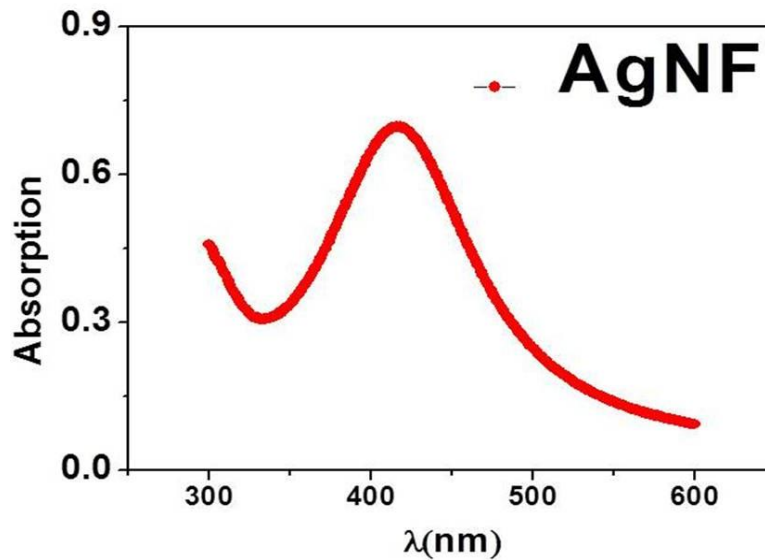


Fig.3.12. UV-Vis absorption spectra of AgNF

TEM images were taken to determine the size and size distribution of the Ag nanoparticles so formed. Fig.3.13 shows the TEM images of our lab made Ag nanofluid. From this we saw that the particles are spherical and very small also.

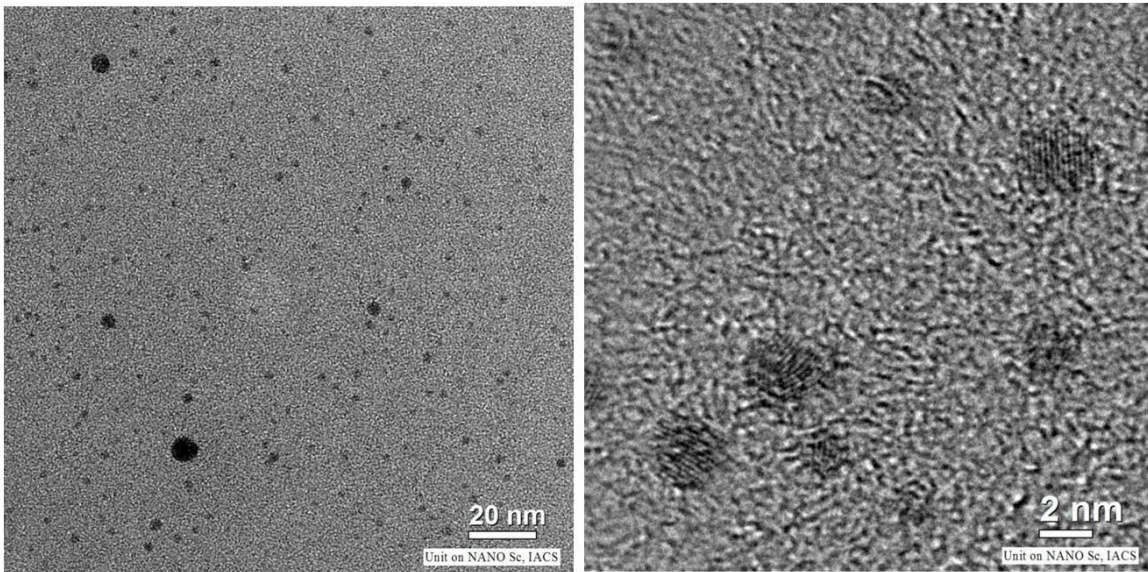


Fig.3.13 TEM image of homemade AgNF

From TEM images we plot the distribution curve of various sizes of the particles with their frequency of occurrence as shown in fig.3.14. It is clear that the average size is 5 ± 2 nm and more over it is very uniform with less distribution in variation of size.

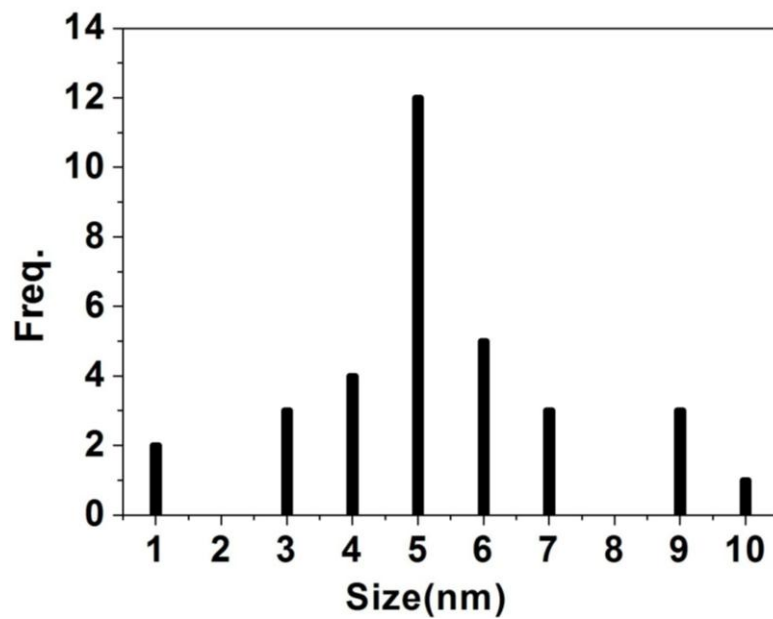


Fig.3.14. Size distribution chart of the Ag nanoparticles

Samples which are shown above are used for carrying out the measurement.

3.5 Synthesis of Gold Nanofluids

Last nanofluid that we synthesize in our lab is the Au NF. It is also prepared by one step wet chemical method. Nanoparticles are dispersed in Ethylene Glycol. Gold tetra Auro Chlorate ($\text{HAuCl}_4 \cdot 3\text{H}_2\text{O}$) is reduced with the help of PVP [8].

Sample is shown in fig.3.15.



Fig.3.15. Photograph of the Au nanofluids after preparation

3.5.1 Characterisation

TEM images of Gold nanofluids were taken with newly installed FEI made TEM facility in our centre. Fig.3.16 shows the TEM images of Au NF at different length scales. HRTEM image of the lattice fringes are shown in fig.3.16.(3)

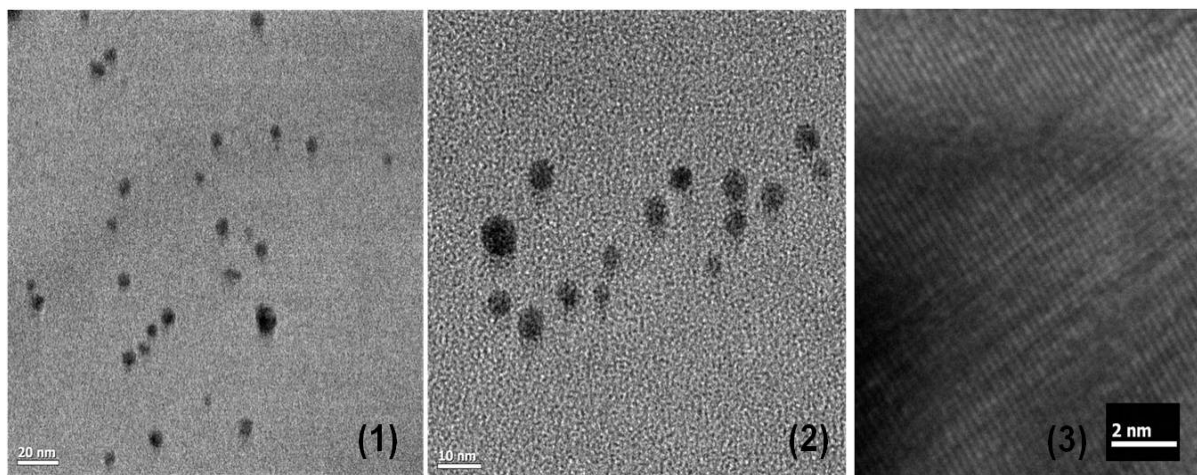


Fig.3.16 TEM, HRTEM image of AuNF taken at different length scale.

Average size of the nanoparticles is found to be around 5 ± 2 nm from the size distribution graph as shown in fig.3.17.

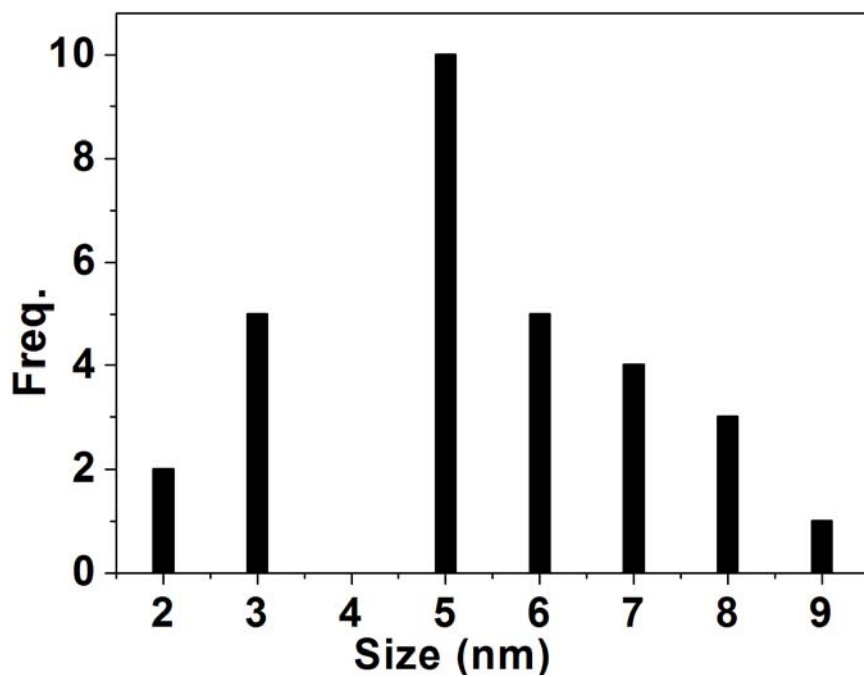


Fig.3.17. Size distribution chart of the Au nanoparticles

For elemental analysis EDX detector of TEM was used. Results are shown in fig.3.18. It is clear that it contains the Au nanoparticles.

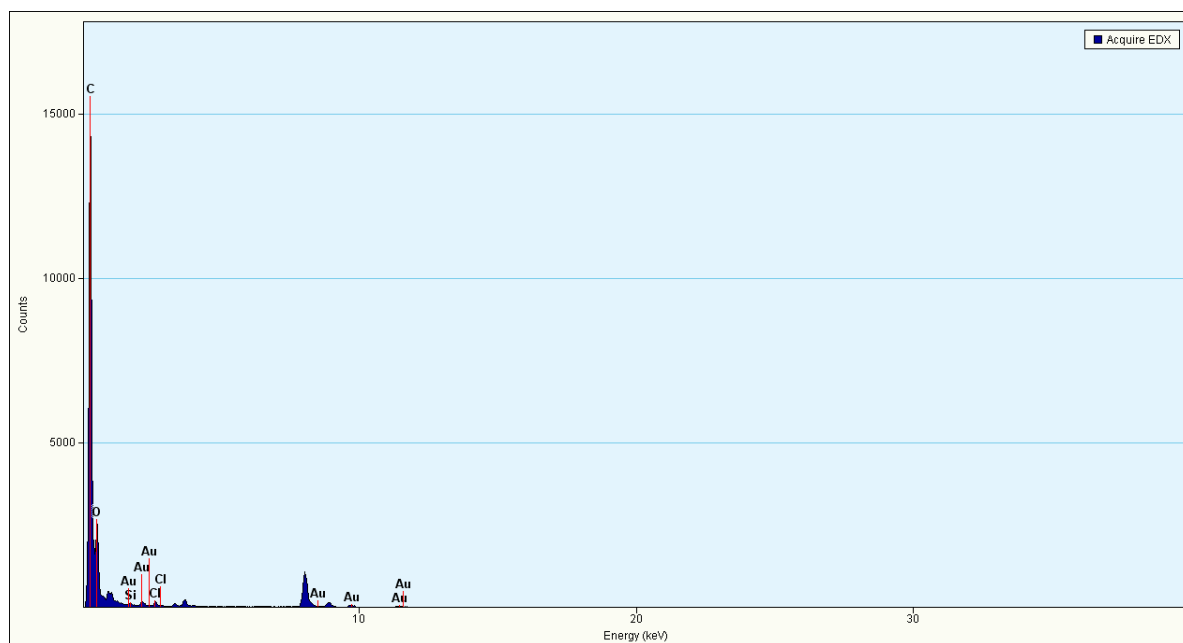


Fig.3.18. EDX spectrum of the Au nanoparticles on Cu grid/matrix

3.6 Synthesis of Gold Nanonetwork

In my thesis work it not only encompasses nanofluids but some newly developed structured materials also. These materials are not spherical particles as for the case of nanofluids. We use Pulsed Laser Deposition (PLD) system for this [9]. This method develops for the synthesis of such Au network structure during the thesis work has not been reported before.

This is simple one step and one pot synthesis of stable assembly of Au nanoparticles into chains in MEG (Mono Ethylene Glycol) medium, using only a solid metallic Au target (no precursors or reducing agent) and a pulsed excimer laser. It is noted that the method, presented here to make stable Au nanoparticle-chain, has the novelty that it is a single step, uses no surfactant or precursor and no reducing agent. The fact that the process uses no chemicals other than the Au target and biocompatible Ethylene Glycol, the Au nanochains so formed are immediately ready to use for any biological applications without any further purifications. The schematic of the set up used in this synthesis is shown in fig.3.19.

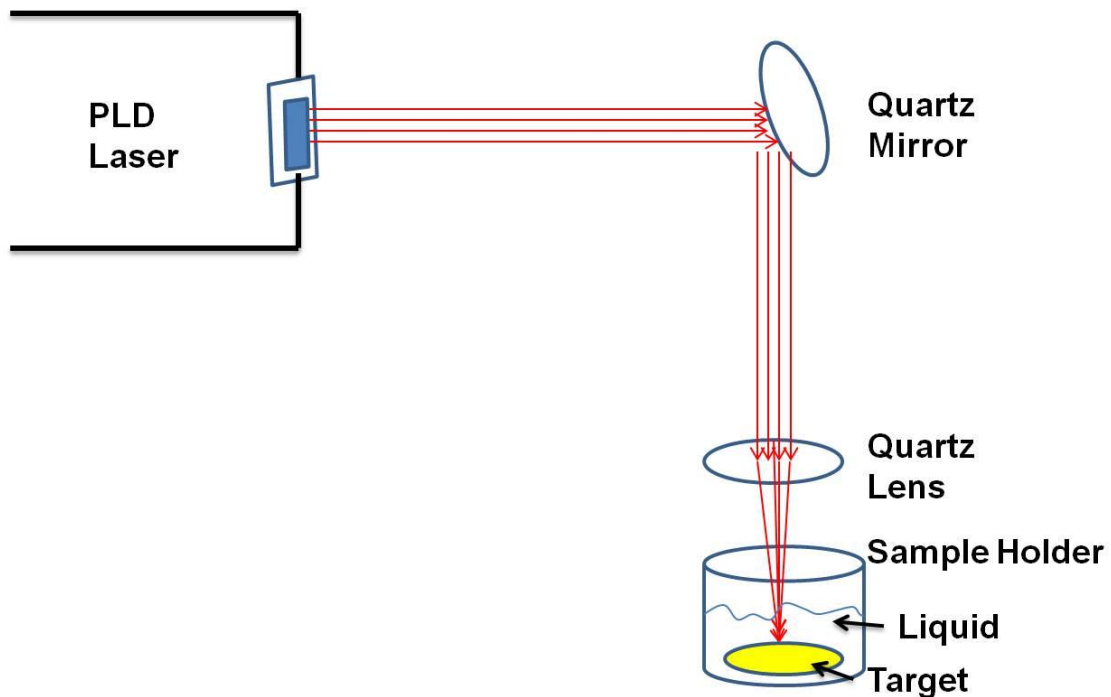


Fig.3.19. Schematic diagram of the PLD set up with allied optics

Surfactant-free Au nanonetworks were prepared by laser ablation of Au metal plate (>99.99%) which was placed on the bottom of quality quartz cuvette (10x20 mm²) (HELLMA GmbH, Germany) filled with 10mL of base fluids like DI water, commercially available Mono Ethylene Glycol (MEG) (GR grade from Merc. Chemicals Co.) and their mixer with different ratios. After proper focusing the laser ablation was performed by using the fundamental (248nm) of KrF gas (Coherent laser, Germany) pulsed laser operating at 5 Hz and energy was 200mJ, spot size was 5x2 mm², the fluence was 2 J/cm² and number of laser shots given was about 5000. All these parameters are optimised by trial and error method over several attempts we got the optimised condition for the growth of such structure. Initially DI water was used as a medium and after firing laser to the gold foil, the nanoparticles start forming inside the medium due to ablation of the outer surface of the gold. Fig.3.20 shows a TEM picture of the Gold nanoparticles thus formed. The HRTEM image of an individual particle is shown in the inset.

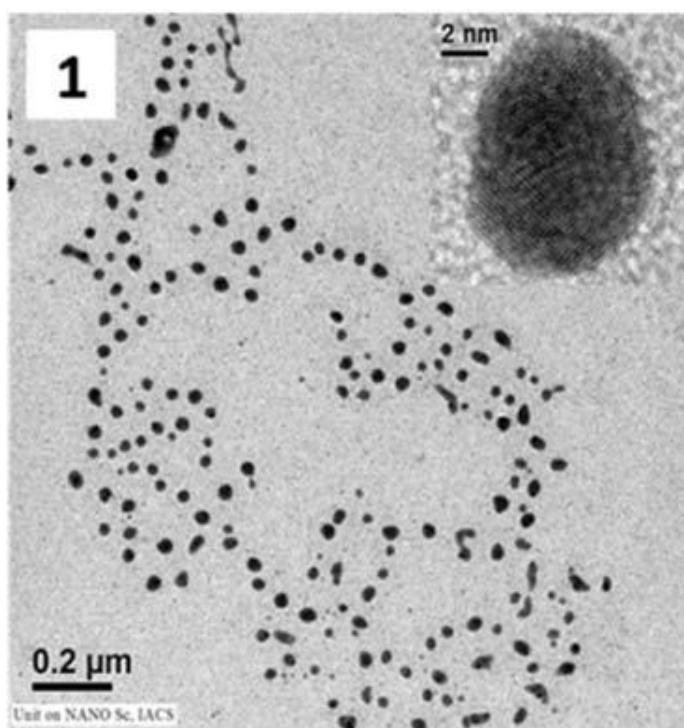


Fig.3.20. TEM image of Au nanoparticles. Inset is HRTEM image

Now the concentration of MEG was increased in the medium by adding MEG to DI such that the volume remains the same. Then MEG was added in DI water with proportion ranging from 25, 50, 75 and 100%. All the samples were made with the same laser fluence as well as the number of shots.

3.6.1 Characterisation

For morphological characterisation SEM, TEM, EDX images were taken using (FE-SEM, FEI HELIOS 600) using 30kV electrons and 200kV JEOL JEM 200CX respectively. TEM and SEM images are shown in fig.3.21. (a),(b),(c).

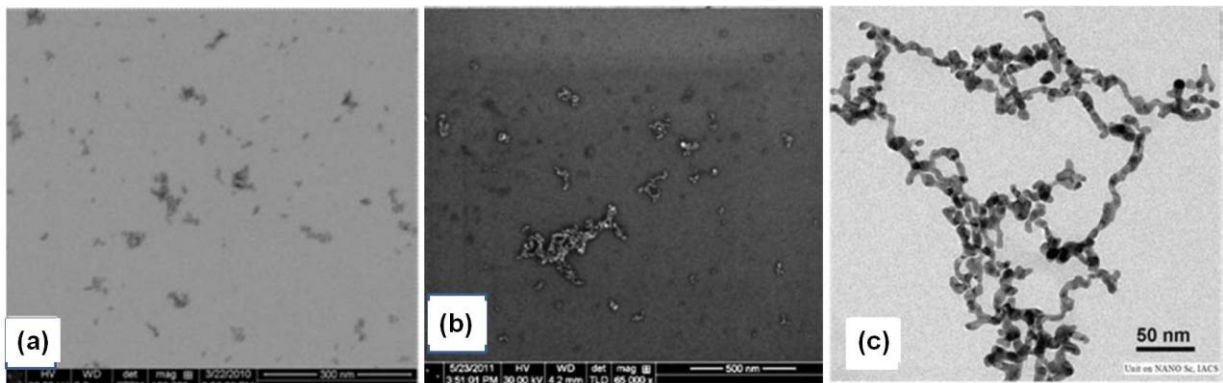


Fig.3.21. Images of the nanoparticles and the networked structure in different samples. (a) for 50% MEG (b) for 75% MEG and (c) for 100% MEG.

Thus when the whole medium is MEG then complete network structure is formed. These network of chains spans over a large surface area when transferred to a solid surface.

We were able to transfer the network on Si (100) wafer (with native oxide, typically 10nm thick) by drop coating. SEM Image in fig. 3.22 shows the typical physical spread of the network of Au nanoparticle chain that spans over lengths more than 5 μ m or more and it can be transferred on to substrates like Si, Glass etc., so that it can be used to make devices using electrodes fabricated by lithography, FIB. As stated, the length scale of the organized structure is thus more than 3 orders of magnitude larger than the individual nanoparticles.

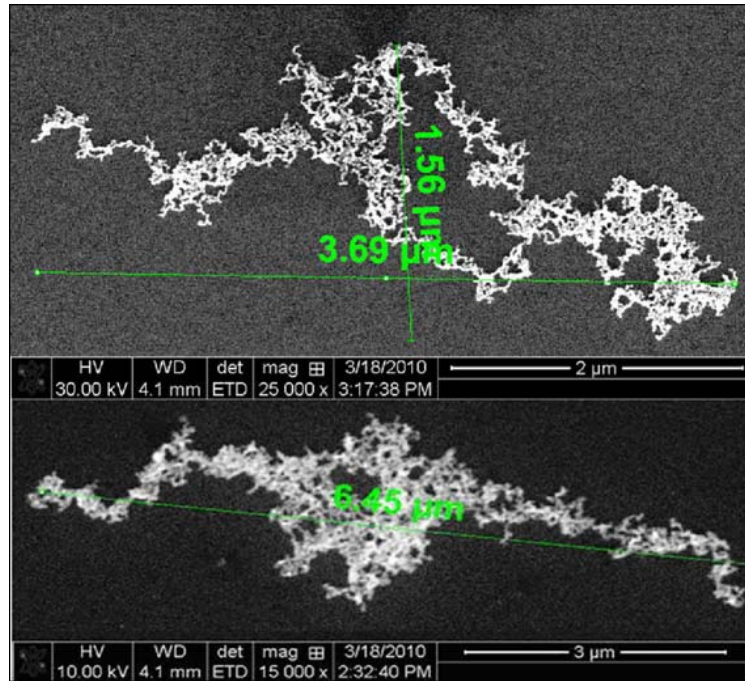


Fig.3.22. SEM images of the network structure after transferred to Si substrate (100)

When we further inspect the structure of these networks at high resolution by TEM, we get the following images of it as shown in fig.3.23. (a), (b), (c).

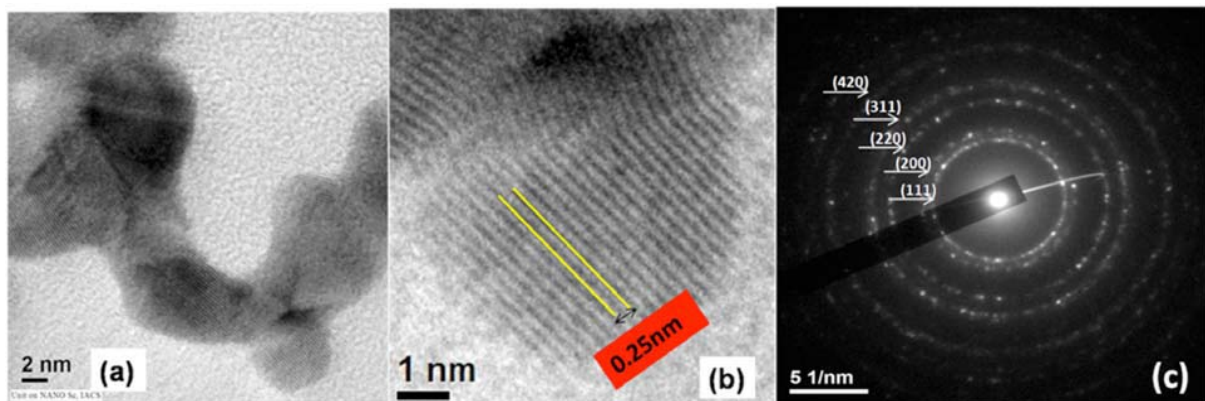


Fig.3.23.(a) TEM image of Au network. (b) HRTEM image (c) Diffraction pattern of Gold

Optical characterisation of the colloids was done by using UV- Vis spectra (400-700nm) of the samples were recorded on a Shimadzu UV-2408 spectrometer.

Fig.3.24 shows the variation of the UV-vis spectra for samples containing different proportion of MEG to DI water. As the proportion of MEG is gradually increased in the solution, there is a corresponding broadening of the absorption spectra to the long wavelength region. The change is in the UV-Visible spectra on the Au chain formation, in particular red-shift of the surface plasmon band and its broadening on formation of chains. Interestingly the coexistence of two species can be seen in the UV-Visible absorption spectra that shows the 520 nm line (from nanoparticles) superimposed on a broad peak due to formation of chains. When the base liquid contains the MEG only, UV-Vis spectra shows a broad absorption extending from 500 to 700 nm and beyond. In this case no plasmon peak is seen at 525nm arising from isolated nanoparticles. The gradual increase of the network structure with MEG concentration indicates that it plays an essential role in the chain formation. There is a transformation from the isolated nanoparticles in pure water to chain formation and a network structure as the percentage of MEG is increased. This observation also allows us to tailor the absorption of the medium by just varying the relative concentration of the DI water to MEG in the base liquid.

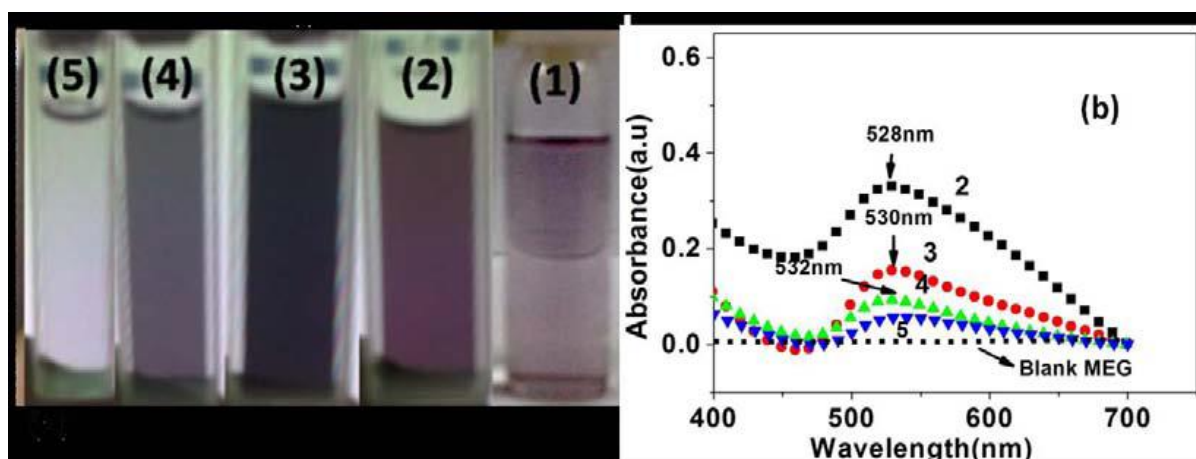


Fig. 3.24. (a) Visual appearance of the samples, (b) Corresponding UV-Vis spectra.

The nanoparticle chains (with fractal type structure) can approach a length even as large as $10\mu\text{m}$. It is thus a continuous and stable assembly that spans a length of nearly 1000 times the smallest entity (the Au nano particle). These network structures are mechanically stable.

3.7 Characterisation Techniques

From above all discussion in this chapter it is clear that our samples are ready to use and their characterisation is also completed.

In this section we will discuss in details the working principal of those characterisation techniques which are used in this chapter. For understanding the working principal of all types of microscope or magnifying apparatus we must understand the basic concept of resolution. This will give the answer to the question why we have to resort to use the e beam for getting much higher resolution than optical signals.

3.7.1 Scanning Electron Microscopy (SEM)

A scanning electron microscope (SEM) is a type of electron microscope that images a sample by scanning it with a high-energy beam of electrons in a raster scan pattern. A typical SEM picture is shown in fig.3.25. It is FEI made model.

In a scanning electron microscope, electrons emanating from a hot tungsten filament (thermionic emission)/sharp tungsten tip (field emission type) are accelerated by a high potential difference and collimated to a sharp beam. The beam traversing through a series of electromagnetic lenses is made to raster the surface of the sample under observation. The high energetic electrons after during interaction with the sample give rise to various signals collected by the respective detectors as a function of beam spot position on the sample giving rise to information of the topography of the sample. The electrons interact with the atoms that make up the sample producing signals that contain information about the sample's surface topography, composition, and other properties such as electrical conductivity.

The types of signals produced by an SEM include secondary electrons, back-scattered electrons (BSE), characteristic X-rays, light (cathodoluminescence), specimen current and transmitted electrons.

Secondary electron detectors are common in all SEMs, but it is rare that a single machine would have detectors for all possible signals. The signals result from interactions of the electron beam with atoms at or near the surface of the sample. In the most common or standard detection mode, secondary electron imaging or SEI, the SEM can produce very high-resolution images of a sample surface, revealing details upto few nm in size. Due to the very narrow electron beam, SEM micrographs have a large depth of field yielding a

characteristic three-dimensional appearance useful for understanding the surface structure of a sample. Back-scattered electrons (BSE) are beam electrons that are reflected from the sample by elastic scattering. BSE are often used in analytical SEM along with the spectra made from the characteristic X-rays. Because the intensity of the BSE signal is strongly related to the atomic number (Z) of the specimen, BSE images can provide information about the distribution of different elements in the sample.



Fig.3.25. FEI made SEM in our lab

The raster scanning of the CRT display is synchronised with that of the beam on the specimen in the microscope, and the resulting image is therefore a distribution map of the intensity of the signal being emitted from the scanned area of the specimen.

Fig.3.26 which is taken from reference [10], illustrates the internal parts of the SEM machine.

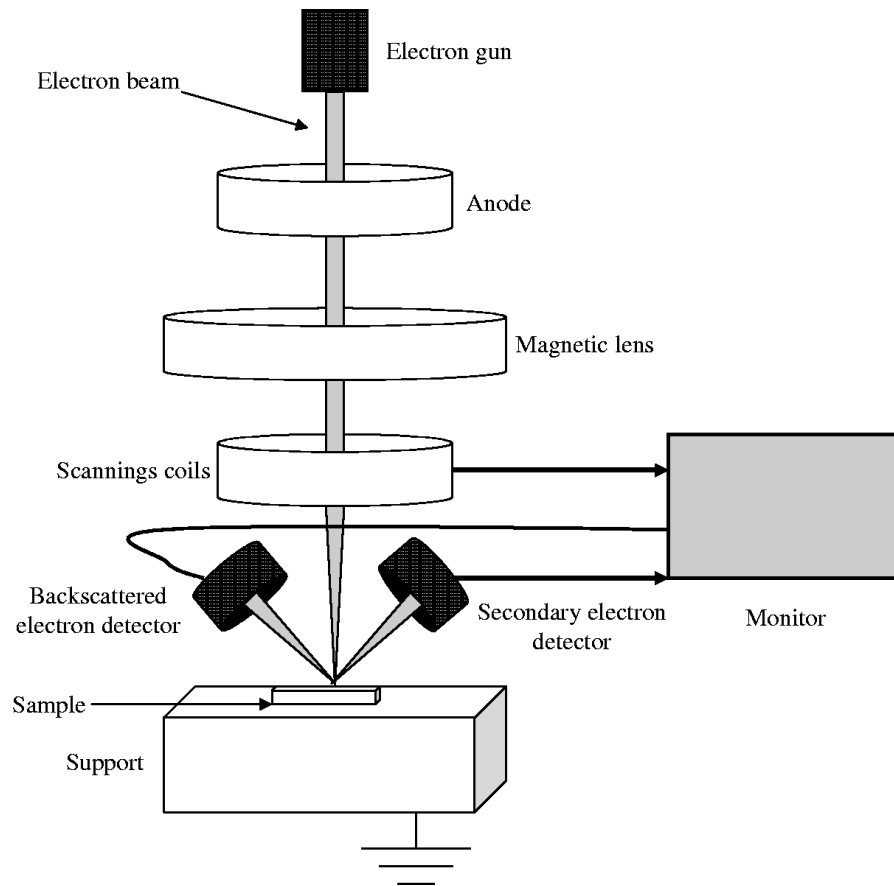


Fig.3.26 Internal structure of SEM [10]

3.7.2 TEM (Transmission Electron Microscope)

This instrument is similar to SEM but there is a basic difference that TEM works in the transmission mode unlike SEM which works in the reflection mode. In this highly energetic electron beams are made to pass through the sample under investigation and the transmitted beam contains the information about the sample after its interaction with it.

The diffraction pattern and image are formed at the back focus plane and image plane of the objective lens. If we take the back focus plane as the objective plane of the intermediate lens and projector lens, we will obtain the diffraction pattern on the screen. It is said that the TEM works in diffraction mode. If we take the image plane of the objective lens as the objective plane of the intermediate lens and projector lens, we will form an image on the screen. It is the image mode. Fig.3.27 which is taken from reference [11] shows a schematic outline of a TEM.

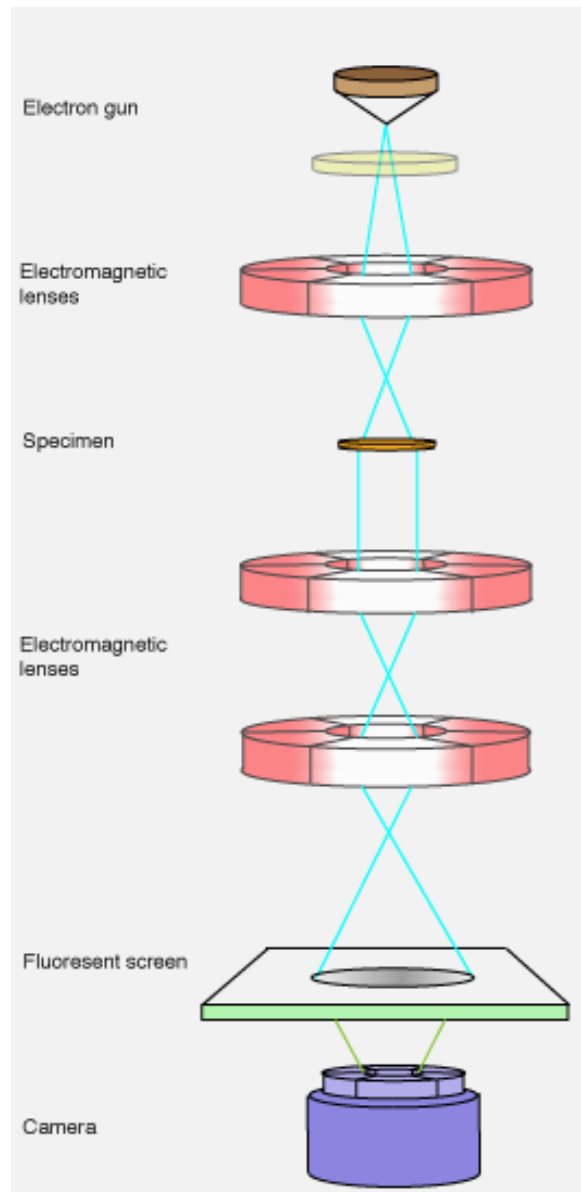


Fig. 3.27 The schematic outline of a TEM.[11]

A TEM contains four parts: electron source, electromagnetic lens system, sample holder, and imaging system. We will explain them as follows

- (a) *Electron source*: The electron source consists of a cathode and an anode. The cathode is a tungsten filament which emits electrons when being heated. A negative cap confines the electrons into a loosely focused beam. The beam is then accelerated towards the specimen by the positive anode. Electrons at the rim of the beam will fall

onto the anode while the others at the center will pass through the small hole of the anode. The electron source works like a cathode ray tube.

- (b) *Electromagnetic lens system:* After leaving the electron source, the electron beam is tightly focused using electromagnetic lens and metal apertures. The system only allows electrons within a small energy range to pass through, so the electrons in the electron beam will have a well-defined energy.
- (c) *Sample holder:* The sample holder is a platform equipped with a mechanical arm for holding the specimen and controlling its position.
- (d) *Imaging system:* The imaging system consists of another electromagnetic lens system and a screen. The electromagnetic lens system contains two lens systems, one for refocusing the electrons after they pass through the specimen, and the other for enlarging the image and projecting it onto the screen. The screen has a phosphorescent plate which glows when being hit by electrons. Image forms in a way similar to photography.

The origin of the image contrast in TEM comes from the variation of intensities of transmitted and diffracted beams due to the differences in diffraction conditions of the electron path depending on the microstructural features. Electrons of 200 kV excitation transmitted through about 0.1 μm thin foil specimen are diffracted according to Bragg's Law, forming a diffraction pattern (consisting of a transmitted and diffracted beam spots). Although diffraction phenomenon is a complex interaction of charged electrons with the periodic potential field of the lattice, Bragg's Law or Laue Conditions are sufficient approximations for usual practical applications. A diffraction pattern is, in the simplest sense, a Fourier transform of the periodic crystal lattice, giving us information on the periodicities in the lattice, and hence the atomic positions

3.7.2.1 High-resolution TEM (HR-TEM)

This is a part of the TEM measurement system. High-resolution TEM in general refers to imaging in which lattice fringes (i.e. crystallographic planes) are observed or atomic resolution is achieved. TEM, HRTEM images are formed from a number of diffracted beams; this multi-beam approach is known as phase-contrast imaging, and is necessary to construct an image of the crystal lattice. HRTEM provides access to much information about the sample, such as analysing crystalline defects and interfaces at the atomic scale, and observing and verifying devices, multilayers, nanocrystals and nanostructures. Just for sake of understanding HRTEM images of some particles are given in fig.3.28

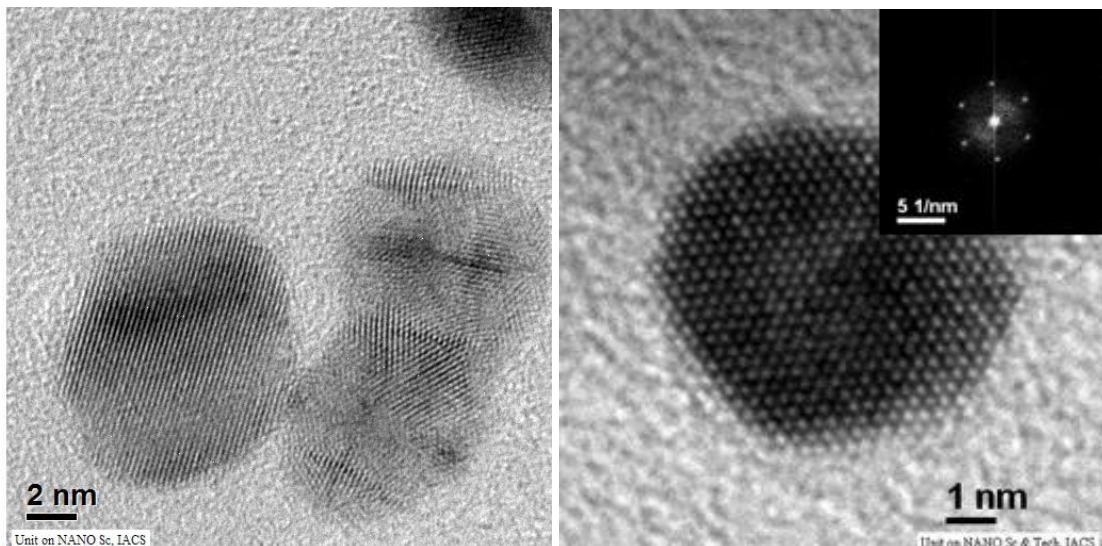


Fig.3.28. HR TEM of Silver & ZnO Nanoparticle

3.7.2.2 Selected-area diffraction (SAD)

A diffraction pattern is made under broad, parallel electron illumination. An aperture in the image plane is used to select the diffracted region of the specimen, giving site-selective diffraction analysis. SAD patterns are a projection of the reciprocal lattice, with lattice reflections showing as sharp diffraction spots. SAD patterns can be used to identify crystal structures and measure lattice parameters. Other uses of SAD include analysis of: lattice matching; interfaces; twinning and certain crystalline defects. SAD

of nanocrystals gives ring patterns analogous to those from X-ray powder diffraction, and can be used to identify texture and discriminate nanocrystalline from amorphous phases. SAD can obtain diffraction information from relatively small volumes.

3.7.2.3 Energy-dispersive X-ray (EDX) spectroscopy

This is a compositional analysis technique. It depends on the Z value of the element. The high energy electron beam can eject electrons from inner-shell atomic orbitals. The resulting vacancies are filled by electrons from higher energy shells; electron energies lost during these transitions are emitted as X-rays. The transitions, and hence X-rays, have energies that are characteristic of the atomic species. Therefore, measuring the X-ray spectrum allows identification of the sample composition. Highly localized information about the elemental composition of the sample can be obtained, with the spatial resolution determined primarily by the probe size. EDXS is a relatively straightforward technique experimentally, but it requires precalibration of the specific EDXS analysis system using standards of known composition.

3.7.3 UV-visible absorption measurement

Absorption of light by solution is one of the oldest and still one of the most useful instrumental methods. The wavelength of light that a compound will absorb is characteristic of its chemical structure. Specific regions of the electromagnetic spectrum are absorbed by exciting specific types of molecular and atomic motion to higher energy levels. Absorption of microwave radiation is generally due to excitation of molecular rotational motion. Infrared absorption is associated with vibrational motions of molecules. Absorption of visible and ultraviolet (UV) radiation is associated with excitation of electrons, in both atoms and molecules, to higher energy states. All molecules will undergo electronic excitation following absorption of light. Thus in this instrument we measure the electronic excitations.

The internal structure of the UV-Vis spectrometer is shown in fig.3.29 which is taken from reference [4].

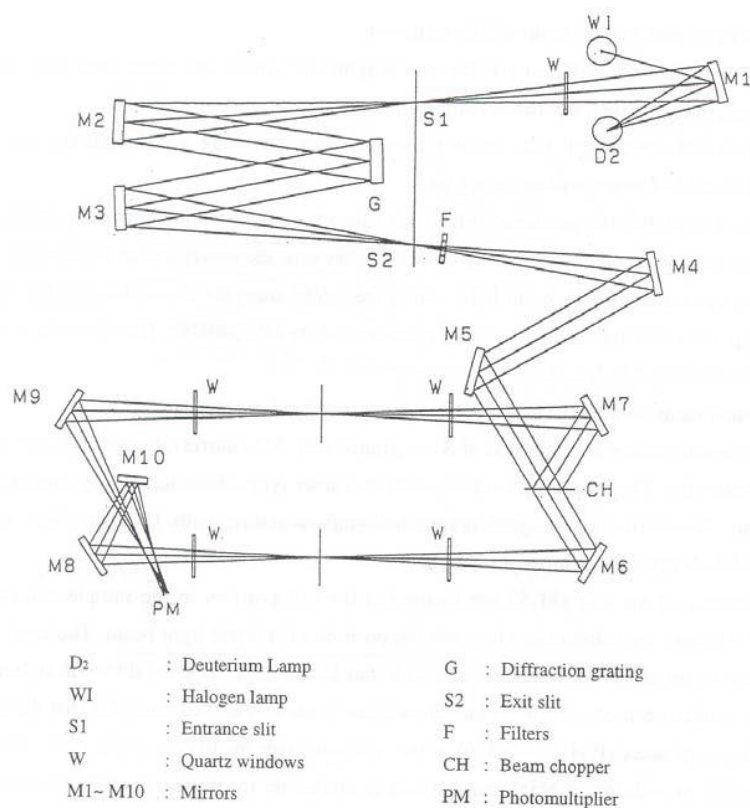


Fig.3.29 Internal structure of the UV-absorption system [4]

The amount of light, I , transmitted through a solution of an absorbing chemical in a transparent solvent can be related to its concentration by Beers Law:

$$-\log (I/I_0) = A = \epsilon . b . c$$

where I_0 = incident light intensity

A = absorbance (a defined quantity, also referred to as the optical density, or OD)

b = cell path length (cm)

c = solution concentration in moles/litre, and

ϵ = molar absorptivity (molar extinction coefficient) litre/mole/cm and is a function of wavelength (λ).

Thus absorption spectroscopy can be used mainly to quantify the amount of chemical present in an unknown solution. The scanning spectrophotometer measures the intensity of transmitted light of a narrow bandpass, and scans the wavelength in order to collect a spectrum. Because absorption is a ratiometric measurement, these instruments generally require the user to measure two spectra, one sample and one blank. The dual beam method is faster, and has the added advantage that lamp drift and other slow intensity fluctuations are properly accounted for in the ratio calculation. Collecting spectra with scanning spectrophotometers is slow, but the instruments often have very high resolving power owing to the use of photomultiplier tube detectors, which can be used with very narrow slit widths. A photodiode array is a 1 or 2 dimensional. Stack of individual photodiode detectors, each of which makes an independent measurement of the incident light intensity at its particular location.

References

- [1] U Ozgur, Y I Alivov, C Liu, A. Teke, M A Reshchikov, S Dogan, V Avrutin, S-J Cho and H Morko, J. Appl. Phys. 98, 041301, 2005
- [2] S. J. Pearton et al. J. Appl. Phys. 93 1, 2003
- [3] P Uthirakumar, B. Karunagaran, S. Nagarajan, E-K Suh and C-H Hong, Journal of Crystal Growth 304, 150, 2007
- [4] Optical Properties of ZnO-based Nanostructured Materials, Doctoral thesis of Dr. M. Ghosh, S.N.Bose Centre, 2008
- [5] <http://cime.epfl.ch/page-26783.html>
- [6] S. ilican, Y. Caglar, M. Caglar, Journal of Optoelectronics & Advanced Materials Vol.10, no.10,p. 2578, 2008
- [7] Raykar, Vijay S.; Singh, Ashok K. Colloid Polym Sci, 286,1667, 2008
- [8] P.-Y. Silvert, K. Tekaiia-Elhsissen, Solid State Ionics, 82, 53-60, 1995
- [9] Rajesh Kr. Neogy, Rajib Nath, Micro and Nanosystems, Vol. 3, No. 4, 1-7, 2011
- [10] www.emeraldinsight.com
- [11] www.cryoem.berkeley.edu

Chapter 4

Chapter 4: Heat Transport Measurement in ZnO Nanofluid.....

4.1 Introduction	117-118
4.2 Measurement process.....	118-121
4.3 Finite Size Effect.....	122-123
4.4 Calibration.	124-126
4.5 ZnO Nanofluid measurement.	127-130
4.5.1 Temperature Dependence.....	131
4.5.2 Volume fraction (ϕ) Dependence.....	131-133
4.6 Analysis of the frequency dependence.....	134-135
4.7 Physical interpretation.....	136-137
4.8 Conclusions.....	137

References

4.1 Introduction

In this chapter we investigate ZnO based nanofluids using 3 ω technique. Our main motivation is to study whether there is any frequency dependency of the thermal parameters. Previous two chapters dealt with the build up of the 3 ω measurement setup and the synthesis of the samples. Before the measurement is done, the regime of the operating frequency (ω) should be chosen. There is some restriction on the choice of frequency of the applied A.C voltage range for scanning the sample depending on the size and thermal properties of heater and the sample which is used for investigation. The operating frequency must be much less than $\frac{\kappa}{C_p L^2}$, the inverse of time required for thermal equilibrium across the film. Where κ is the thermal conductivity, C_p is volumetric specific heat of the material of the film/heater and L is smallest dimension of the film at $x = 0$ plane (i.e inplane).

To avoid back reflection, thermal wavelength of the liquid sample should be greater than the width of the film. The frequency dependent thermal diffusion length is given as

$$\lambda_{th} = \sqrt{D/2\omega}, \text{ where } D = \text{Thermal diffusivity} = \kappa/\rho C_p = 9 \times 10^{-8} \text{ m}^2/\text{sec for Ethanol [1].}$$

When we plot the λ_{th}/W vs the frequency we got behaviour as shown in fig.4.1.

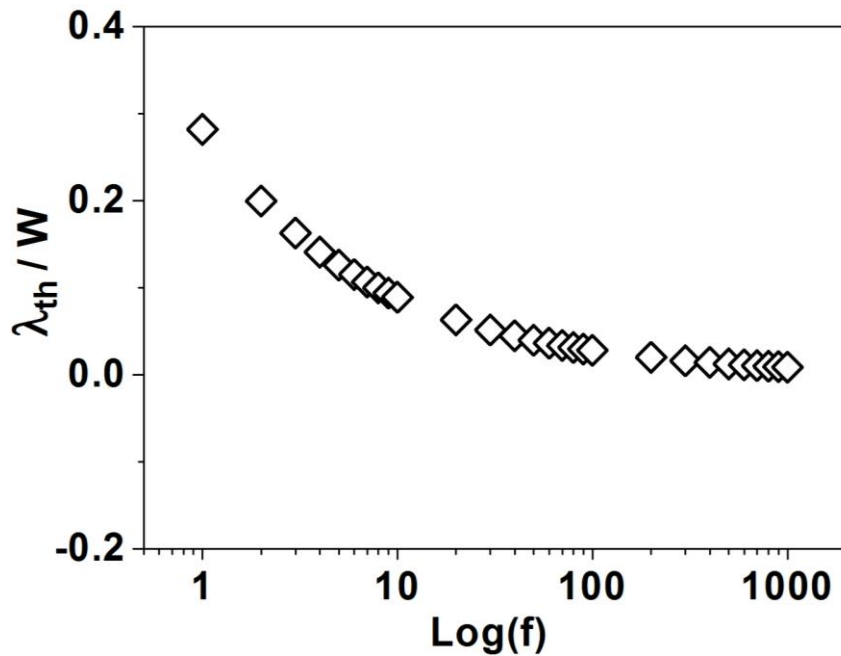


Fig.4.1. Plot of the ratio λ_{th}/W w.r.t frequency

The following part of the introduction describes some of the measurement, namely the size of the heater and the thermal diffusion length

From above we find that at the two extreme frequencies $\omega=1\text{Hz}$ & 1000 Hz , the corresponding wavelengths are $\lambda_{\text{th}}\sim 5\mu\text{m}$ & $90\mu\text{m}$.

This gives the lower bound on the frequency coming from the characteristics time for heat to leak/dissipate to the surrounding temperature bath. So the width of the film must be greater than the $200\mu\text{m}$ to start scan with frequency starting with 1Hz . Keeping above figures in mind we have taken a heater of width 0.3mm .

Wider films are used for low frequency range and narrower films are for higher frequency range of the applied a.c voltage. Another thing is that there must be good thermal contrast between the films and substrate and thermal conductivity of the film must be less than the thermal conductivity of the sample which is to be investigated. When we used this heater for measurement we found that after 1 KHz , the signal becomes very small in magnitude and reaches the resolution of the instrument. Thus for our heater upper limit of frequency comes out to be less than 1 KHz . Thus we cover three decades of frequency range $1\text{Hz}-1\text{ KHz}$.

4.2 Measurement process

We are using heater simultaneously as a thermometer so we have to find the temperature oscillation at the heater due to the periodic oscillating joule heating produced as a result of the applied oscillating voltage. The temperature oscillation at the heater is obtained by solving the heat diffusion equation with the boundary condition being that of an infinite plane sinusoidal heat source. Heater geometry is shown in fig.4.2 with the heater lying in $x=0$ axis plane with the substrate and the liquids are in the beneath of it i.e $x<0$ region.

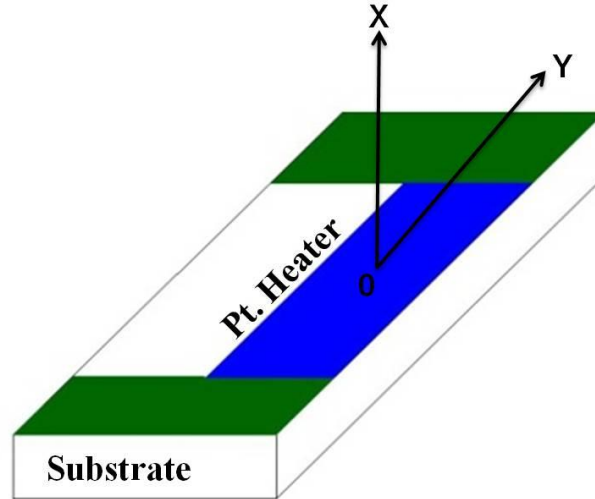


Fig.4.2 Heater geometry on the glass substrate

The relevant equations are given in the work of Birge et.al 1987 [2]

Heater is assumed to be infinitely narrow line source of heat on the surface of an infinite half volume. We solve the 1-D heat conduction equation as given in eqn.4.1 [3].

$$C_p \frac{\partial}{\partial t} T(x,t) = \kappa \frac{\partial^2 T(x,t)}{\partial x^2} \quad [4.1]$$

Where C_p and κ are the (possibly frequency dependent) are the specific heat and thermal conductivity of the medium surrounding the heater. Applying the boundary condition being that of an infinite plane sinusoidal heat source we have the eqn.4.2.

$$\kappa \frac{\partial T}{\partial x} \Big|_{x \rightarrow 0^-} = j_q = \frac{P}{A} = \frac{I_0^2 R_0}{2 * area} [1 + \cos(\omega t)] \quad [4.2]$$

where P=Power across the film, A= Area of the film

The heater lies in the $x=0$ plane and heat is only diffusing in one direction—into the substrate—which is assumed to be a homogeneous solid filling the space $x < 0$.

The dc component of the power merely sets up a linear temperature gradient in the sample cell and since the measurement is done in frequency space this does not affect the measurement. We have calculated the average temperature change introduced by dc power in the cell is about 0.5 K over the set temperature of the cell.

Assuming the solution to be as given by eqn.4.3

$$T(x, t) = T_0(x) + \delta T_{2\omega} e^{i(kx + \omega t)} \text{ for } x < 0 \quad [4.3]$$

We get the oscillating temperature δT as
$$\delta T_{2\omega} = \frac{\text{power}}{\text{area}} \frac{e^{-i\pi/4}}{\sqrt{2\pi f C_p \kappa}}$$

This is the case when there is no liquid in the sample bath. For the case when there is a liquid in the bath there is some modification in the above equation. For the case when heat flows into both substrate (S) and liquid (L) the boundary condition is modified to eqn.4.4

$$\kappa_L \left. \frac{\partial T(x, t)}{\partial x} \right|_{x \rightarrow 0^+} - \kappa_S \left. \frac{\partial T(x, t)}{\partial x} \right|_{x \rightarrow 0^-} = j_q = \frac{P}{A} \quad [4.4]$$

The two derivatives are calculated on both sides of the film

this yield
$$T(x = 0, t) = T_0(x = 0) + \delta T_{2\omega} e^{i2\pi f t}$$

where magnitude of temperature oscillation is given by eqn.4.5

$$\delta T_{2\omega} = \frac{P}{A} \frac{e^{-i\pi/4}}{\sqrt{2\pi f} (\sqrt{(C_p \kappa)_S} + \sqrt{(C_p \kappa)_L})} \quad [4.5]$$

Thus there is an extra additive term, in the denominator due to the liquid so there is a lowering in the value of $V_{3\omega}$ voltage.

The approximation of the infinite plane source is valid for $W \gg \lambda_{th}$, where W (2b) is the narrowest dimension of the heater in the plane of the substrate. In this approximation, the

technique is sensitive to the combination $\sqrt{C_p \kappa}$. Connection between Z and $C_p \kappa$ is given by eqn.4.6

$$Z e^{i\phi} = \frac{2area}{\alpha^* power} \sqrt{2\pi f} V_{heater}(3\omega) = \frac{e^{-i\pi/4}}{(\sqrt{(C_p \kappa)_s} + \sqrt{(C_p \kappa)_L})} \quad [4.6]$$

$$|Z_s| = \frac{1}{\sqrt{(C_p K)_s}} \text{ for substrate \&} \quad [4.7]$$

$$|Z_{NF}| = \frac{1}{\sqrt{(C_p K)_s} + \sqrt{(C_p K)_L}} \text{ in sample/Nanofluid} \quad [4.8]$$

The $\sqrt{(C_p \kappa)_L}$ value for the liquid may be obtained by making measurements with the substrate only and then with liquid and subtract away $\sqrt{(C_p \kappa)_s}$.

In a normal fluid the temperature oscillations at the heater will lag in phase behind the heat oscillation.

Experimentally we determine the phase, ϕ , and the normalized magnitude, Z, of the complex 3ω voltage signal, $V_{heater}(3\omega)$ given by [4]

$$\text{From eqn.4.7 \& 4.8 we obtain the } (C_p K)_L = \left[\frac{Z_s - Z_L}{Z_L} \right]^2 (C_p K)_s \quad [4.9]$$

From eqn.4.9 we calculated the $C_p \kappa$ value of the different liquid samples like heat transfer fluids, nanofluid etc.

4.3 Finite Size Effect

The Above calculation is based on the assumption that width of the film is almost infinite but in actual condition it is not so particularly at the low frequency end, consequently some error creeps in the final result. The one-dimensional diffusion model only hold as long as the thermal diffusion wavelength is much smaller than the width of the heater ($\lambda_{th} \ll W$) so that for the wave edges of the film becomes invisible i.e becomes infinite for them. If this is not the case, edge effects will be present and must be taken into account.

To counteract this error we have to include the effect of the finite size (width) of the film in the calculation. For this some correction factors [4] (which is multiplicative in nature) has to bring in as shown in eqn.4.10.

$$Ze^{i\phi} = Z_w e^{i\phi_w} \left[\frac{e^{-i\pi/4}}{(\sqrt{C_{pS}\kappa_S} + \sqrt{C_{pL}\kappa_L})} \right] \quad [4.10]$$

where the finite-size contribution, ϕ_w to the measured phase, ϕ .

Expression for this phase correction factor, ϕ_w is given by eqn.4.11 [3]

$$\phi_w = \frac{1}{W} \sqrt{\frac{\kappa_S}{2\pi f C_{pS}}} \quad [4.11]$$

and correction to the Z is multiplicative factor is given by eqn.4.12

$$Z_w = 1 - \phi_w = 1 - \frac{1}{W} \sqrt{\frac{\kappa_S}{2\pi f C_{pS}}} \quad [4.12]$$

A plot of the variation of the Z_w vs. f is shown in fig.4.3

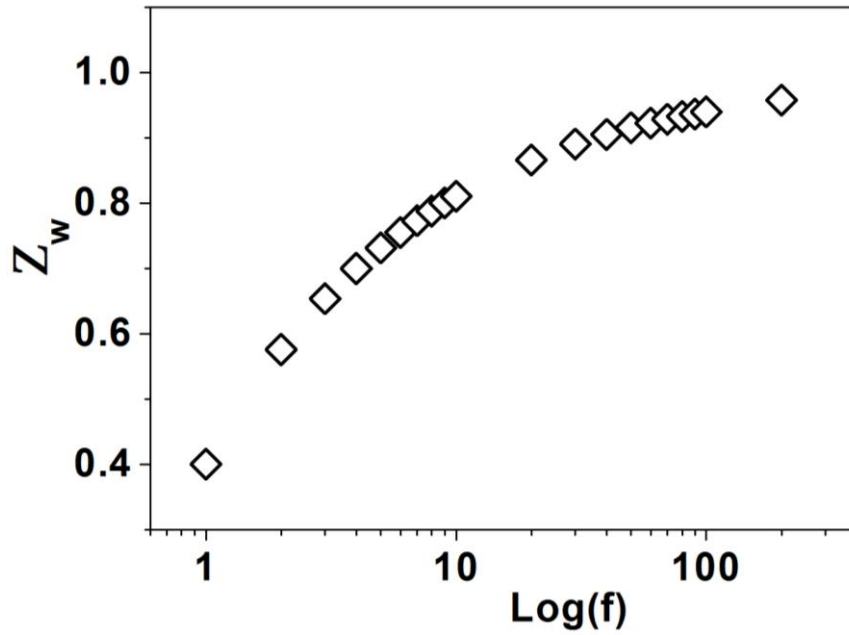


Fig.4.3 Variation of the Z_w vs f

By these correction factors we can get the correct values out of the measurement.

These correction factors are more important in the low frequency regime where the diffusive thermal wavelength ($\lambda_{th} = \sqrt{D/2\omega}$) becomes comparable to the width of the film, and in the high frequency end this correction factors becomes redundant as explained below

$$f \rightarrow \infty \Rightarrow (\phi_w \rightarrow 0) \Rightarrow (Z_w \rightarrow 1)$$

In our system for the given film and the given liquid the range of frequency available for scanning is ($1\text{Hz} < f (= \omega/2\pi) < 1\text{ KHz}$), However, for frequencies below 5Hz corrections for finite heater dimension have been applied. Size of the film we have taken is $300\mu\text{m}$

4.4 Power dependence

The first test we have to establish that the signal that we are getting from the output of the LIA which is set for determining the third harmonics detection. Since from chapter 2 we showed that $V_{3\omega} = \frac{1}{2} I_0 R_{\omega}$, as R_{ω} proportional to T_{ω} which is again proportional to I^2 .

So $V_{3\omega}$ is ultimately proportional to I^3 or V^3 .

If we plot $V_{3\omega}$ vs cube of the applied voltage then we should get a straight line. We have shown this measurement in fig.4.4 for the base fluid Ethanol.

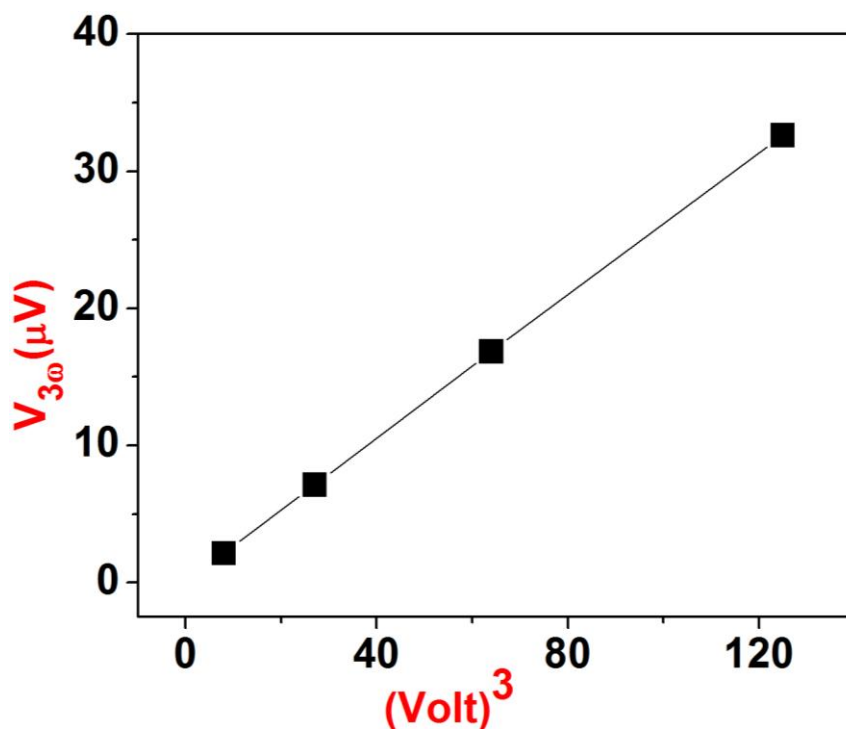


Fig.4.4. Graph showing the V^3 dependence of 3ω signal for Ethanol

From above graph it is clearly showing the linear dependence of $V_{3\omega}$ voltage on the V^3 of the applied voltage V was varied between 2V to 5V. This is the signature of the 3ω voltage. This observation established that we are getting a pure 3ω signal from the sample (from our measurement set up) which is the key for determining the thermal properties of a system by 3ω method.

Typical power produced in the heater is about 25mW at 5V of the input voltage.

From eqn.4.5 if there is no liquid surrounding the heater the phase ϕ , approaches 135° . Thus for substrate the phase should approach to 135 (degree).

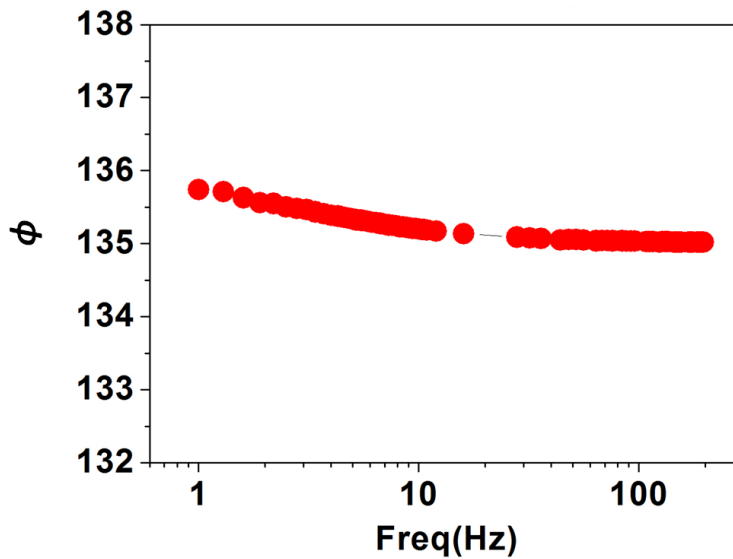


Fig.4.5 Variation of the Phase w.r.t the frequency for the bare substrate

Graph plot in fig.4.5 again validating out measurement system which shows that phase ϕ of the bare substrate (glass) is almost constant (135 degree) with the variation of frequency as expected also. Deviation at the lower frequency comes from the finite size effect.

Typical Third harmonic voltage ($|V_{3\omega}|$) for the substrate is shown in fig.4.6. Here we have used different excitation voltages. As the amplitude of the applied voltage is increased there is a proportional increase in the magnitude of 3ω voltage response. We apply the highest excitation voltage across the film for getting the maximum joule heating so that the response voltage is maximum and thus reducing the error etc.

In SR 830 model LIA, 5V is the maximum value that we can use for excitation of the sample. So our all measurements were performed at 5V excitation voltage.

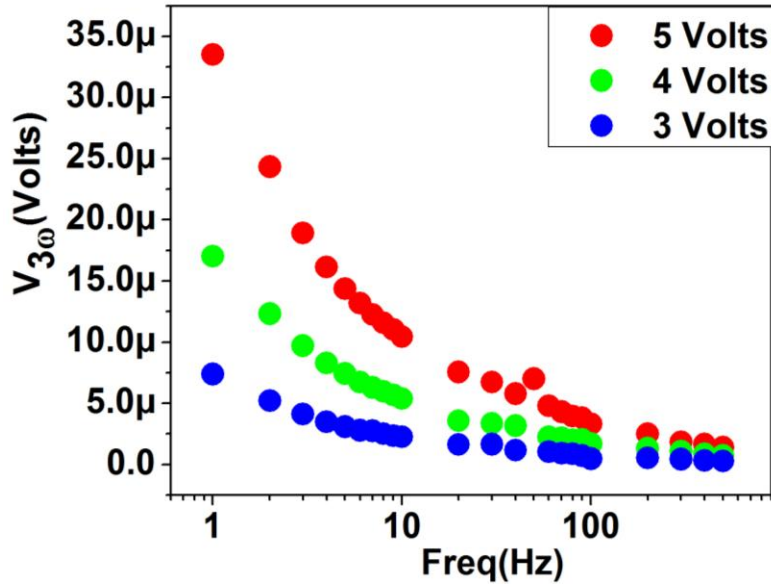


Fig.4.6. $V_{3\omega}$ voltage for substrate with variation in frequency of the input excitation

We calibrate the apparatus by measuring $C_p\kappa$ values for some standard liquids and then compare this with the available ones. Values for Ethanol and Substrate (soda lime glass) are shown in Table 4.1

Samples	$C_p\kappa$ [1] ($J.W/m^4K^2 \times 10^{-6}$)	Measured ($J.W/m^4K^2 \times 10^{-6}$)	Error (%)
Ethanol (30 °C)	0.4	0.3 ± 0.1	25
Glass (soda lime)	1.05	1.17 ± 0.5	10

Table.4.1 Fluids with their available and measured $C_p\kappa$ values

After the completion of the standardisation of the measurement set up we proceed for the samples that we are intended for my thesis work i.e nanofluids containing different types of nanoparticles and compare their properties with their corresponding bare base fluids in which these nanoparticles are dissolved for nanofluid formation.

4.5 ZnO Nanofluid measurement

The reported data on thermal conductivity of nanofluids are mostly based on static measurements. In this work we report an unusual phenomenon that the enhancement of heat transport through these nanofluids may actually depend on the frequency, when the measurement is done using a dynamic method. The enhancement of the parameter

$$C_p \kappa \quad (C_p = \text{heat capacity and } \kappa = \text{thermal conductivity})$$

was found to be strongly frequency dependent. It reaches a limiting large value at a low frequency and at higher frequency $C_p \kappa$ is close to that of the base fluid. The measured enhancement of $C_p \kappa$ can be substantial and it increases when the temperature is increased. The experiment was carried out in nanofluid containing

ZnO nanocrystals (dia. ~ 10 nm) in suspension in Ethanol (volume fraction of solid $\sim 1.5\%$). The frequency dependent dynamic measurements were carried out using the 3ω technique described below briefly. This work has two aspects:

- (1) to investigate whether the thermal transport has frequency dependence, an issue that has not been reported before in the context of nanofluids and
- (2) to report on a nanofluid containing ZnO that has not been investigated earlier. ZnO being an optical material with fundamental absorption in the UV (~ 3.3 eV) gives us a handle to address the solid content of the nanofluid optically.

Then we take the real part of the output 3ω signal from the LIA. Graph in fig.4.7, shows the raw $V_{3\omega}$ data taken during the measurement by frequency scan on base fluid Ethanol and ZnO Nanofluid.

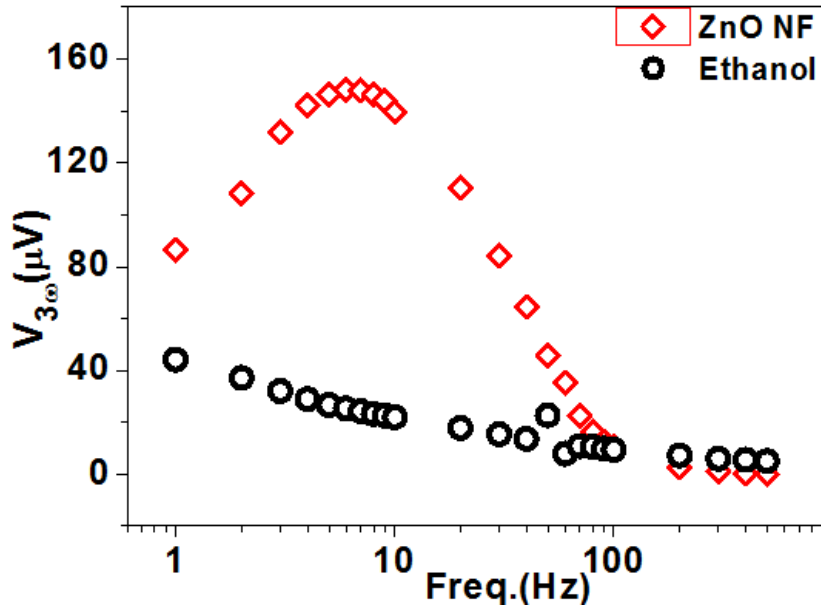


Fig.4.7. $V_{3\omega}$ vs freq. data for ZnO nanofluid and Ethanol at room temperature.

From above data it is clear that in the case of base fluid only i.e Ethanol the $V_{3\omega}$ voltage is very small and the dependence on frequency is shallow. When the ZnO Nanofluid was brought in to the picture there is a huge increase in the $V_{3\omega}$ response and there is also a clear indication of strong frequency dependence behaviour. This is a very interesting observation in the field of thermal conductivity enhancement in nanofluids.

This data is then converted in terms of more physical thermal parameters C_p and κ . For this we first convert the 3ω signals of each samples i.e Substrate, Ethanol and ZnO Nanofluids to its corresponding normalised value is Z_S , Z_{Eth} and Z_{NF} and then find the $C_p\kappa$ of the substrate by using eqn.4.7, denoted by $(C_p\kappa)_S$.

This value is used in the calculation of $C_p\kappa$ for each liquid samples by using eqn.4.9.

Results in terms of $C_p\kappa$ for Ethanol and ZnO nanofluid is shown in fig.4.8

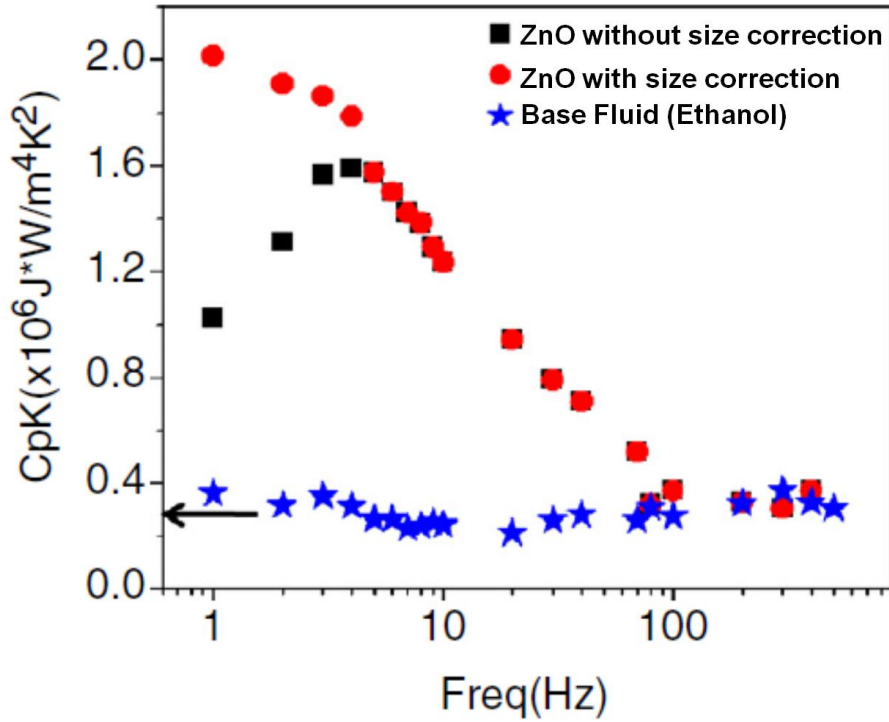


Fig.4.8. Variation of the $C_p\kappa$ of ZnO nanofluid and ethanol at 40°C . The estimated $C_p\kappa$ based on the Maxwell equation is marked in the figure. The data for the nanofluid show the as measured data (referred to as uncorrected) and that corrected for finite heater size.

Red curve shows the actual $C_p\kappa$ trend of ZnO w.r.t frequency variation. The data on the base fluid Ethanol is also shown in the same graph. The product $(C_p\kappa)_{NF}$ shows a clear enhancement compared to that of the ethanol. Interesting is the observation that, for the nanofluid $(C_p\kappa)_{NF}$ has a clear frequency dependence.

In the low frequency region ($f < 5\text{Hz}$) there is a sharp peak in the experimental data for ZnO but there is no physical reason for the occurrence of this peak and we show that arises from finite heater width. Actually in the low frequency range the diffusive thermal wavelength becomes comparable to the width of the film which violates the assumption of 1D planar heater as the lateral dimension of the heater must be long compared to the thermal wavelength if not then above equations are not valid and the result will be erroneous. So we applied the correction for the finite size correction.

Original experimental $C_p\kappa$ data for the ZnO is shown by the black (square) data points. In order to obtain the size corrected data red (circle) for this we have to calculate the Z_w the correction factor for the given film for each frequency. A plot of these values is shown in the fig.4.9 below.

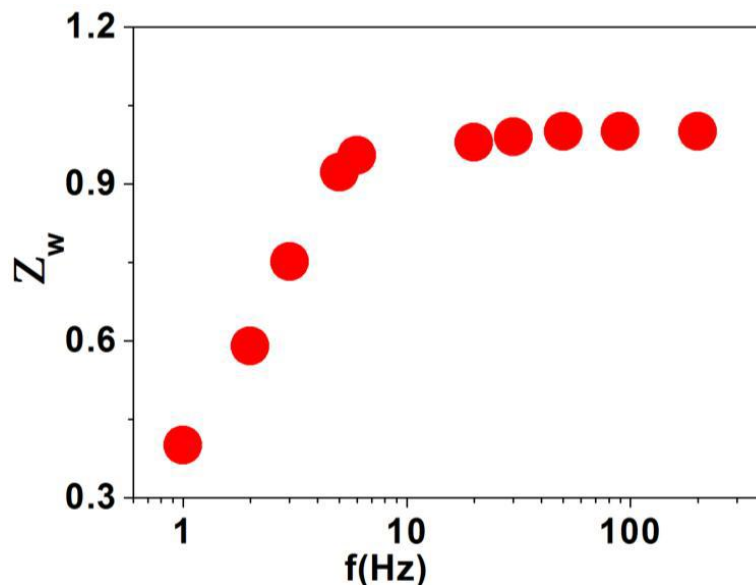


Fig.4.9. Plot of the size correction factor w.r.t freq. for ZnO nanofluid.

We then multiply the original Z with this factor at each frequency to obtain the corrected value of Z i.e Z_c given by the eqn.4.13.

$$Z_c = Z_w * Z \quad [4.13]$$

This corrected Z value is put in the original eqn.4.9 to obtain the corrected red curve. This is the process of size correction of the datas.

This is a very important observation, which is at core of this thesis work. This observation has a very important implication in the field of thermal conductivity enhancement of nanofluids. Static measurements of thermal conductivity in nanofluid the enhancement has constant and relatively small magnitude, but with dynamic measurement nanofluid shows a constant enhancement up to certain frequency with considerable magnitude (4 to 5 times the base fluid) and then slowly merge with the value of the base fluid at the higher frequency $> 100\text{Hz}$. For frequency $> 1 \text{ kHz}$, the value of the measured 3ω voltage is very small and the error in the data increases. The base fluid ethanol has a very shallow frequency dependence of $C_p\kappa$.

4.5.1 Temperature Dependence

The temperature plays an important role in the enhancement of thermal conductivity enhancement of nanofluid. It is normally found that there is an increase in the enhancement with the increase of operating temperature. We have also found the same trend. Graph in fig.4.10, shows the raw 3ω signals for ZnO nanofluid at three temperature 20, 30 & 40 °C respectively along with that of base fluid Ethanol.

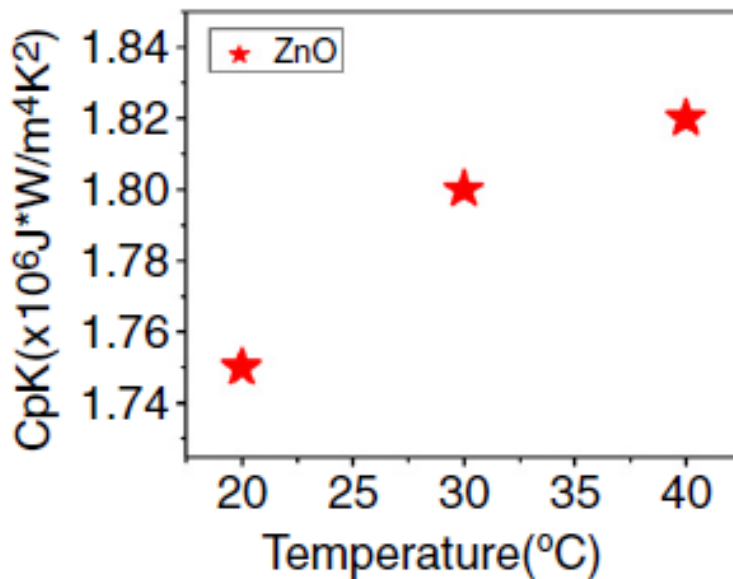


Fig.4.10 The variation of $C_p\kappa$ with temperature at any arbitrary frequency 3 Hz (say).

It is clear that the enhancement of $(C_p\kappa)_{NF}$ also depends on the measuring temperature. It increases as the measuring temperature is increased, although the increase is only 4%. This enhancement is not coming from base liquid since it has no frequency dependence of $C_p\kappa$ for ethanol (blue colour) as shown in fig.4.12.

4.5.2 Volume fraction (ϕ) Dependence

To establish that the observed frequency dependence as well as the enhancement of $(C_p\kappa)_{NF}$ is solely due to the presence of the nanoparticles in the base fluid, we have also measured the $(C_p\kappa)_{NF}$ product as a function of the volume fraction.

For making the ZnO nanofluids with different concentrations we dilute the mother solution step by step by adding the base fluid to it and the volume is kept constant. In this way solutions with different volume fractions (ϕ) is achieved.

The data for different volume fractions (ϕ) at a given temperature are shown in fig.4.11. The scaling with the volume fraction is apparent. The maximum volume fraction of the ZnO in the nanofluid used here is $\leq 1.5\%$ ($\phi \leq 0.015$).

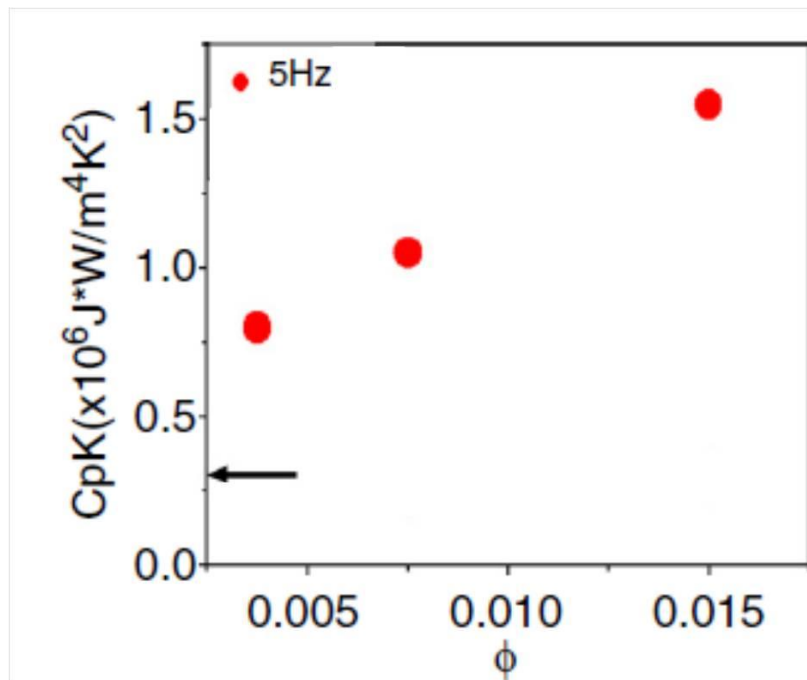


Fig.4.11. Concentration dependence of $(C_p\kappa)_{NF}$ at three different volume fractions (ϕ) of the ZnO nanoparticles. The value for the base fluid (ethanol) is marked for reference.

The enhancement of the $(C_p\kappa)_{NF}$ product is seen to change at even lower volume fractions as can be seen from fig.4.12. For $\phi > 0.005$, the dependence is linear and at lower ϕ the dependence is steep. At higher frequency (>100 Hz), the change in $(C_p\kappa)_{NF}$ with ϕ is small and is of the order of the error in the data.

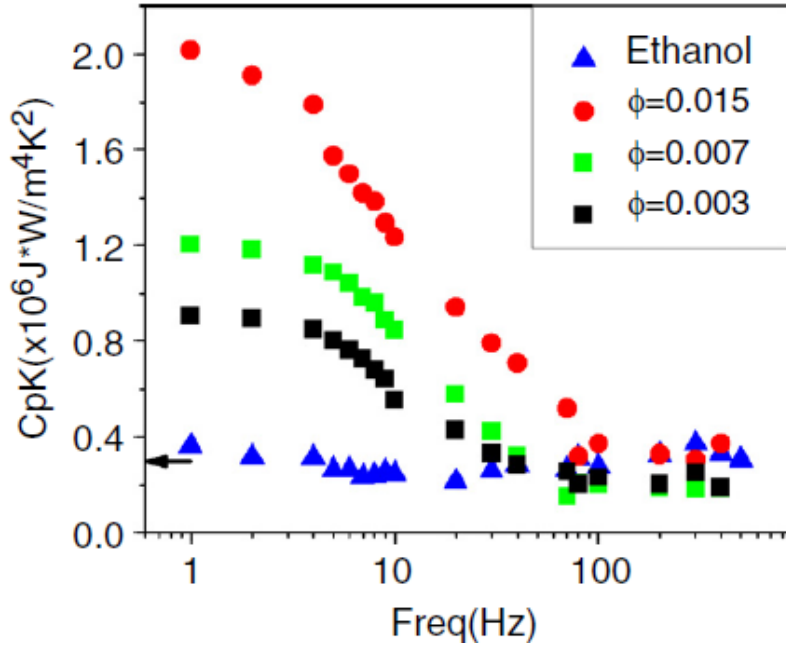


Fig.4.12. Dependence of $(C_p\kappa)_{NF}$ on ZnO concentration (ϕ) at different measurement frequencies. The ethanol value is marked. At 100 Hz, the change in $(C_p\kappa)_{NF}$ on solid loading is similar to the resolution in the data.

We note that the density as well as the specific heat $(C_p\kappa)_{NF}$ of the nanofluids is expected to be not much different from that of the base liquid at such a low volume fraction of ZnO. This has been validated experimentally for the base fluid (ethanol). We also note that the observed $(C_p\kappa)_{NF}$ for the base fluid ethanol has no (or very little) frequency dependence. Thus, the change as well as the frequency dependence observed in $(C_p\kappa)_{NF}$ of the nanofluid can be expected to be mainly from the change in the thermal conductivity κ_N . Using the C_p values of ethanol we can obtain the frequency dependent κ of the nanofluid. We find that the enhancement of thermal conductivity in the low frequency limiting range can be about four to five times that of the original base liquid at a loading fraction $\phi \sim 0.015$ [5].

Using Maxwell's effective medium theory (EMT) for non contacting spherical particles [6] the effective thermal conductivity of the nanofluid has been evaluated by using the corresponding values of the host and the dispersed particle. The estimated value obtained by this method for ZnO nanofluid is marked in fig.4.8 by an arrow. This turns out to be much less than the experimental one.

4.6 Analysis of the frequency dependence

The main observations in this work are two-fold. First, to show that nanofluid containing ZnO nanoparticles can give a rather high value of the parameter $(C_p \kappa)_{NF}$. As ZnO is a cheap and benign material, a nanofluid containing ZnO is expected to have a good application potential. Second, and more importantly we find that there is a rather strong dependence of the parameter $(C_p \kappa)_{NF}$ on the measuring frequency. At low frequency ($f < f^* \approx 10$ Hz) the enhancement is large and it reaches a frequency independent value. However, at higher frequencies $f > f^*$, there is a rapid decrease of the enhancement and for $f \geq 100$ Hz all of the concentrations it shows a frequency independent value. This is definitely a new observation and has not been observed in other nanofluids.

The cause of this frequency dependence behaviour is exactly not known but we suggest some likely scenario that might explain the observation and will also bring out its relevance. It has been reported recently that even in stable nanofluids, there can be thermo-diffusion assisted local aggregation that can enhance thermal conductivity and this can have time dependence over long timescales [9, 10]. If it happens that the enhancement of heat conduction is due to local aggregation of the solid nanoparticles (whatever the reason), the solid like aggregated region in the nanofluid also has to respond to the oscillating temperature field $\delta T_{2\omega}$.

Suppose the length scale of the aggregation is L_A .

The thermal response of the region (determined by the thermal diffusivity D) will occur on characteristic timescale of τ_c given by eqn.4.12

$$\tau_c \approx L_A^2 / D \quad [4.12]$$

At low frequency the local aggregation can follow the oscillating temperature (at $2f$) gradient leading to large enhancement of $(C_p \kappa)_{NF}$. If the temperature oscillation is faster (high frequency end) than the timescale τ_c , it will not follow the temperature gradient at higher frequency. We thus expect the response of the system to have a clear dependence on the measuring frequency and the response $(C_p \kappa)_{NF}$ is expected to follow the relation of the type given by eqn.4.13

$$\frac{(C_p \kappa)_{NF}(f)}{(C_p \kappa)_{NF}(f=0)} = \frac{1}{\sqrt{1 + \left(\frac{f}{f_c}\right)^2}} \quad [4.13]$$

where $(C_p \kappa)_{NF}(f)$ is the value at the measuring frequency f and $(C_p \kappa)_{NF}(f = 0)$ is the limiting low frequency value, $f_c =$ corner frequency.

The corner frequency f_c is related to the timescale τ_c . The frequency f is the frequency of the excitation current, leading to the temperature oscillation occurring at frequency $2f$. Thus, the corner frequency will be related to the timescale of thermal relaxation by the relation by eqn.4.14

$$\tau_c \approx \frac{1}{4\pi f_c} \quad [4.14]$$

We find that the observed data at a given concentration and temperature fit eqn.4.13 very well. From the observed fit we find the value of the corner frequency f_c . The typical corner frequency is around 10 Hz. The timescale is thus around $\tau_c \approx 8$ ms.

The characteristic time of the thermal relaxation time can be linked to a characteristic length scale L_A . From eqn.4.12 we can get the value of it via the expression $L_A \approx \sqrt{\tau_c D}$

The thermal relaxation occurs over this length scale. Using the experimental value of D we find $L_A \approx 20\text{--}25 \mu\text{m}$.

The scale of the frequency dependence associated with the phenomena shows that this occurs on a length scale much larger than the particle size. If the explanation is indeed correct this will mean that the observed large enhancement of the thermal parameter $(C_p \kappa)_{NF}$ at low frequency occurs due to aggregation of the nanoparticles in the fluid over length scales that extend over a few tens of microns. Though there are suggestions of more than one mechanism that can lead to aggregation that will enhance the thermal parameters, there was no direct estimation of the length scale. The frequency dependence of $(C_p \kappa)_{NF}$ thus gives us a way to estimate the length scale associated with the aggregation [5].

4.7 Physical interpretation

It has been reported recently that aggregation of nanoparticles plays an important role in the enhancement of thermal conductivity beyond Maxwell limit [6].

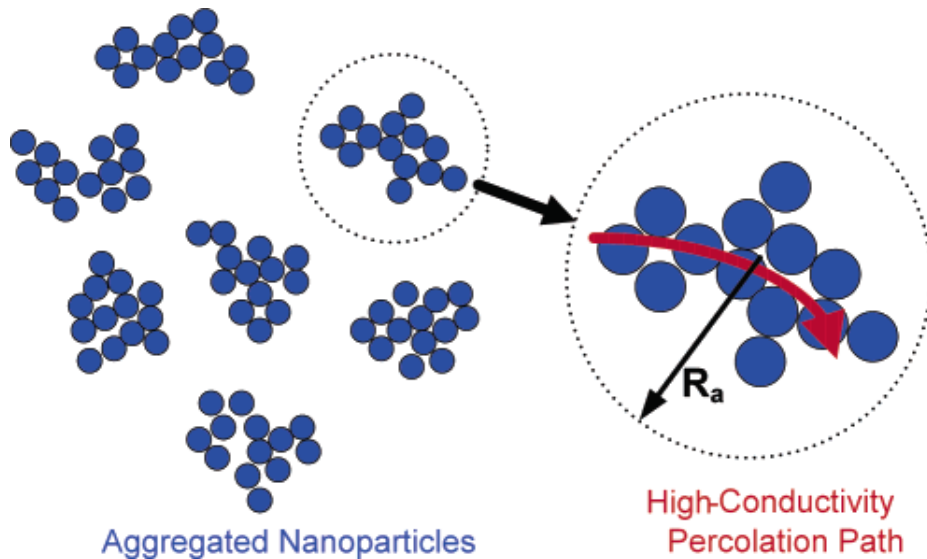


Fig.4.11. High conducting percolating path created by agglomerating of nanoparticles

Aggregation and thermo diffusion are time dependent phenomena [9, 10, 11] therefore will induce a time dependent thermal conductivity. There is a thermo diffusion assisted aggregation of nanoparticles. Thermodiffusion affects the amount of aggregation across a temperature gradient by imposing a concentration distribution and variation in the aggregation time constant [12]. The thermal conductivity distribution is affected through its direct relationship with the concentration and progress of aggregation.

Particles will be well dispersed at time, $t=0$ and then will start to agglomerate to form multiple aggregates as shown in the fig. Aggregation will decrease the Brownian motion due to the increase in the mass of the aggregates, whereas it can increase k due to percolation effects in the aggregates, as highly conducting particles touch each other in the aggregate.

Thus thermal conduction paths can arise through percolating amorphous like interfacial structures.

Aggregates are characterized by their radius of gyration (R_a) [13] as shown in above fig. 4.11, these individual aggregates will have higher conductivity than the liquid; they can be considered as the new “particles” with an effective radius of R_a and they will enhance the κ of the nanofluid. However, this enhancement will decrease as the aggregates continue to

agglomerate to make much bigger aggregates. As $t \rightarrow \infty$, all the nanoparticles will agglomerate to form one large aggregate, at which time the nanoparticles will not enhance k further. Therefore, the enhancement in κ due to aggregation will be maximum for well-dispersed aggregates, somewhere between the two extremes at $t = 0$ (no aggregation) and $t \rightarrow \infty$ (complete aggregation).

As we go to higher frequency side the time t also increase and may be at the upper limit almost all the particles get agglomerate and show no increase in thermal conductivity.

4.8. Conclusions

We report here an interesting frequency dependent enhancement in the $(C_p \kappa)_{NF}$ of ZnO nanofluid containing ~ 10 nm ZnO nanoparticles. This most likely arises due to an enhanced κ and the enhancement is substantially more than what is expected from simple effective medium theory. The enhancement increases with temperature and scales with nanoparticles concentration. The observation of the frequency dependence of $(C_p \kappa)_{NF}$ is a new phenomenon. The frequency dependence has a characteristic frequency scale. We proposed local aggregation as a likely cause for the frequency dependence.

In this chapter we find the expressions and values for the product $(C_p \kappa)$ and not the individual quantities separately. If we can separate these quantity then we can have more insight in the system and able to concentrate on a single parameter.

In the 5th chapter we will be dealing with this matter and along with measurements in some more types of nanofluids and other nanostructures.

References

- (1) Lide D R 2000–01 Handbook of Chem. and Phys 81st edn (Boca Raton, NY: CRC Press)
- (2) N.O. Birge, S.R. Nagel, “Wide-frequency specific heat spectrometer”, AIP, 1987
- (3) H. S. Carslaw and J. C. Jaeger, Conduction of Heat in Solids (Clarendon, NY, 1959)
- (4) Menon N, J. Chem. Phys. 105, 5246, 1996
- (5) R.K.Neogy and A.K. Raychaudhuri, Nanotechnology 20, 305706, 2009
- (6) Maxwell J C 1873 A Treatise on Electricity and Magnetism (Oxford: Oxford Univ. Press)
- (7) Gharagozloo P E et al, Appl. Phys. Lett. 93, 103110, 2008
- (8) Feng Y, J. Phys. D: Appl. Phys. 40, 3164, 2007
- (9) Koblinski, P. et al. Mater. Today, 36, June 2005
- (10) Russel, W. B. et al. Colloidal Dispersion; Cambridge University Press: Cambridge, U.K.
- (11) Hunter, R. J. Foundations of Colloid Science; Oxford University Press: New York, 2001
- (12) P. E. Gharagozloo et.al, Appl. Phys. Letts **93**, 103110, 2008
- (13) Prasher R, Nano Letters vol.6, 1529, 2006

Chapter 5

Chapter 5: Measurements in ZnO and ZnO with PVP Nanofluids.....

5.1 Introduction	144-145
5.2 Results.....	145-146
5.3 Separation of C_p and κ measurements.....	147
5.3.1 Measurement process of Thermal Conductivity (κ).....	147
5.3.1.1 Measurement Theory.....	147-148
5.3.1.2 Experimental Results.....	148
5.3.1.2.1 ZnO and ZnO + PVP Nanofluid.....	148-149
5.4 Calculation of temperature distribution of the heater.....	150
5.4.1 Substrate.....	150-151
5.4.2 Liquid.....	151-152
5.5 Discussion.....	153-156
5.6 Conclusion.....	156

References

5.1 Introduction

Chapter 4 is the first discovery of the effect, that the effusivity parameter ($C_p\kappa$) is indeed frequency dependent. It has been reported recently that even in stable nanofluids, there can be thermo-diffusion assisted local aggregation that can enhance thermal conductivity and this can have time dependence over long timescales [1, 2].

In this chapter we would explore this hypothesis with further experiments. We have chosen ZnO and ZnO with surfactant PVP, which prevents agglomeration and thus inhibits local aggregation. It is expected that this should affect the frequency dependence in a straight forward way that the surfactant will lead to inhibiting the local aggregation. We will compare the different parameters like thermalisation time constant and spatial length for thermalisation etc. of these two correlated systems, to reach a conclusion.

In continuation to the previous work described in chapter 4, we further conducted the measurement on

(a) ZnO Nanofluid

(b) ZnO nanofluids in which ZnO particles are coated with protective PVP layer.

The debate behind the mechanism for the enhancement in thermal conductivity beyond the EMT theory was largely fuelled by limited experimental characterization of the nanofluid systems and consequently lack of information. However, a number of recently reported experimental studies strongly suggest that nanoparticles aggregation plays a significant role in the thermal transport in nanofluids. In particular, Hong *et al.* demonstrated by light scattering measurements that Fe nanoparticles aggregate into micron size clusters. Lee *et al.* demonstrated the critical importance of particle surface charge in nanofluid thermal conductivity. The surface charge is one of the primary factors controlling nanoparticle aggregation.

In chapter 4, it has been shown that for ZnO nanofluids without surfactant, aggregates in the spatial scale 10-20 μm , can explain the frequency dependence of the enhanced thermal conductivity. So it is clear that one of the reason for such frequency dependence may be due to the formation of local clustering by these particles. Such local clustering can be prevented by adding surfactants. In this chapter we have investigated what happens to the thermal transport enhancements when a surfactant is added to such nanofluids. If there is frequency

dependence of the enhanced thermal transport it would imply likely existence of a length scale in the problem. We have calculated the aggregation length scale for the nanoparticles cluster and thermal relaxation time for heat diffusion in such clusters. If our hypothesis is correct then we should be getting a different length and time scale for the same system if it is stabilized by using a surfactant. Since aggregation depends on the stability of the nanofluid. We can alter this aggregation process by altering its stability and tendency to produce local aggregation using surfactant that inhibits local aggregation.

So we carried out our measurement on both the stable and unstable ZnO nanofluids.

In chapter 4 we have reported the measurement on a bare ZnO nanofluid without surfactant which has a relatively shorter shelf life, due to the agglomeration of the nanoparticles.

5.2 Results

Details of the measurement and result for the bare ZnO case are explained and discussed in chapter 4 of this thesis. In this chapter we do mainly measurement on ZnO with PVP. However, we rearranged all the data in terms of analysis of $\delta T_{2\omega}$, that was not done in chapter 4.

In this chapter we report experiment with ZnO nanofluid with protective PVP coating. During preparation of ZnO nanofluid we put PVP in the solution and the resulting ZnO nanofluid so formed is stabilised. This has been discussed in details in chapter 3. It is found to have a shelf life above a month. We take this as a sample for measuring the $C_p \kappa$ values of it. First we take the data with the bare substrate and then dipped the heater inside the ZnO+PVP solution. The data taking procedure is the same as that in chapter 4. We do not repeat it here to avoid duplication. Data shown in fig.5.1.

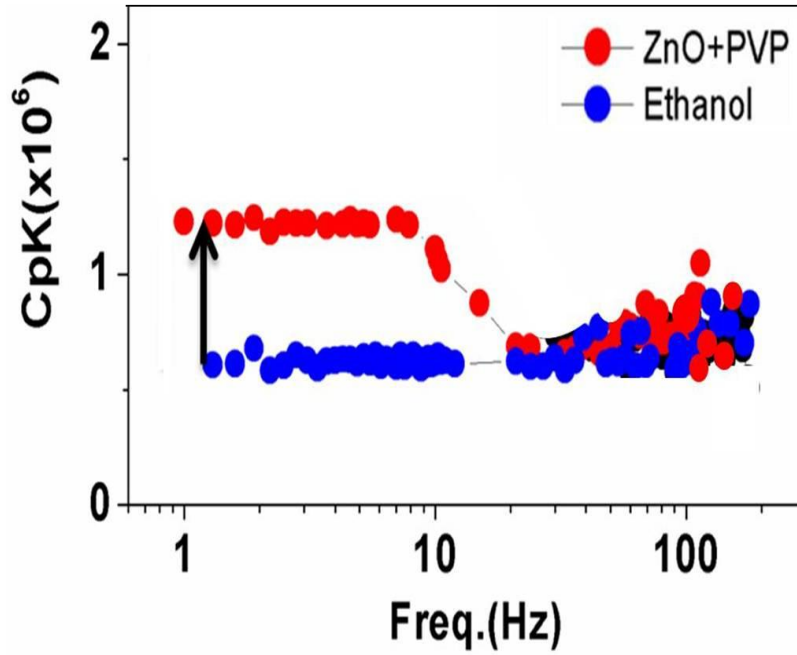


Fig.5.1. $C_p\kappa$ values shown w.r.t Ethanol

For this case there is an enhancement at low frequency effusivity $C_p\kappa$ and the relative value comes out to be (for $f < 5\text{Hz}$)

$$\frac{(C_p\kappa)_{ZnO}}{(C_p\kappa)_{etha}} \approx 2.6$$

This can be compared to the relative enhancement for ZnO without PVP which comes out to around 4. Both the samples have the same loading fraction as made by the same process and PVP has just been added for the synthesis of the stable one.

Thus there is a reduction in the ratio for stable ZnO when compared with the bare ZnO nanofluid. This result indicates that agglomeration property of the nanoparticles dispersed in the base fluids has an important role to play for showing enhanced effusivity. This provides a direct confirmation of our hypothesis that the local thermally assisted aggregation is a factor that enhances thermal properties in nanofluids.

Thus in both the case we got an enhancement in the ratio of $C_p\kappa$ values. We found that for the nanofluid containing metal nanoparticles have higher enhancements than containing semiconductor nanoparticles. This may be because of the higher thermal conductivity of metals than the semiconductors. For frequency $> 100\text{ Hz}$, the value of the measured 3ω voltage is very small and the error in the data increases also it reaches the resolution of the measuring instrument.

5.3 Separation of C_p & κ

In this section we will discuss our attempt to separate the coupled parameters in the term $C_p\kappa$. It is important to know that the enhancement observed in $C_p\kappa$ is coming due to C_p or κ . So to ascertain it we determine the thermal conductivity κ of each sample separately.

5.3.1 Measurement process of Thermal Conductivity (κ)

Measurement of thermal conductivity is also done by the same set up that we have constructed in our lab. For measurement of thermal conductivity, the container is filled with sample and the line heat source/film is inserted at the centre of the Cu container dipped inside the constant temperature bath (Julabo F32 model) and allowed to equilibrate to bath temperature. Then a current is send through it for measuring the thermal conductivity.

5.3.1.1 Measurement Theory

As in the case of the hot-wire method [3] where a metal wire is inserted and suspended in a liquid acts as both heater and thermometer. A sinusoidal current at frequency ω is passed through the metal wire and generates a heat wave at frequency 2ω . The temperature rise at frequency 2ω in the metal wire can be deduced by the voltage component at frequency 3ω . Thus, the average temperature rise of the strip can be obtained from the amplitude of temperature oscillations can be calculated from the equation. We take the real part of temperature amplitude from the eqn.5.1

$$\Delta T_{2\omega} = \frac{2V_{3\omega}}{IR\alpha} \quad [5.1]$$

where I=current, R=resistance of the heater, α = Temp. Coeff. of resistance and all voltages are rms values.

By this way we determine the temperature oscillations experimentally by the 3ω setup.

The thermal conductivity of the liquid, κ , is determined by the slope of the 2ω temperature rise of the metal wire versus the frequency. via the eqn.(2) of [4].

$$\Delta T_{2\omega} = \frac{-P_L}{2\pi\kappa} \ln \omega \quad [5.2]$$

From this slope is calculated and then inserting in eqn.5.3 to finally get the thermal conductivity value of the liquid in which this heater is dipped.

$$\kappa_s = \frac{-P_L}{2\pi} \left(\frac{\partial T_{2\omega}}{\partial \ln \omega} \right)^{-1} \quad [5.3]$$

Where κ_s = thermal conductivity of the substrate &

P_L = power/length

Thus eqn.5.3 provides the way to determine the thermal conductivity from the real part of the temperature oscillation for a solid sample/substrate.

For liquid sample, neglecting boundary mismatch, the measured k can be approximated as [5]

$$\kappa = \kappa_l + \kappa_s$$

where κ_l = thermal conductivity of the liquid & κ_s = thermal conductivity of the substrate

$$\kappa_s + \kappa_l = \frac{-P_l}{2\pi} \left(\frac{\partial T_{2\omega}}{\partial \ln \omega} \right)^{-1} \quad [5.4]$$

For liquid system we get the effective thermal conductivity value as shown in eqn.5.4 and to get the thermal conductivity value for the liquid, we have to subtract the thermal conductivity value of the substrate from it.

5.3.1.2 Experimental Results

Experimental results for the thermal conductivity measurement for all are listed below.

From the raw $V_{3\omega}$ data we find the temperature oscillation of the metal wire which occurs at twice the frequency of the applied voltage i, e 2ω (so it is denoted as $\delta T_{2\omega}$).

5.3.1.2.1 ZnO and ZnO+PVP Nanofluid

In fig.5.2 we show the temperature oscillation for both the ZnO and ZnO with PVP nanofluids plotted w.r.t applied frequency.

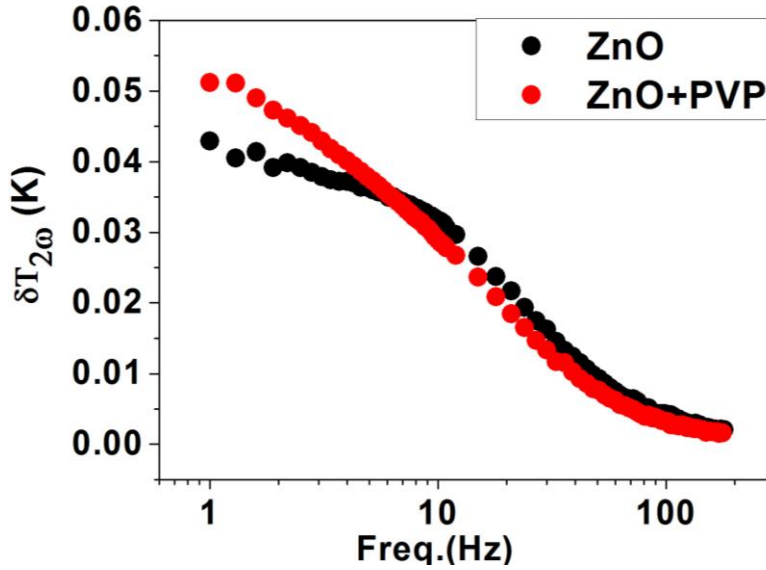


Fig.5.2. Temperature oscillation vs the frequency

We calculate the enhancement ratio in κ for both the nanofluids w.r.t base fluids as our motto is to measure the effective enhancement ratio for the nanofluids. It is found that when the measurement is made in low frequency limit, we get the thermal conductivity of the specimen, but loses the information on specific heat. Similarly at the high frequency side we get the information on specific heat but at the cost of information on thermal conductivity [6]. Thus we calculated the κ from the slope of the curve at the low frequency end ($< 10\text{Hz}$). Tabulated values of these enhancement ratios that we get in κ and $C_p\kappa$ values separately are given in the table 5.1.

Method	ZnO	ZnO+PVP
Slope of $\delta T_{2\omega}$ curve	$(\kappa)_{ratio} \sim 4.2$	$(\kappa)_{ratio} \sim 2.3$
From 3ω method	$(C_p\kappa)_{ratio} \sim 4$	$(C_p\kappa)_{ratio} \sim 2.7$

Table.5.1. Nanofluids with corresponding enhancement ratio of $C_p\kappa$ and κ w.r.t base fluid.

5.4 Calculation of temperature distribution of the heater

In this section we try to fit the experimental results with that of calculated one. In this work temperature oscillation of the heater is measured so we try to find the distribution of the temperature profile due to the periodic heating of the heater in both the case of bare substrate and the liquid by solving the heat equation of the system.

5.4.1 Substrate

We determine the thermal conductivity of the substrate, base fluids and nanofluids by the above process. We fit this temperature distribution with the theoretical model.

Consider an infinitely thin and infinitely long heater on the surface of a semi-infinite medium of thermal conductivity κ . The ac power per unit length used to heat this line is P_L . The steady-state solution to the heat equation of the system is a thermal wave of the form [7]

$$\delta T(r) = \frac{P_L}{\pi\kappa} K_0(qr)$$

where K_0 is the zeroth order modified Bessel function, and for substrate case we have

$$q = \sqrt{(2\omega\rho C/\kappa)}i = \sqrt{(12.56 \times 10^6 f)}i$$

The steady-state solution for the average temperature on the heater/sensor then becomes eqn.5.5

$$\delta T = \frac{P_L}{\pi k} \int_0^\infty \frac{\sin^2(Kb)}{(Kb)^2 (K^2 + q^2)^{1/2}} dK \quad [5.5]$$

K is the integration variable in Fourier space, $2b=W$ =Total width of the heater=300 μ m.

The temperature for the substrate is shown fig.5.3.

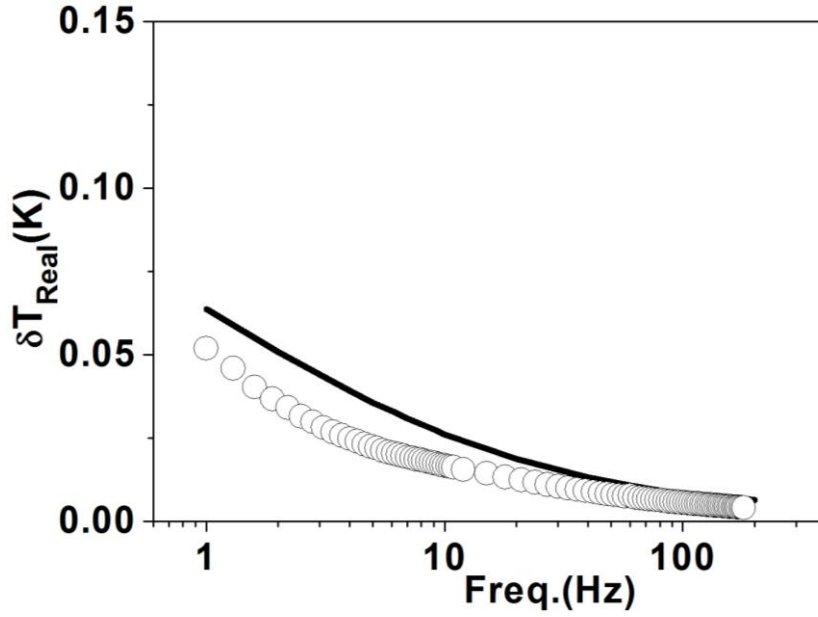


Fig.5.3. Model fit (line) on the substrate's experimental result (circle)

5.4.2 Liquid

Above is the case when we consider that heat flow is in to the substrate only (i.e along x axis) but when the heater is dipped inside the liquid sample then there is a heat dissipation in both side of the heater can be thought to be sandwich between substrate and the liquid in this case. Matrix formalism [8] provides an exact solution for the case of a strip-heater between two media.

$$\delta T = \frac{P_L}{\pi k} \int_0^{\infty} \frac{\sin^2(Kb)}{(Kb)} \frac{1 + \gamma_s}{\gamma_l + \gamma_s + \gamma_s \gamma_l R} dK \quad [5.6]$$

Where $\gamma_i = \kappa_i \sqrt{K^2 + q_i^2}$ and R= Interfacial resistance

For the liquid case (Ethanol), $q = \sqrt{(2\omega\rho C/\kappa)}i = \sqrt{(15.3 \times 10^7 f)}i$

$$\kappa_s = 1 \text{ W/mK} \quad \& \quad \kappa_l = 0.21 \text{ W/mK}$$

After plotting the real part of the temperature with the frequency is shown in fig.5.4.

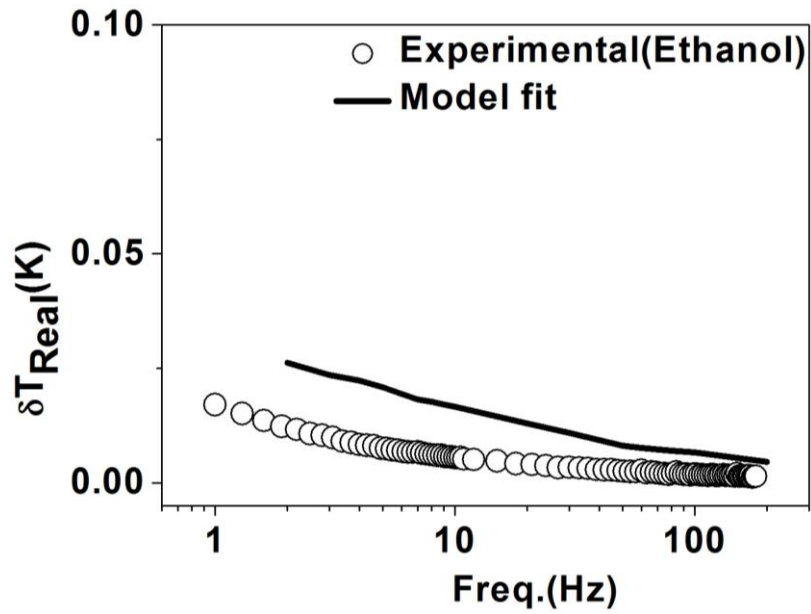


Fig.5.4. Matrix model fit to the Ethanol data

We have done these calculations to match the fluctuating temperature of the heater with that obtained during the experiment. All the calculation of the complex integrals are performed by using Wolfram Alpha computational Knowledge engine [9]

5.5 Discussions

For ZnO and PVP coated ZnO nanofluids we got the following results. We plot both the plots for bare ZnO and stable ZnO nanofluids w.r.t the base fluid as shown in fig.5.5.

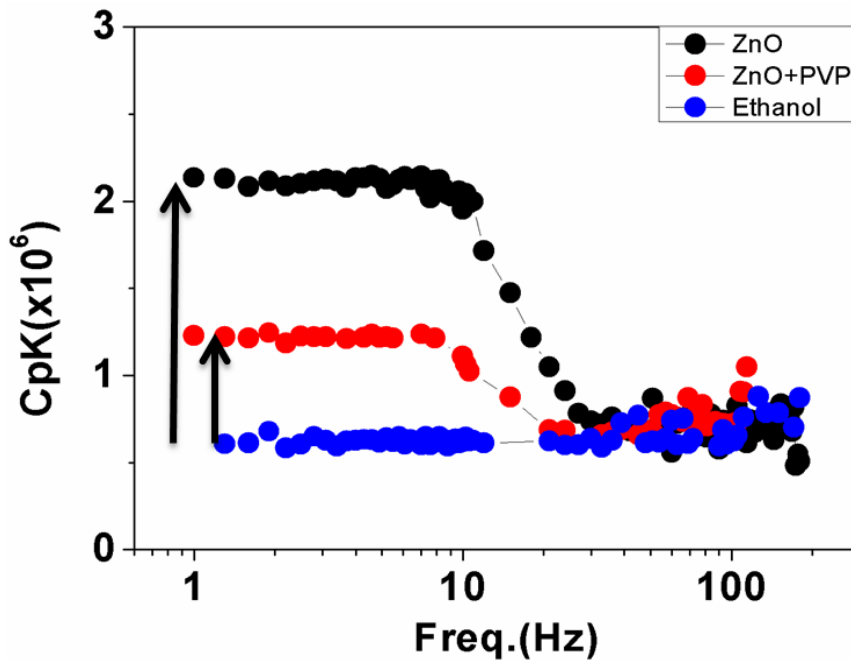


Fig.5.5. Frequency dependence of both bare ZnO and ZnO with PVP.

The experimental results show that there are large enhancements of the thermal parameter $C_p\kappa$ at low frequency. This enhancement is suppressed at high frequency. For bare ZnO nanofluid, there is about four to five times enhancement in the κ value compared to the value of the base fluid Ethanol at room temperature.

At low frequency ($f < f^* \approx 10$ Hz) the enhancement is large and it reaches a frequency independent value. However, at higher frequencies $f > f^*$, there is a rapid decrease of the enhancement and for $f \geq 100$ Hz all of the concentrations show a frequency independent value. This is close to the base fluid value.

For the stable PVP stabilized ZnO nanofluid we found that enhancement in $C_p\kappa$ is reduced although the nature of the frequency dependence is similar.

Particle surface treatment is important. Several studies have demonstrated that thermal transport behaviour is strongly affected by the presence or absence of chemical species attached to particle surfaces. Surfactants can improve the dispersion properties and long-term

stability of nanofluids. The Kapitza (thermal) resistance of the nanoparticle-fluid interface may also be strongly affected by species attached to the surface. Surface species could impact particle mobility and the extent of liquid ordering.

Since the stability of the nanofluid is increased due to the protective PVP layer on the nanoparticles there is a reduction in the aggregation probability of the nanoparticles consequently reduction in $C_p \kappa$.

We can calculate the time constant of thermal relaxation of the aggregate. The $C_p \kappa$ data shows an behaviour similar to that of an electrical component called low pass filter (1st order) which allows low frequency signals but attenuates signals with frequency higher than that the cut off/corner frequency. By using this analogy we calculate the corner frequency in our case.

Experimental data are fitted with the nth order low pass filter response type eqn.5.7; we can find the corner freq., f_c

$$\frac{(C_p \kappa)_{NF}(f)}{(C_p \kappa)_{NF}(f=0)} = \frac{1}{\sqrt{1 + \left(\frac{f}{f_c}\right)^{2n}}} \quad [5.7]$$

where $(C_p \kappa)_{NF}(f)$ is the value at the measuring frequency f &

$(C_p \kappa)_{NF}(f=0)$ is the limiting low frequency value.

We fit this to both the curves and one such fit for the stable ZnO is shown in fig.5.6

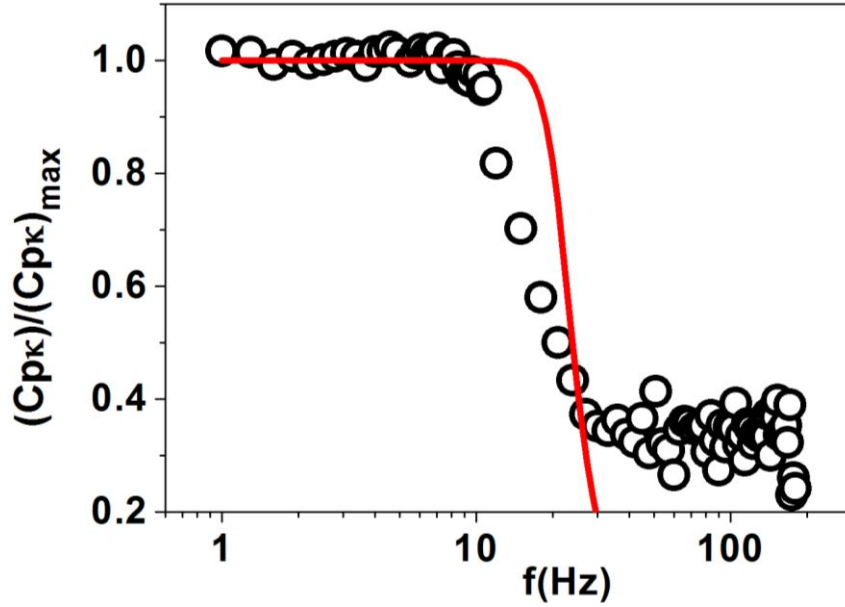


Fig.5.6. First order low pass filter response fit for stable ZnO.

The frequency f is the frequency of the excitation current, leading to the temperature oscillation occurring at $2f$. Thus, the corner frequency will be related to the timescale of thermal relaxation by the relation shown in eqn.5.8

$$\tau_c = (4\pi * f_c)^{-1} \quad [5.8]$$

The characteristic time of the thermal relaxation time can be linked to a characteristic length scale L_A using the eqn.5.9.

$$L_A = (\tau_c D)^{1/2} \text{ where } (D=9 \times 10^{-8} \text{ m}^2/\text{sec}) \quad [10] \quad [5.9]$$

The scale of the frequency dependence associated with the phenomena shows that this occurs on a length scale much larger than the particle size. If the explanation is indeed correct this will mean that the observed large enhancement of the thermal parameter $(C_p \kappa)_{NF}$ at low frequency occurs due to aggregation of the nanoparticles in the fluid over length scales that extend over a few tens of microns

Values obtained for the different parameters for the ZnO nanofluids are summarised in table 5.2.

Nanofluid system	$f_c(Hz)$	$\tau (ms)$	$L_A(\mu m)$
ZnO	23±1.5	4±3	18±2
ZnO+PVP	43±2.3	2±1	13±2

Table 5.2. Nanofluids with corresponding characteristics length and time scale.

For stable nanofluids or colloids, the repulsive forces between particles must be dominant. According to the types of repulsion, the fundamental mechanisms that affect colloidal stability are divided into two kinds, one is steric repulsion, and another is electrostatic (charge) repulsion, shown in fig.5.7. For steric stabilization, polymers are always involved into the suspension system, and they will adsorb onto the particles surface, producing an additional steric repulsive force [11] which helps in keeping the particles separated from each other.

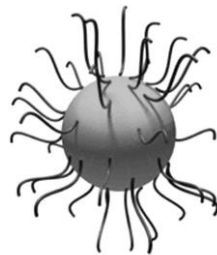


Fig. 5.7 Demonstration of the steric effect of the polymeric dispersant

PVP is an efficient agent to improve the stability for ZnO nanofluid. Due to this steric hindrance there is a decrease in the tendency of agglomeration of the nanoparticles so there is a decrease in the both size of the cluster and thermal relaxation time. Consequently there is a decrease in $C_p \kappa$ enhancement.

5.6 Conclusion

Thus in this chapter we have shown the effect of using the stabilizer and its role in suppression in the thermal conductivity of the nanofluid. This observation supports the hypothesis that aggregation of nanoparticles to form cluster and provides high conducting paths for heat conduction thus showing enhancement in thermal conductivity in nanofluids.

References

- [1] Gharagozloo P E et al, Appl. Phys. Lett. 93, 103110, 2008
- [2] Feng Y, J. Phys. D: Appl. Phys. 40, 3164, 2007
- [3] J. H. Blackwell, J. Appl. Phys. 25, 137, 1954
- [4] D.G. Cahill, Review of Scientific Instruments 61/2, 802, 1990
- [5] Byoung Kyoo Park, Jaesung Park, and Dongsik Kim, Review of Scientific Instruments 81, 066104, 2010
- [6] Lu, Yi and Zhang, Rev.Sci.Instrum.72,2996, 2001
- [7] H.S. Carslaw and J.C.Jaeger, Conduction of heat in Solids (Oxford University Press, Oxford, 1959), p.193
- [8] J. H. Kim, A. Feldman, and D. Novotny, J. Appl. Phys. 86, 3959, 1999
- [9] <http://www.wolframalpha.com>
- [10] Lide D R 2000–01 Handbook of Chemistry & Physics 81st ed. (Boca Raton, NY: CRC Press)
- [11] Wei Yu and Huaqing Xie, Journal of Nanomaterials Volume 2012, Article ID 435873, 17 pages

Chapter 6

Chapter 6: Measurements in Metal Nanofluids.....

6.1 Introduction	163-164
6.2 Results... ..	165
6.2.1 Silver Nanofluids.....	165-167
6.2.2 Au Nanofluids.....	168-169
6.2.3 Au Network.....	170-171
6.3 Discussion.....	172-173
References	

6.1 Introduction

In Chapter 6, we investigated the nanofluids with metallic contents and in particular investigated what happens to the thermal parameters when one changes the morphology of the metallic contents to chain like structure. Effect of morphology of the nanomaterials in the nanofluid has been investigated before as discussed in Chapter 1. However, the metal nanoparticles can be engineered to a very different morphology which is very different from isolated Nanoparticle morphology. In particular, we investigated a novel type of nanofluids that contain Au chains or Au network (Au NW) that was made by a one-pot synthesis method using an excimer laser described in details in chapter 3. We compared the nanofluids with Au nanoparticles with the nanofluid contains Au chains. We started this chapter by measurements on Ag nanofluids with surfactant where the nanoparticle has somewhat smaller size (~5nm).

The metal nanofluids which are measured in this chapter are listed below.

- (a) Silver nanofluid
- (b) Gold Nanofluids and
- (d) Gold Nanonetworks.

We started with the Silver nanofluid. We have chosen Silver for using it as metal nanofluids because it is one of the most common metal nanofluids which can be synthesised easily on large scale in one step method for commercial applications. The nanofluid that we make contain Ag nanoparticle with average size~5nm, which is somewhat in the lower range of nanoparticle used for making Ag nanofluids.

Gold nanofluids are the most versatile class of nanofluids. There are lots of research works going on in this material. Multi-functional Au nanoparticles assembled in different types of morphology are being pursued by different groups [1]. This is a challenge for material scientists investigating functional materials to exploit the multifunctional properties of Au nanoparticles in assemblies. Gold is one of the metals with the most positive electron affinity and thus disperses easily. Alcohols like MEG (Mono Ethylene Glycol), PEG (Poly Ethylene Glycol) were found to be the best solvent for this system. Therefore, these combinations give the most stable nanometre-sized colloidal dispersion. The motivation for using Au

nanoparticles ranges from device application of nanoparticles to biomedical (due to its biocompatibility) that includes imaging as well as cancer therapy. In recent years hybrid materials containing water soluble polymers (like Chitosan) attached to nanoparticles are being used for biomedical applications [2].

Particularly Au nanoparticles-Polyethylene Glycol (PEG) hybrid nanocomposites are finding in vivo applications in radiation therapy [3]. Au nanoparticles coated with polymers have been attached to MEG through chemical means [4]. The fact that the process uses no chemicals other than the Au target and biocompatible Ethylene Glycol, the Au nanochains so formed are immediately ready to use for any biological applications without any further purifications. Also Au is very stable and bio compatible.

The synthesis and characterisation of the nanofluids are given in chapter 3.

6.2 Results

6.2.1 Silver nanofluid

Silver nanofluid used in this experiment was synthesized by microwave assisted chemical reduction method as described in chapter 3. The average size of the nanoparticles is about 5nm. The Ag concentration is 1% by volume in the nanofluid. Frequency dependent thermal measurements are done following the procedure described in chapter 2.

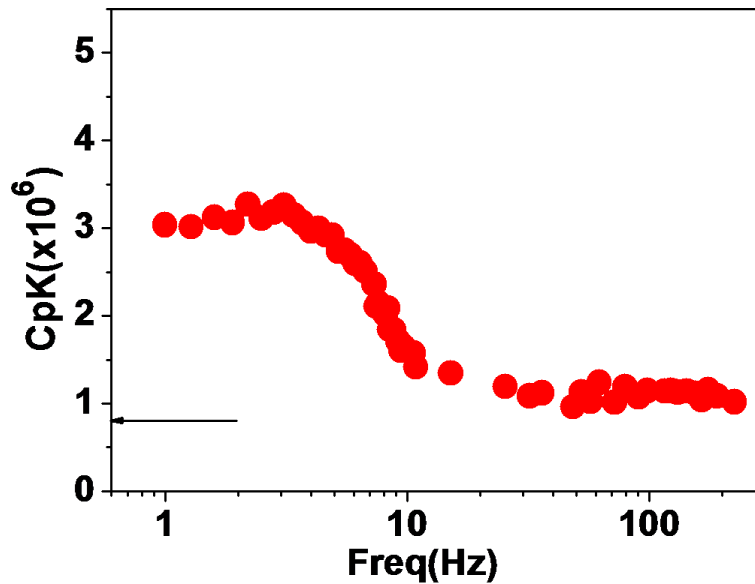


Fig.6.1 Enhancement of $C_p\kappa$ of Ag Nanofluid w.r.t Ethanol value (shown by arrow)

The $C_p\kappa$ value (corrected for finite size effect) is shown in fig.6.1. It is seen that below 3Hz there is a large enhancement of $C_p\kappa$. However the $C_p\kappa$ value becomes close to the Ethanol for frequency > 50 Hz.

If we calculate the enhancement ratio in $(C_p\kappa)$ values for Silver nanofluid it comes out to be about 6 times than that of ethanol.

$$\frac{(C_p\kappa)_{Ag}}{(C_p\kappa)_{etha}} \approx 6$$

In case of nanofluid containing the metal nanoparticles the enhancement is greater than that containing of semiconducting particles like ZnO.

Like the case of ZnO nanofluid when we can fit the response shown in fig. 6.1 with 1st order low pass filter type response eqn. We get the corner frequency f_c , from this we can find the thermalisation time and length scale for the Silver nanoparticle agglomerates by using $D=9 \times 10^{-8} \text{ m}^2/\text{sec}$ [5] for Ethanol. These calculated values are listed in table 6.1.

Nanofluid system	$f_c(\text{Hz})$	$\tau (\text{ms})$	$L_A(\mu\text{m})$
Ag	10 ± 0.7	7.9 ± 0.3	26 ± 0.1

Table 6.1. Nanofluids with corresponding characteristics length and time scale.

Thermal conductivity measurement

Again we employed the slope method for finding the thermal conductivity of the silver nanofluids. Fig.6.2 shows the temperature fluctuation of the heater in the Ag Nanofluid.

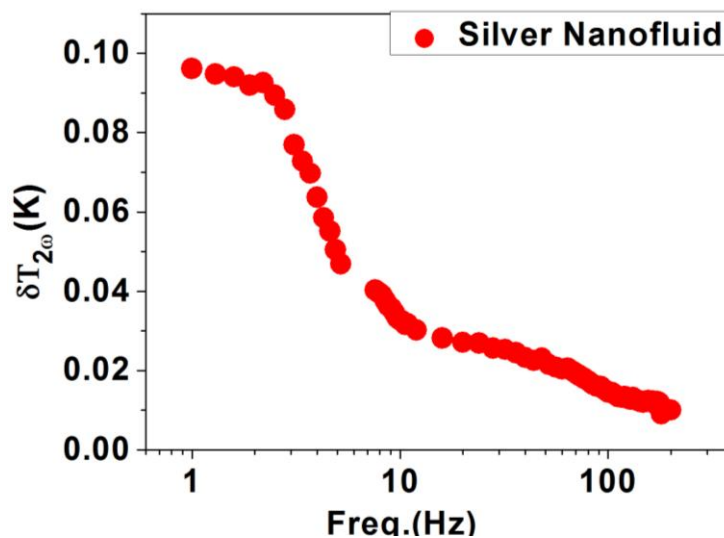


Fig.6.2. Temperature oscillation vs. the frequency for Ag nanofluid

Again we derived the enhancement ratio of the Silver nanofluid w.r.t the base fluids get the similar results for the metal nanofluid as we get for the oxide one. Results are shown in table

6.2. We calculate the thermal conductivity of this nanofluid. It comes out to be six times of the base fluid value.

Method	Ag Nanofluid
Slope of $\delta T_{2\omega}$ curve	$(\kappa)_{\text{ratio}} \sim 6.3$
From 3ω method	$(C_p \kappa)_{\text{ratio}} \sim 6.5$

Table.6.2. Nanofluids with corresponding enhancement ratio of $C_p \kappa$ and κ w.r.t base fluid.

But for the metal nanofluid the ratio of enhancement is much larger. It was also shown by many groups that thermal enhancement for metal nanofluid is greater than any oxide nanofluid [6]

6.2.2 Au Nanofluids

At the end, we carried out the measurement in the Gold (Au) nanofluid containing dispersed Au nanoparticles and then the Au nano network structures both dispersed in the base fluid MEG with volume fraction 0.026. We tried to compare the thermal performance of the network structure over the dispersed spherical nanoparticles in the same base fluid.

We calculated the $C_p\kappa$ variation of these samples as shown in fig.6.3. From the data it is clear that there is again a frequency dependency in $C_p\kappa$ values. The enhancement observed in case of AuNP w.r.t base fluid ($0.7 \times 10^6 \text{ JW/m}^4\text{K}$ [5]) is almost 8.5 times hence we have developed such a network structure of Gold which can significantly enhance the thermal conductivity of the base fluid.

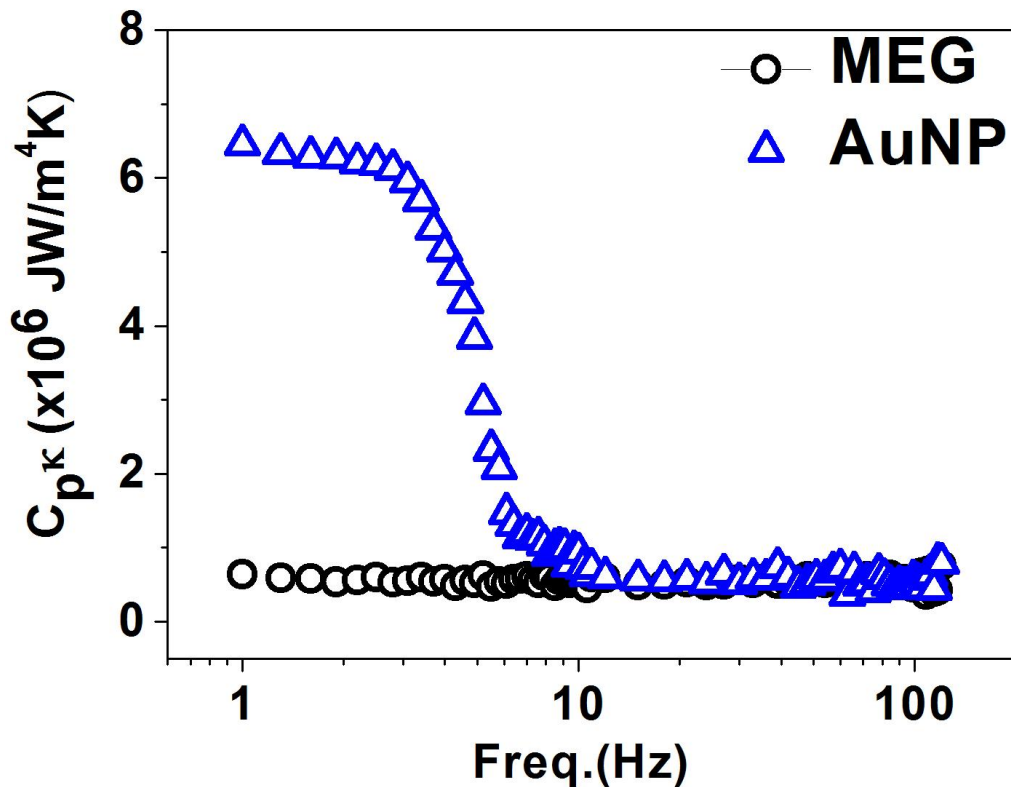


Fig.6.3. Enhancement of $C_p\kappa$ of Ag Nanofluid w.r.t MEG value

Thermal Conductivity Measurement

We determine the thermal conductivity of these by the slope method by calculating the temperature fluctuation using the 3ω signals. Such temperature variation is shown in fig.6.4.

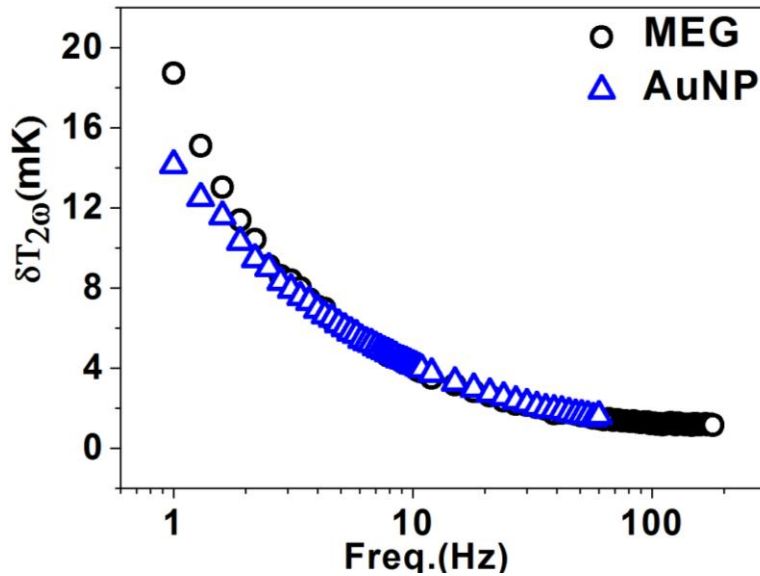


Fig.6.4. Temperature oscillation vs. the frequency curve for MEG, Au nanofluid (AuNP)

From the slope (low freq. end) of the above values we calculate the thermal conductivity of these nanofluids as

$$\kappa_{AuNP} = 1.7 \text{ W / mK}$$

Thus thermal conductivity for the network structure is much more than that of nanoparticles.

We have summarised the above results for Gold samples are given in the table 6.3.

Method	AuNP	AuNW
Slope of $\delta T_{2\omega}$ curve	$(\kappa)_{\text{ratio}} \sim 8.5$	$(\kappa)_{\text{ratio}} \sim 11.5$
From 3ω method	$(C_p \kappa)_{\text{ratio}} \sim 8.1$	$(C_p \kappa)_{\text{ratio}} \sim 11.2$

Table.6.3. Nanofluids with corresponding enhancement ratio of $C_p \kappa$ and κ w.r.t base fluid

From above discussion we can say get that the enhancement in $C_p\kappa$ values is due to the thermal conductivity κ and it also remains almost constant at those values for the lower frequency regime ($<10\text{Hz}$).

6.2.3 Au Network

It is the most interesting sample in our thesis. It is different from all previous samples, in which the particles are spherical and very small in the range 5-10nm. But this Au network is with different morphology. In this small Au nanoparticles get attached with each other by polymer links formed due to the laser ablation. These are very stable and rigid. These chains are formed by the single step, one pot, and surfactant free method [7]. Since we are making this in non chemical process we can find the amount of gold (weight fraction) induced into the solution during the synthesis process (as there is no particular shape/volume of the chains). We determine this from the difference in the weight of the target before and after the laser ablation process. We can find out the mass removed in a single shot and then multiplied with the total number of shots applied during the synthesis. By this way we find the volume fraction of such network which comes out to be 0.03.

These chains are formed and suspended in the solution during the time of formation of the chains.

After this we conducted our measurement on this solution. The result is shown in fig.6.5.

We have found that there is a huge enhancement in the $C_p\kappa$ values w.r.t the MEG value.

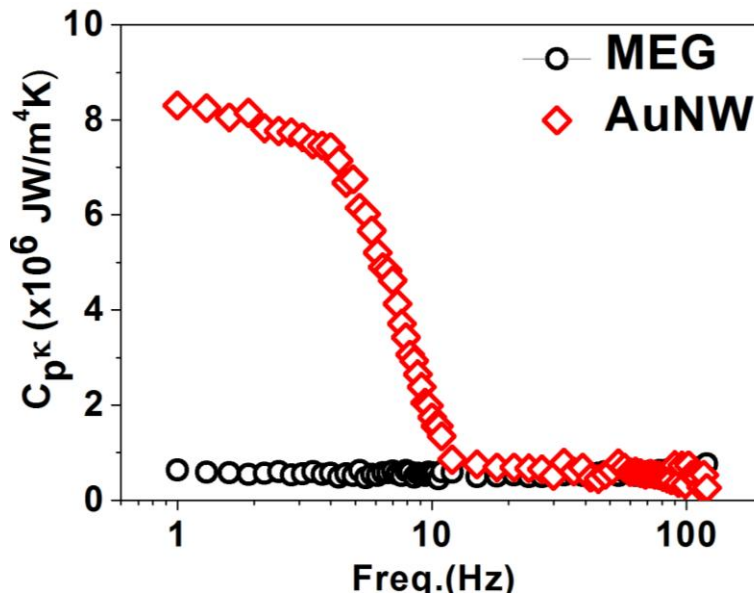


Fig.6.5. Enhancement of $C_p\kappa$ of Au Nanonetwork w.r.t MEG

There is frequency dependence associated with it. At higher frequency side it merges with the value of the base fluid, MEG.

To find the thermal conductivity separately we find the temperature oscillations of the heater in the nanonetwork solution from the $V_{3\omega}$ signal. We got the result as shown in fig.6.6.

From the slope of the curve at lower frequency side gives the information of the thermal conductivity of the sample. We find that the thermal conductivity of this solution as

$$\kappa_{AuNW} = 2.3 \text{ W / mK}$$

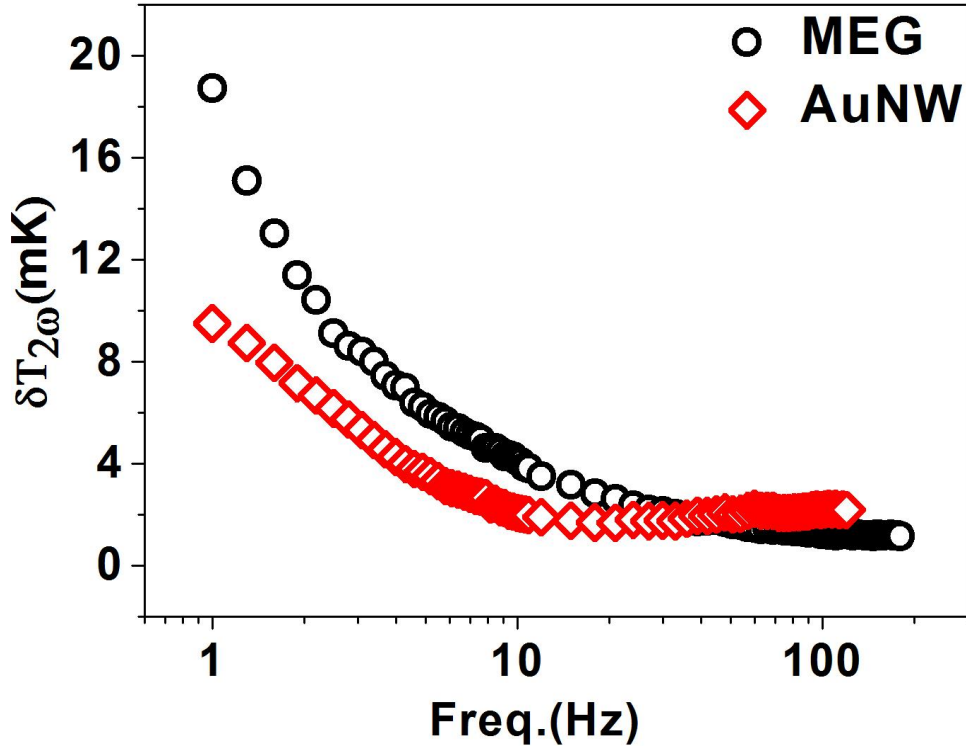


Fig.6.6. Temperature oscillation vs. the frequency curve for MEG & Au network (AuNW).

and for the AuNW it comes out to be almost 11 times. Thus we found that the clusters of Au networks can act as good filler in heat transfer fluids for application in heat management systems as the enhancement with Au network is found to be the highest among the samples we have used for the experiment.

6.3 Discussions

We compare the results of the measurements for both the case of the Au nanofluids. Results are listed in table 6.4. It is shown that enhancement for the case of Au nanonetwork is about eleven times that of the base fluid MEG.

Method	AuNP	AuNW
Slope of $\delta T_{2\omega}$ curve	$(\kappa)_{\text{ratio}} \sim 8.5$	$(\kappa)_{\text{ratio}} \sim 11.5$
From 3ω method	$(C_p \kappa)_{\text{ratio}} \sim 8.1$	$(C_p \kappa)_{\text{ratio}} \sim 11.2$

Table.6.4. Nanofluids with corresponding enhancement ratio of $C_p \kappa$ and κ w.r.t base fluid

By the 1st order low pass filter response fit we find the corner frequency (f_c) for both the case and calculated the thermalisation time and the spatial extent of the aggregation of the nanoparticles by using $D=9.7 \times 10^{-8} \text{ m}^2/\text{sec}$ [5] for MEG. These values are listed in table 6.5.

Nanofluid system	$f_c(\text{Hz})$	$\tau (\text{ms})$	$L_A(\mu\text{m})$
AuNP	3.6±0.3	22±0.3	46±0.1
AuNW	4.5±0.2	17±0.1	41±0.2

Fig.6.5.Nanofluids with corresponding characteristics length and time scale.

In the case of other type of nanofluids where particles are separated and when they form a cluster (due to thermo diffusion) they conduct. But for the network structure (as shown in fig.6.7) the individual nanoparticles are connected tightly with each other and such huge enhancement for the case of the network is due to the long chain structure. These continuous structures provide the backbone for the heat transport through the connected nanoparticles over a large length scale. For such enhancement it is important that the network structure are formed and simultaneously suspended in the base fluid. The structure shown in fig.6.7 is the TEM image of a typical network when they are transferred to Cu grid. They are not formed by the cohesive force between them or with the substrate when they are they are transferred to them.

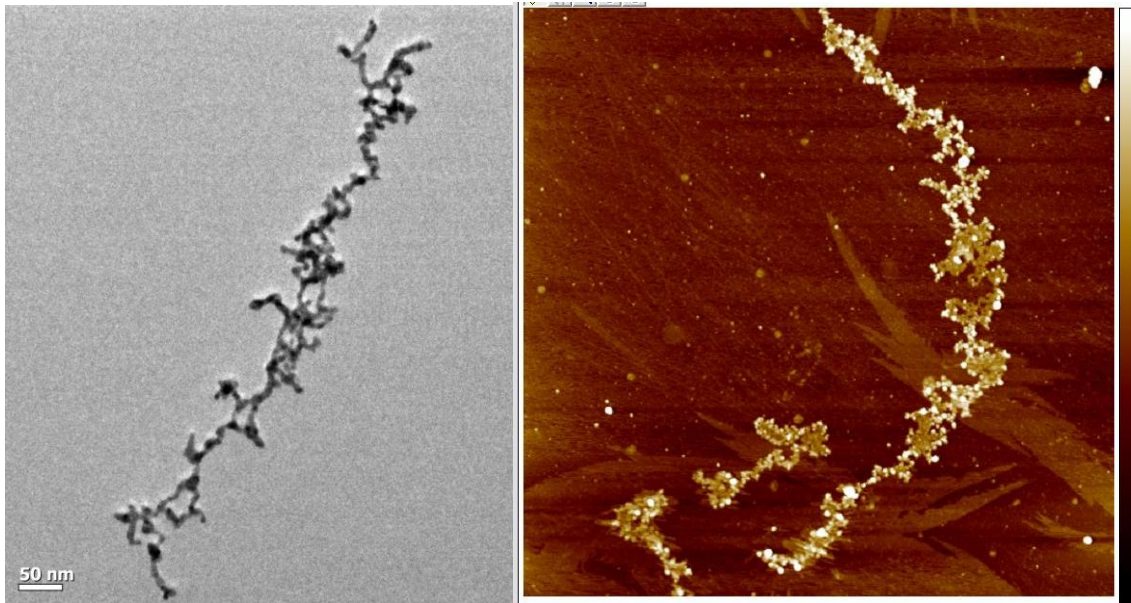


Fig.6.7.TEM & AFM images of an elongated Au network structure.

We have experimentally shown that these networks are formed in the solution itself. Thus this network structure shows more improved thermal conductivity than those of ordinary (general sense) nanofluids.

If we want to compare the effective enhancement in the $C_p\kappa$ for all the nanofluids, we normalise the individual $C_p\kappa$ values with the corresponding volume fraction and all these values are shown in the table 6.6.

Sample	ϕ (%)	$C_p\kappa$ ($\times 10^6$)	$C_p\kappa/\phi$
ZnO	1.5	2	1.3
ZnO+PVP	1.5	1.3	0.8
Ag	1	3	3
AuNP	2	6.5	3.2
AuNW	3	8.5	2.8

Table.6.6.Nanofluids with corresponding normalised $C_p\kappa$ values.

We find that Gold nanofluids (AuNP) have the highest enhancement of the thermal parameters (per unit vol.fraction).

References

- [1] Amir Fahmi, Anthony D'Aléo, René M. Williams, Luisa De Cola, Nabil Gindy, and Fritz Vögtle, *Langmuir*, 23 (14), pp 7831, 2007
- [2] Linlin Wu, *Journal of Physical Chemistry C*, 112, 319, 2008
- [3] Chi-Jen Liu et.al. *Phys. Med. Biol.* 55, 931, 2010
- [4] Teresa Pellegrino et.al. *Nanoletters* 4, 703, 2004
- [5] R. C. Weast, *CRC Handbook of Chemistry and Physics*, CRC Press, Boca Raton F, 1987
- [6] Chapter 12 of *Cutting Edge Nanotechnology*, ISBN: 978-953-7619-93-0, In Tech Published, Croatia, 2010
- [7] Rajesh Kr. Neogy, Rajib Nath, *Micro and Nanosystems*, Vol. 3, No. 4, 1-7, 2011

Summary and conclusions of the thesis

(a) Experimental contributions

- » The synthesis of good quality, different types of nanofluids. These were characterized for the structure and microstructure using tools like XRD, TEM and HRTEM.
- » Fabrication of the high quality Pt thin film for using it as a heater and as well as thermometer.
- » This report is based on using an electrical conducting thin Pt film as a planar heater and temperature sensor simultaneously. The thin Pt film is on a glass substrate, and measurements are made with and without liquid on the other side of the heater. High precision thermal conductivity measurement setups (based upon 3ω technique) have been prepared to study the thermal parameters of liquid samples. This can measure a temperature oscillation (δT) of the order of few mK sitting at room temperature. The necessary hardware and software for measurement automation was also developed simultaneously.
- » Successful fabrication & simultaneous assembly free Gold nanoparticles into micron size structured network by the bottom up method through the process of PEGylation. These network structures shows many interesting properties like enhancement in thermal conductivity etc.
- » We measure thermal conductivity and effusivity separately for the nanofluids.

(b) Physics contributions

- » For the first time we have shown that the thermal conductivity enhancement in the case of Nanofluids can have a frequency dependence over a certain range of the applied frequency and this enhancement is much larger than as predicted by the classical Effective Medium Theory (EMT).

- » Our experiment supports the local aggregation model for the enhancement in thermal conductivity in nanofluids. We have devised a method to calculate the characteristics time constant and length scale over which the aggregation of the nanoparticles takes place.

Scope for future work

- (1) A Molecular Dynamics (MD) simulation work can be done in order to estimate the enhancement in the thermal parameters of the nanofluid theoretically.
- (2) The frequency range of scanning of the current setup needs to be extended for getting more information about the system beyond the frequency range (1 Hz- 1 KHz) on both the ends. For this two heaters (wider and thinner) can be used simultaneously.
- (3) More experiments can be done on different nanofluids by varying shapes, sizes and the environment of the nanoparticles.
- (4) Temperature variation can be done over a wide range both below and above the room temperature.

List of Publications

- (1) Frequency dependent enhancement of heat transport in a nanofluid with ZnO Nanoparticles,
R K Neogy and A K Raychaudhuri, *Nanotechnology* 20 (2009) 305706

- (2) Synthesis of micron sized Gold network structure by assembling individual Gold nanoparticles by Laser assisted PEGylation method
Rajesh Kumar Neogy and Rajib Nath, *Micro and Nanosystems*, 2011, 3

- (3) Dielectric Constant Enhancement of Ethylene Glycol by Au Nano Networks
Rajesh Kumar Neogy and Rajib Nath, *Nanoscience and Nanotechnology Letters* 4, 409-413, 2012

- (4) Effect of surfactant on the frequency dependent enhancement in thermal conductivity for Nanofluid containing ZnO nanoparticles.
Rajesh Kumar Neogy, A. K. Raychaudhuri (to be submitted for review)

The End...